Department for Landscape, Spatial and Infrastructure Sciences

Institute of Surveying, Remote Sensing and Land Information

Head of the Institute: Atzberger, Clement (Univ. Prof. Dr. rer.nat.)

Advisors:

- Atzberger, Clement (Univ. Prof. Dr. rer.nat.)
- Vuolo, Francesco Dr.

Title: Assimilation of Leaf Area Index into the crop growth models GRAMI and SAFY to monitor maize crop: a case of study in the Marchfeld region.

Dissertation for obtaining a doctorate degree at the
University of Natural Resources and Life Sciences, Vienna

Submitted by:
Javier Esteban Portillo

Vienna, October 2016

Abstract

Simple crop growth models (CGM) integrated with Leaf Area Index (LAI) retrieved from earth observation (EO) data allow monitoring crop growth at regional and plot scales. The global research objective of this study was to develop a method based on the GRAMI and SAFY crop growth models to estimate maize yield in the Marchfeld region, characterized by a restricted availability of input data. Maize yield data were collected for the seasons 2013 and 2014. The LAI was estimated by the CLAIR model from Landsat and DEIMOS data with a NRMSE of 12%. The assimilation of LAI into the crop growth models was analyzed for four approaches. The Look up Table (LUT) and Particle Swarm optimization (PSO) methods were tested at plot and pixel scale. Ensemble Kalman Filter (EnKF) and Particle Filter (PF) were implemented at pixel scale. The sensitivity analysis of LUT and PSO showed that for efficient calibration of the GRAMI and SAFY models, satellite-based LAI observations should be available every 15 days for LUT and 20 days for PSO. The average LAI random error should be smaller than 20%. SAFY calibrated at plot scale by PSO achieved a better performance compared to GRAMI with an estimation error at plot scale (EEP) of 12.5% and at regional scale (EER) of 0.2%. The calibration techniques performed well in forecasting maize yield one to two months before harvesting with an EER of 3% and 7.1% respectively. The yield estimation accuracy was increased by using pixel data. The EEP was reduced to 8.3% using SAFY calibrated at pixel scale for a reduced number of free parameters. The updating at pixel scale showed a good performance. The EEP using EnKF was 9.7% and the EER 2.3%. Moreover, the time of processing was reduced by 17 times compared to the PSO calibration at plot scale. PF showed in average for both crop seasons better accuracy than EnKF. The calibration of the SAFY model at plot scale using PSO and the updating at pixel scale using PF yielded a suitable average accuracy both at regional (2.5%) and plot scale (10.5%). Additionally, the low computational demand of PF makes the updating of SAFY at pixel scale possible even for larger regions.

Keywords: agricultural remote sensing, crop growth modeling, maize, GRAMI, SAFY, particle swarm optimization, ensemble Kalman filter, particle filter.

Zusamenfassung

Die Assimilation des aus Fernerkundungsdaten abgeleiteten Blattflächenindexe (Leaf Area Index, LAI) in einfache Wachstumsmodelle erlaubt das Monitoring des Pflanzenwachstums auf regionaler Ebene als auch auf Schlagebene. Das Forschungsziel der vorliegenden Arbeit ist die Entwicklung einer Methode zur Schätzung des Maisertrages in der Region Marchfeld, basierend auf den Wachstumsmodellen GRAMI und SAFY bei einer geringen Verfügbarkeit von Eingangsdaten. Hierzu wurden Maisertragsdaten für die Wachstumsperioden 2013 und 2014 erhoben. Der LAI wurde mit dem CLAIR-Modell aus Landsat- und DEIMOS-Daten mit einem NRMSE von 12% geschätzt. Die Assimilation des LAI in die Wachstumsmodelle wurde für vier verschiedene Methoden untersucht. Look Up Tables (LUT) und Partikelschwarmoptimierung (PSO) wurden für die schlag- und pixelspezifische Assimilation getestet. Ensemble Kalman Filter (EnKF) und Particle Filter (PF) wurden hingegen nur pixelspezifisch umgesetzt. Eine Sensitivitätsanalyse von LUT und PSO zeigte, dass für eine optimale Kalibrierung der genannten Modelle satellitenbasierte LAI-Beobachtungen alle 15 Tage für LUT und alle 20 Tage für PSO verfügbar sein sollten. Der durchschnittliche LAI-Zufallsfehler sollte unter 20% liegen. Das auf Schlagebene kalibrierte SAFY-Modell erzielte bessere Ergebnisse im Vergleich zum GRAMI-Modell, mit einem Schätzungsfehler auf Schlagebene (estimation error at plot scale, EEP) von 12,5% und auf regionaler Skala (estimation error at regional scale, EER) von 0,2%. Die Kalibrierungstechniken zeigten ein bis zwei Monate vor der Ernte gute Ergebnisse in der Prognose des Maisertrages mit EERs von 3% bzw. 7,1%. Die Verwendung von pixelbasierten Daten erhöhte die Genauigkeit der Ertragsschätzung. So konnte der EEP bei der Kalibrierung von SAFY mit einer verringerten Anzahl von freien Parametern auf 8,3% reduziert werden. Update mit pixelspezifischen Daten brachte gute Ergebnisse: der EEP mittels EnKF betrug 9,7% und der EER 2,3%. Zudem konnte die Prozessierungszeit im Vergleich zur PSO-Kalibrierung auf Schlagebene um das 17fache verringert werden. Im Durchschnitt zeigte PF eine bessere Genauigkeit für beide Erntezyklen als EnKF an. Die Kalibrierung des SAFY-Modells auf Schalgebene mittels PSO und das Update mit pixelbasierten Daten mittels PF ergaben eine ausreichende durchschnittliche Genauigkeit auf regionaler Ebene (2,5%) und auf Schlagebene (10,5%). Eine wichtige Schlussfolgerung ist, dass aufgrund des geringeren Prozessierungsaufwandes ein pixelspezifisches Update von SAFY selbst für größere Gebiete ermöglicht wird.

Schlüsselwörter: Landwirtschaftliche Fernerkundung, Wachstumsmodellierung, Mais, GRAMI, SAFY, Partikelschwarmoptimierung, Ensemble Kalman Filter, Partikelfilter.

Acknowledgement

I thank the Instituto Nacional de Tecnología Agropecuaria (INTA-Argentina) for delivering a grant in order to attend my PhD study at BOKU University. My deepest gratitude to GÁNDARA Fernando (Msc), PECORARI Carlos (Dr), GUEVARA Edgardo (Dr) and Meira Santiago (Msc) who supported the submission of my PhD project. I thank the Institute of Surveying, Remote Sensing and Land Information of BOKU for admitting me to PhD studies since without the admission, the grant and the attendance of the study would have not been possible.

My sincere gratitude extends to the individuals who contributed to the accomplishment of my study. First and foremost, I would sincerely to thank my advisers ATZBERGER Clement (Ao. Univ. Prof. Dr.techn.) and VUOLO Francesco (Dr), for their guidance during the whole study period. This work would not be in the current shape without the dedication and friendly support from my supervisors.

I want to thank the researchers of the Institute of Surveying, Remote Sensing and Land Information (IVFL). My appreciation extends specially to KLISCH Anja (Dr) for her technical support and constructive comments.

I want also to use this opportunity to thank everyone who supported me throughout the whole period of the study with special gratitude to BIBLl Detlef (Dr), TRIPP Gerhard (Msc) and FERREYRA Adriana (AUS). I am thankful for their friendly advises during my study. My warm appreciation extends to all my family members for all their encouragement and support.

I thank the contribution of the farmers of the Marchfeld region who allowed me to take field measurements and provided information of the maize plots. I have to thank the Statistics Austria (Statistik Austria, Feldfruchternteerhebung) and the Zentralanstalt für Meteorologie und Geodynamik (ZAMG) for the data provided.

Finally, my deepest gratitude to DUCHEMIN Benoît (Dr) who made available the code of the SAFY crop growth model.

Table of contents

1. Introduction

Agricultural activities have a strong impact on natural resources and societies. Agriculture contributes between 5 to 32 % of the GDP (Gross Domestic Product) of urbanized and agriculture-based countries, respectively (World Bank, 2008). Agricultural activities still represent the most important source of employment in emerging markets, being for example responsible for more than half of total employment in sub-Saharan Africa and South Asia.

As a result of the increasing global population and changing diets, an escalation in food consumption has been observed over the last decades. This trend is expected to continue within the 21st century (Gehlhar and Coyle, 2001). Alexandratos & Bruinsma (2012) predict that the global food consumption per capita will increase from 2411 kcal per person and day in 1969/1971 to 3130 kcal in 2050. Cereals such as wheat, rice and maize are the main source of energy. They provide about 60% of the total daily kilocalories consumed in developed countries and 80% in developing countries (Awika, 2011). Moreover, in the last decades the demand of cereals such as maize has sharply increased because of its use for animal feeding and energy production (Edgerton, 2009).

The worldwide increase in food demand strongly contrasts with limited resources (water and land) as well as the need to protect habitats and halt deforestation (Foley et al., 2011). In this context, a collective action is necessary to reduce the risks of food shortages, scarcity of water resources and energy (Thenkabail, et al., 2012). Matching food demand and food production is a Millennium Development Goal (MDG) of the United Nations (UN). World leaders have committed to the goal of "Zero hunger" for 2030 (UN, 2016) and "it's what humanity deserves" (WFP, 2016).

As food demand is expected to rise in the future, it is becoming increasingly important for scientists and decision-makers to reliably and timely estimate yields at regional and national levels (Chahbi et. al., 2014; Rembold et al., 2013). Such information is for example useful to identify yield gaps and areas suitable for agricultural intensification (Lobell, 2013). Forecasting crop yields also allows planners and decision makers to understand and address markets, and reliable agricultural information enables governmental and international agencies to execute contingency plans (Liu, et al 2014a). Tools, which allow estimation of crop production, help to manage the way food is produced, stored and distributed. An accurate monitoring of crop yield is also essential for commodity trade, detecting of regional crop failure and greatly supports humanitarian aid (Pino, 2001; Rizzi, 2005; Padilla, et al 2012; Ma et al, 2013a). Finally, objective and timely production-related information also provides an important input to agricultural insurances (De Leeuw et al., 2014).

Currently, in most countries agricultural statistics are still obtained by conventional techniques based on information delivered by regional referents, agricultural input providers or the use of sampling techniques. Such methods are in most cases subjective, costly, time consuming and susceptible to large errors (Liu, et al 2014a; Wu et al, 2012). At the same time, the information is often provided with significant delays, making it less useful (Atzberger et al., 2013a).

Mathematical models of environmental systems such as agricultural crops, formalize the interaction of the object of interest with its (environmental) drivers, conditions and management. The formalization is based on theoretical knowledge and/or empirical evidence, thereby allowing to understand how the system works and to predict its behavior. In the context of agricultural crop yield forecasting, crop growth models (CGM) describe the main physiological mechanisms which occur in the crop and its interaction with the environment (Delécolle et al., 1992). A crop growth model simulates the temporal evolution of state variables (for instance biomass and leaf area index) as a function of driving variables such as meteorological data and further input variables such as soil and crop characteristics as well as management practices (Mansouri et al, 2014). The models thereby

summarize and formalize current knowledge of the main processes determining crop yield, update model state variables in regular updating intervals (daily, weekly, monthly) and ensure a consistent evolution of crop development (phenology) and growth variables (Delécolle et al., 1992).

Thanks to the capability of CGM to mimic crop growth, it is feasible to assess the effects of management and climatic scenarios as well as to identify possible practices increasing crop yield (Faivre et al., 2004; Lobell, 2013). Using available weather data as well as weather forecasts, it is for example possible to build different temporal scenarios. Then, based on these scenarios, different agricultural practices can be proposed to minimize the (negative) weather impact on crop production (Royce et al., 1998; Hoogenboom et al., 2000). Similar approaches can be used to assess future impacts of climate change (Shin, et al., 2009; Ferreyra et al., 2001).

Crop growth models have been implemented initially as a research tool within experimental frameworks (Spitters, 1990, Boote, et al. 1996). In the last decades, they have been used at regional scale aiming to estimate crop state over larger areas. The regional application of these complex models is hampered by their high input requirements, which are practically impossible to obtain over large areas with a sufficient degree of confidence. Therefore, formally correct, CGMs typically suffer from inaccurate input variables (mainly related to climate, soil and management). If the models are not constraint by measurements, errors in CGMs accumulate over time and finally lead to erroneous crop growth and yield simulations.

Remote sensing is a technique which allows acquiring spectral and temporal information from remote platforms (Shanahan et al, 2001). EO data provide relatively inexpensive, synoptic, objective and homogenous observations, which can be geographically and temporally registered. Thanks to these characteristics, remote sensing is considered an efficient tool for providing standard, high quality information on agriculture (Tsiligirides, 1998) and for constraining CGMs (Maas, 1998). The continuous monitoring of the Earth surface by satellites fits very well with the dynamics of agricultural activities. This is an importance asset for CGM calibration and, in consequence, for yield assessment (Ozdogan, 2010).

Contrary to many other (natural) vegetation types and biomes, agricultural crops are relatively easy to assess remotely because of their (genetical) homogeneity. Indeed, for crops, the spectral signatures resulting from canopies of different leaf area index (LAI), with different leaf pigmentation and soil optical properties are relatively well modeled using various radiative transfer models (Jacquemoud et al., 2009). Important crop status variables such as LAI and fAPAR also correlate well with remotely sensed vegetation indices such as the Normalized Difference Vegetation Index (NDVI) (Baret & Guyot, 1991).

Since a few years, the use of remote sensing data has been boosted by the huge amount of high-quality data available obtained from sensors with different technical configurations, such as Landsat-8, DMC (Disaster Monitoring Constellation) or Sentinel-2. This new generation of sensors is building virtual constellations, able to deliver multi-spectral images with a spatial resolution in the range of 10 to 30 meters and a temporal revisit frequency of a few days. Hence, compared to very high spatial resolution (VHR) sensors such as WorldView-2/3 or Pleiades, global agricultural activities can be continuously monitored with reduced lag times and at lower costs. Only high revisit frequencies allow following the growth of agricultural crops and detecting and assessing disturbing events like hail damages or insect infestations. Obviously, a high revisit frequency is worth little if the data is expensive and/or if the spatial resolution is not able to resolve small fields (De Wit, 2012; Machwitz et al, 2014). In this respect, freely available data from the European Sentinel-2 mission with 10m GSD and a 5-daily revisit time is a long awaited game changer for agricultural applications (Immitzer et al.,

2016). First comparative assessments also show a close spectral match between Landsat-8 and Sentinel-2 (Vuolo et al., 2016).

Crop growth models and remote sensing techniques complement well each other in various agricultural tasks. Crop growth models provide excellent means of simulating detailed physiological processes taking into account weather, soil and management conditions, etc. On the downside, CGMs are difficult to parameterize at regional scale due to lack of sufficiently detailed information regarding management practices and soil conditions, etc. Obviously, any shortcoming in model parameterization results in erroneous simulations –summing up until the end of the growing period when the yield information is derived. Remote sensing, on the other hand, does provide only very little information on crop physiology (and only little information on crop phenology), but offers abundant information on crop status over large areas at high spatial resolution and with high temporal (revisit) frequency. For instance, remote sensing provides a detailed description of some important crop status variables (e.g. leaf area index), which may be used to constrain and correct CGM simulations (Dadhwal, 2003). The combination of remote sensing and crop models therefore allows taking advantage of the synergy of the two approaches (Delécolle et al., 1992).

Aware of the close link between EO and CGM Maas and co-workers conducted successfully the early work to combine remote sensing data and crop models to reduce the errors and uncertainties in crop growth simulations at regional scale. An example of a CGM specifically designed to integrate external data sources aiming at calibrating model parameters is GRAMI. The model was developed by Maas (1992) and consists of a group of integrated equations based on the light-use efficiency (LUE) theory (Monteith, 1977). Duchemin et al (2008) developed the "Simple Algorithm For Yield estimate" (SAFY). The model was built following a logical sequence similar to GRAMI. However, unlike GRAMI, in SAFY the speed of the plant senescence can be parameterized and the efficiency of conversion of FAPAR to biomass is modified by a factor which depends on the daily air temperature.

The combination of simplicity along with the feasibility to use remote sensing data for parameter calibration enables this kind of models to be implemented in regional crop monitoring programs (Padilla et al., 2012).

GRAMI and SAFY models have been implemented to estimate biomass and yield of several crops in different regions. For instance; Ko et al (2006) tested GRAMI performance for cotton, Atzberger el al. (2001) and Padilla et al (2012) for wheat and Yeom et al. (2015) for rice among other examples. Moreover, SAFY was implemented for wheat (Duchemin et al., 2008), maize and sunflower (Claverie et al., 2012) and barley and wheat (Chahbi et al, 2014).

For these examples most of the model parameters were defined from literature or were estimated using experimental data. Thereafter, a reduced group of parameters was calibrated, with a low inter-correlation.

The calibration of simple CGMs such as GRAMI and SAFY by assimilating EO data is not a trivial issue. One problem relates to the ill-posedness of the inverse problem. Ill-posed problems are caused when similar fits between measured and estimated state variable may be achieved for different parameter combinations. (Kabanikhin, 2008). For instance, a similar good fitting between simulated and observed leaf area index (retrieved from EO-data) can often be obtained by different combinations of model parameters. However, these combinations potentially produce different estimations of crop yield.

The reduction of free parameters is the alternative mostly used to minimize the ill-posed effect in the calibration of (inter-) correlated parameters. This is implemented under the assumption that the fixed parameters are representative of the crop variability in the study area. This assumption is valid if

there is sufficient information about the crop/s of interest and the study area is relatively homogenous. Otherwise, the estimations obtained by the CGM might be inaccurate. Therefore, if the CGM is implemented in a heterogeneous study area and there is no possibility to carry out field experiments; it is mandatory using a methodology which allows obtaining accurate crop estimations with a minimum requirement of input data.

Our experiment is carried out under the hypotheses that the crop growth models GRAMI and SAFY integrated with remote sensing observations are able to estimate maize yield with a suitable degree of accuracy with few inputs available.

Focusing on the accuracy of maize yield estimation, the research questions are:

- Which model parameters must be calibrated first and foremost?
- Which is the best strategy to calibrate multiple (inter-)correlated parameters?
- How does the temporal frequency and error of the remote sensing observations affect model calibration?
- How early in the crop season one can accurately forecast maize yield?
- Which of the two simple crop growth models GRAMI and SAFY has the best performance to estimate maize yield?

1.1. Objetives of the research

The global research objective is to develop an assimilation method based on a simple crop growth model to estimate maize yield in the Marchfeld region with a minimum input data requirement. The specific research objectives were:

(1) assessing the sensitivity and correlation of the parameter of two simple crop growth models;
(2) testing calibration techniques and the combination of calibration with updating to calibrate a maximum number of inter-correlated parameters;
(3) establishing the critical calibration period, the suitable error level and the minimum number of LAI observations required for an accurate calibration of the model parameters;
(4) assessing the ability of SAFY and GRAMI to forecast maize yield, one to two months before harvesting;
(5) comparing the performance of SAFY and GRAMI models to estimate maize yield.

2. Retrieval of vegetation bio-physical variables using EO data

2.1. Introduction

The objective of the bibliographical review was to summarize the state-of-the-art of EO data assimilation in crop growth models. The first part of the revision presented in this chapter is focused on mapping/retrieval of biophysical vegetation variables. The chapter is divided in four sections; in sections 2.2 to 2.4 are introduced and compared techniques to retrieve bio-physical variables considering advantages and disadvantages of approaches ranging from simple empirical regressions to complex radiative transfer models. In section 2.5 an overview is presented regarding the retrieval of bio-physical variables. Aspects related to the assimilation of the retrieved bio-physical variables in the CGMs are addressed in the second part of the bibliographical revision in chapter 3.

Being aware of the impossibility to cover all aspects associated with EO-based crop monitoring, valuable reviews in near-by fields are included in Table 1.

2.1.1 Quantitative analysis of Research

Aiming to assess the relevance of the topics discussed in chapters 2 and 3 was carried out a thematic research on SCOPUS and Thompson Reuters websites. The number of publications in (i) CGM and (ii) EO-data assimilation in CGM is depicted in **Figure 1.** The searching keywords used to assess the number of publications were "crop growth model", "crop growth model + remote sensing", "crop growth model + remote sensing/LAI + forcing", "crop growth model + remote sensing/LAI +calibration", "crop growth model + remote sensing/LAI + updating", "crop growth model + ensemble Kalman filter", "crop growth model + particle filter". The number of publications per decade is expressed as a percentage with respect to the total number of publications considered. Both topics show a strong increase over time. However, publications dealing with assimilation of EO data in crop models show a sharper growth in the last decade, compared to the CGM publications. This probably reflects a growing demand for information about crop growth at different spatial scales which can be provided through EO data assimilation. At the same time, availability of high resolution (deca-metric) EO data strongly increased.

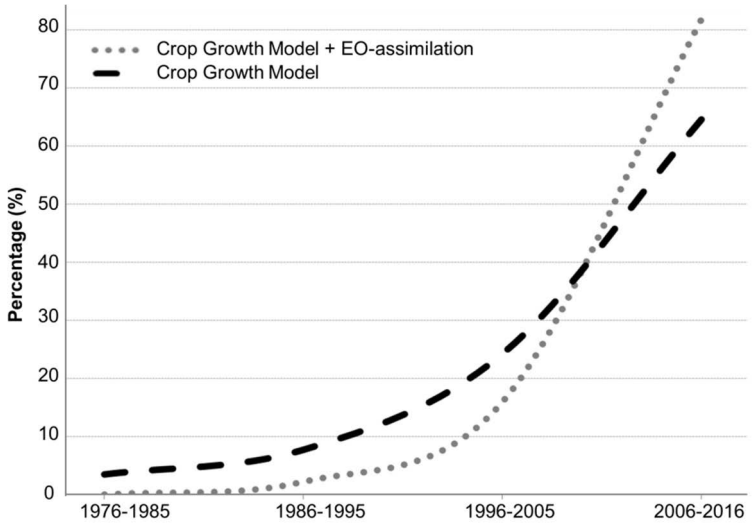

Figure 1. Research publications about CGM and CGM+EO assimilation during the past four decades. Values are expressed as percentage with respect to the total number of publications. Data from SCOPUS and Thompson Reuters.

Table 1. Valuable review papers about bio-physical variables retrieval and assimilation in CGMs

Topic	Content	Source
Agricultural remote sensing	Remote sensing applications in classification, monitoring of phenology and production estimation	Calvao & Pessoa, 2015
	Remote sensing in agricultural monitoring, modeling, and management	Shi, et al., 2014
	Regional to global application of remote sensing in agriculture; overview of operational monitoring systems	Atzberger, 2013a
RS and yield forecasting	Synergy of remote sensing and biophysical/ eco-physiological process models	Inoue, 2003
	Crop monitoring by low resolution remote sensing data	Rembold et al., 2013
Retrieval of crop state variables	Review of methods to derive canopy state variables from EO data	Dorigo, et al., 2007
	Reviews of algorithms for estimating land surface variables using optical remote sensing	Liang, 2007
	Review of currently available LAI estimation algorithms	Baret & Buis, 2008
	Presentation of emulators models to approximate the functioning of RTMs and to speedup model inversion	Rivera et al., 2015
	Evaluation of different retrieval methods on their ability to estimate leaf area index (LAI) using Sentinel-2 images	Verrelst et al., 2015a
Assessment of crop area	Review of mapping and yield forecasting of rice	Mosleh et al., 2015
	Review of soft computing classification techniques for crop mapping	Murmu & Biswas, 2015
Crop growth models	Conceptual review about crop models	Oteng-Darko, et al., 2013
	Applications of crop growth models in agricultural meteorology	Rauff & Bello, 2015
	Review about crop models structure, evaluation, parameter estimations and model improving	Dumont, et al., 2012
	Fundaments and review of 'School of de Wit' crop growth models	Bouman, et al., 1996
Assimilation techniques	Overview of assimilation of remote sensing data in hydrological models	Xu,X., 2014
	Review of multivariate and multiscale assimilation of observational data	Montzka, et al., 2012
	Overview of EO data assimilation techniques in agricultural crop growth models	Delecolle et al., 1992
Use of filter techniques	Presentation, implementation and discussion about the Ensemble Kalman Filter	Evensen, 2003
	Review of Bayesian algorithms for nonlinear/non-Gaussian focused on particle filters	Arulampalam, et al., 2002

2.1.2. General classification of bio-physical retrieval techniques

The most natural link between crop growth models and remote sensing (RS) is established via the crop's leaf area index (LAI). LAI is often used for connecting RS and CGM as this bio-physical variable determines both the reflected signal captured by the remote sensor as well as the crop's radiation interception capacity as modeled in crop growth models. Other bio-physical variables such as fractional cover (fCOVER), the fraction of photosynthetically active radiation absorbed by the canopy (fAPAR), plant chlorophyll concentration or phenological stage may also be used to connect EO and CGM, either alone or in combination with LAI (Dorigo et al., 2007).

Crop bio-physical variables can be remotely retrieved using (1) empirical methods, (2) semi-empirical approaches or (3) physically-based radiative transfer models, (Baret & Buis, 2008; Atzberger et al., 2015; Verrelst et al., 2015b). Definitions of LAI as well as methodologies for LAI retrieval are discussed in Zheng and Moskal (2009) and Baret & Buis (2008).

2.2. Empirical methods

Empirical methods consist in establishing regression equations (linear or nonlinear) between the biophysical variable(s) of interest and remote sensing observations (spectral signatures or vegetation indices) using experimental data (Liang, 2007). Two broad classes can be distinguished:

- Mono-variate models mostly based on vegetation indices
- Multi-variate ("chemometric") methods using the spectral reflectance values as predictor variables

The empirical approach is schematically represented in **Figure 2**. The procedure has been divided in model and variable estimation.

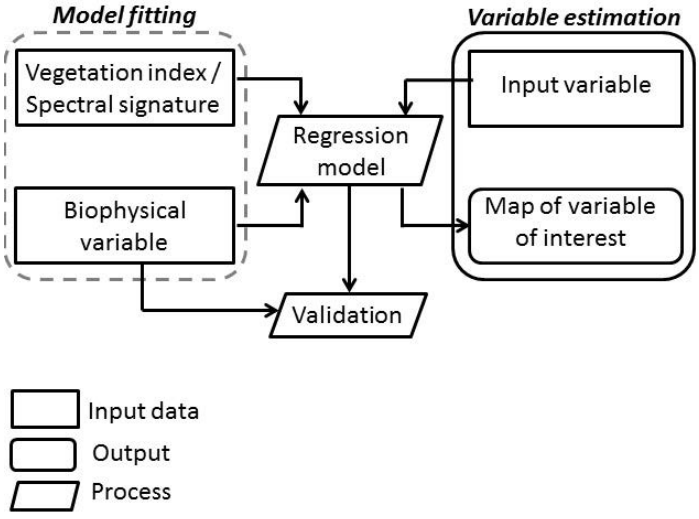

Figure 2. Empirical method to estimate biophysical variable (adapted from Verrelst et al., 2015b).

2.2.1. Mono-variate approaches

Spectral vegetation indices (VI) have been extensively used to map LAI, fAPAR, canopy and leaf chlorophyll content and many other biophysical variables (Dorigo et al., 2007). VIs have also been found useful for quantifying the effects of various stresses on crop growth (Wiegand et al., 1986).

One of the most widely used VI is the normalized difference vegetation index (NDVI) first proposed by Rouse (1973). Richardson et al. (1992) derived a logarithmic relationship to express the NDVI as a function of the LAI taking into account the non-linearity between NDVI and LAI. Non-

linear relations were also established by Yang et al. (2007), who fitted NDVI and LAI using an exponential model.

Numerous vegetation indices have been proposed for LAI retrieval and calibrated for different phenological stages and crops. Development of vegetation indices was mainly motivated by the wish to reduce apparent saturation effects observed for NDVI; for instance, SAVI (Huete, 1988), MSAVI (Qi et al., 1994), EVI (Huete, 1999), Green NDVI and Green-Blue NDVI indices (Wang et al, 2007) were developed in this spirit.

Of particular interest for LAI retrieval is the red edge inflection point (REIP), as this index is insensitive to soil brightness variations and does not saturate with increasing canopy chlorophyll content (Baret & Guyot, 1991). Analyzing experimental data, Filella and Penuelas (1994) for example observed a high correlation between plant chlorophyll content and wavelength of the red edge peak. Additionally, they found a close relation between LAI and the area of the red edge peak. Thenkabail et al. (2000a) used ground-level hyperspectral reflectance measurements of cotton, potato, soybeans, corn, and sunflower to determine the optimum spectral bands for mapping crop biophysical variables. The bands with optimum performance were localized in the red (650 nm to 700 nm), green (500 nm to 550 nm) and near-infrared (900 nm to 940 nm) part of the electromagnetic spectrum, together with a moisture sensitive band centered at 982 nm. Obviously, to estimate REIP, one needs hyperspectral sensors or satellites such as Sentinel-2 with dedicated bands in the red edge spectral region.

To evaluate the performance of VIs derived from multispectral satellite sensors, Das and Seshasai (2015) compared hyperspectral indices such as Red Edge Normalized Difference Vegetation Index (RENDVI), Plant Senescence Reflectance Index (PSRI) and Normalized-Difference-Infrared-Index (NDII) against simple difference index (SDI), simple ratio (SR) and NDVI derived from synthetic AWiFS, OCM-2 and MODIS data. The results showed a close correlation between the various types of indices. A relatively recent review about vegetation indices and canopy variables retrieval is presented in Glenn, et al. (2008).

2.2.2. Multi-variate approaches

Instead of using only a single variable (e.g. a VI) for predicting a crop's biophysical variable, it is also possible to establish multi-variate regression equations between the recorded spectral signature and the sought bio-physical variable(s). Such approaches have been used for a long time in laboratory spectroscopy for example for the analysis of food samples (Wold, S. & Sjostrom. M, 1977); hence the name "chemometric", "full spectrum" or "spectroscopic" method. Sometimes these techniques are also coined "machine learning techniques".

Within the remote sensing context, a number of studies demonstrated for example the high potential of partial least square regression (PLSR) for estimating LAI (Li, et al., 2014a). Other widely used modeling techniques include multiple linear regression (MLR), principal component regression (PCR), random forest regression (RFF), the use of support vector machines (SVM) and neural nets (NN) (Caicedo, et al. 2014; Xie, et al., 2014). Compared to mono-variate approaches, the multi-variate methods generally achieve higher accuracies (Atzberger et al., 2010a). Care has to be taken, however, not to overfit the data. A good overview of different empirical techniques is given in Verrelst et al., (2015b).

2.2.3. Drawbacks of empirical approaches

The main disadvantage of the empirical approach is the poor transferability of developed models to other conditions (Baret and Buis; 2008). Problems arise as the relationship between remote sensing

data and the crop biophysical variable depends on additional factors such as soil spectral properties, canopy architecture, development stage, leaf optical properties, illumination and viewing geometry (Baret and Buis; 2008). Therefore, the model developed in a specific context (site, environment and observation conditions) is often only suitable for similar conditions (Danson et al., 2003). For instance, Serrano et al. (2000) found that LAI was overestimated when using equations obtained under nitrogen deficient conditions.

The most important fundamental drawbacks of empirical approaches (and in particular of VIs) have been summarized below (Danson et al., 2003):

- lack of generality and transferability: new equations may be required when the crop type or measurement conditions change. This makes empirical models unsuitable for multi-temporal, multi-site, multi-crop or multi-sensor conditions;
- lack of consistency: the 'best' VI often varies with the measurement conditions;
- reliance on experimental data: field measurements are required to define the relationship with the biophysical property of interest; acquisition of reference information is costly and time demanding;
- little usage of prior knowledge: for example, the solar position and sensor viewing conditions may be calculated for any measurement but this readily available information is usually not used;
- under usage of spectral information; VIs use solely data in two or three spectral wavebands instead of making use of all available spectral channels.

2.3. Semi-empirical methods

Semi-empirical approaches are very similar to empirical approaches with the main difference that either i) the empirical database is replaced by synthetic data (e.g. le Maire al., 2008), or ii) the models' functional type is derived from physical knowledge such as Beer's law (Baret & Guyot, 1991).

2.3.1. Predictive equations

Instead of using experimental data to calibrate empirical models, le Maire et al. (2008) argued that the creation of a large (synthetic) database containing reflectance spectra and their corresponding canopy characteristics has several advantages:

- many canopy characteristics are represented as thousands of spectra can easily be simulated;
- the influence of each characteristic can be totally decoupled from that of others; and
- the effect of a particular crop characteristic on the spectra is based on physical knowledge (e.g. a radiative transfer model).

Therefore, spectral models developed from such large simulated databases may potentially be applied to a wide range of measurement conditions; this led to the label "predictive equations" (Haboudane, et al., 2004). Obviously, the approach relies on the capacity to correctly simulate the reflectance of a wide range of canopies (e.g. the correctness of the employed radiative transfer model). Additionally, the representativeness of the simulated database is also critical. As noted in Atzberger et al. (2015), the main drawback of the approach is that if often focuses on a few spectral bands (combined in a VI) therefore underusing available spectral information from most current (multi-spectral) sensors. The working principle of predictive equations is depicted in **Figure 3**.

2.3.2. Simplified canopy reflectance models based on Beer's law

The second semi-empirical approach focuses on using a physically-based functional form for the empirical model. An appropriate functional form is for example given by Beer's law (Baret & Guyot, 1991). It states that the relation between LAI and reflection is exponential:

$$\rho = \rho_{\infty} - (\rho_{\infty} + \rho_{soil}) \times exp(-k \times LAI) \quad (1)$$

The model implies that the canopy reflectance (ρ) equals the soil reflectance (ρ_{soil}) in case of LAI=0. For dense canopies (e.g. LAI approaching infinity), the canopy reflectance equals the infinite canopy reflectance (ρ_{∞}). The exponential factor k mimics the spectrally dependent absorption of leaves, respectively, the differences in leaf angle distribution (Baret & Guyot, 1991). As a consequence, the spectral reflectance either decreases or increases with increasing LAI, depending on whether the soil reflectance is higher or lower than the leaf reflectance. The "speed" of reflectance change depends on the absorption coefficient (k) which is for example high in the visible spectral region (chlorophyll absorption) and low in the near infrared. All other conditions being identical, k will be higher for planophile crops (e.g. soybeans) compared to erectophile crops (e.g. corn) as soil coverage decreases with increasing leaf angle.

The approach was used for instance by Baret & Guyot (1991) and by Liu et al., (2012) for estimating LAI using vegetation indices. Vuolo et al., (2013) applied a similar semi-empirical model to derive time-series of LAI maps using an exponential relationship between LAI and the Weighted Difference Vegetation Index (Clevers, 1989) and reported a good performance. The parameters estimated for one site (Austria) also achieved reasonably good results in a second study site (Italy) and *vice versa*. In Atzberger et al., (2015) a comparison of empirical and semi-empirical approaches for estimating LAI is presented. It was concluded that none of the approaches outperforms the other.

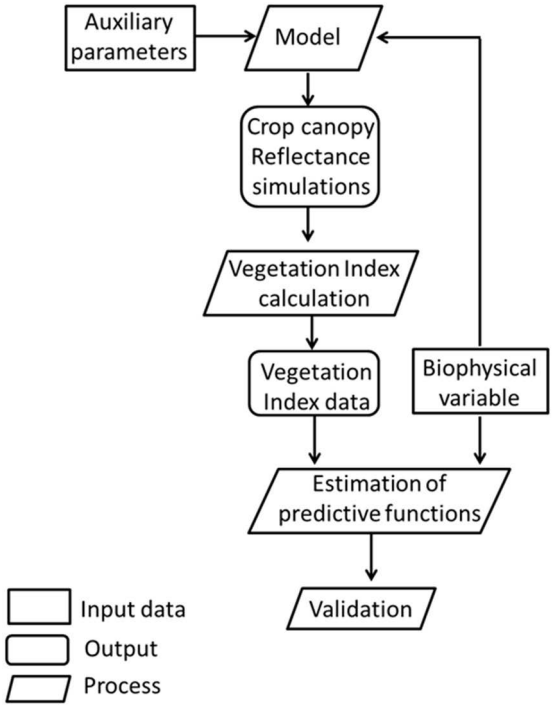

Figure 3. Semi-empirical "predictive equation" method to estimate biophysical variables.

2.4. Physical methods

Physical methods are based on the principles of radiation propagation within a canopy (Myneni and Ross, 1991; Goel, N.S, 1989). Radiative transfer models (RTM) describe – using physically-based

formulas – the relationship between canopy structure, leaf and soil optical properties and the resulting top-of-canopy bidirectional reflectance for a given illumination and observation geometry (Baret & Buis, 2008). Thanks to their foundation in physics, RTM offer the capability to be applied under different conditions (Dongwei et al, 2010).

Besides being useful for the estimation of vegetation bio-physical variables, RTMs also provide means to understand and model the light interception by plant canopies. This enables the interpretation of vegetation reflectance (but also transmittance and absorbance) in terms of biophysical characteristics. For that reason, RTM have been widely used to define and optimize spectral indices, to test possible sensor configurations and inversion strategies, among other applications (Jacquemoud et al., 2009).

Using RTMs, structural and biochemical variables are estimated in a process called "inversion of canopy RTM" (Jiang, et al, 2014b). A simple flowchart of the physical inversion approach is depicted in Figure 3.

2.4.1. General conditions affecting RTM performance.

The performance of the physical approach to retrieve biophysical variables depends on several factors, such as the quantity and quality of the available spectroradiometric information, the choice of the radiative transfer model and its suitability for a particular kind of vegetation canopy (model assumptions), the available *a priori* knowledge regarding important model parameters, and the choice of the inversion procedure (Weiss et al., 2000). In a recent paper, Verrelst et al. (2015a) have demonstrated the huge impact of the selected cost function on the retrieval accuracy, which moreover depends on the selected bio-physical variable. Other studies have pointed out the influence of an appropriate feature selection (Atzberger, 2010b; Darvishzadeh, et al., 2011; Atzberger et al., 2013b; Cernicharo, et al., 2013). A simple flow chart of RTM is presented in Figure 4.

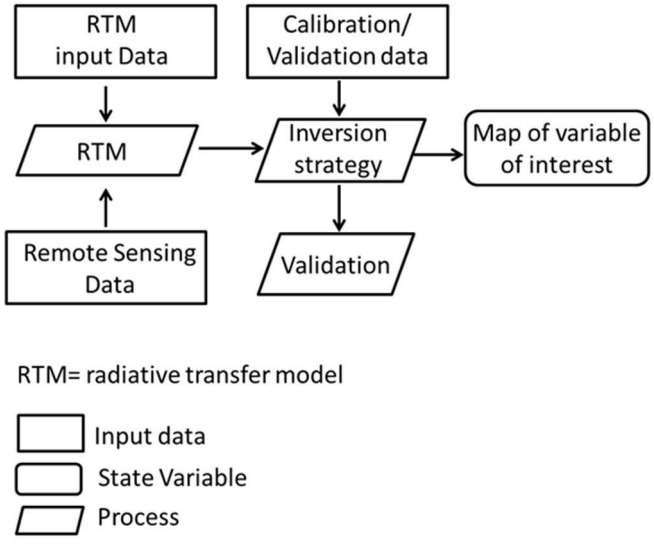

Figure 4. Physical approach to estimate biophysical variables (adapted from Verrelst et al., 2015b).

2.4.2. Examples of RTM's used in agricultural remote sensing.

The most widely used RTM is the PROSAIL model (Jacquemoud et al., 2009). PROSAIL combines the leaf optical properties model PROSPECT (Jacquemoud & Baret, 1990) and the canopy reflectance model SAILH (Verhoef,. 1984). This permits to simulate the top-of-canopy spectral (bi-directional) signature between 400 and 2500 nm as a function of structural variables such as LAI and leaf angle

(ALA) as well as soil brightness and leaf pigment and water content. An important constrain of SAILH models is the assumption of a horizontally continuous vegetation canopy, while many crops are planted as row structure. Yao et al (2008) found that at least two kinds of models should be adopted for corn canopy at different growth stages, i.e. row structure model for early growth stage (before plant elongation) and homogeneous canopy model for later growth stage (after plant elongation). Other widely used RTM are SCOPE (Van der Tol, et al., 2009), GeoSAIL (Huemmrich, et al., 2001), SLC (Verhoef & Bach, 2007) and 4SAIL (Verhoef, et al., 2007). Web-based tools have been published by Jochem Verrelst and his co-workers to make many of these models available to a wider audience (so called ARTMO website –http://ipl.uv.es/artmo/). The difficulties encountered to inter-compare competing RTMs is well documented – however with a focus on forests – in recent work of Widlowski and co-workers (e.g. Widlowski et al., 2013; Widlowski et al., 2015).

2.4.3. Model inversion algorithms.

The goal of inversion RTM algorithms is to minimize the mismatch between observed and simulated state variables. The most widespread algorithms are numerical optimization (Vohland, et al., 2010, Xiao, et al. 2009) and Look up Tables (LUT) (Dorigo et al, 2009; Locherer, et al., 2015; Hedley; et al., 2009). Genetic algorithms are sometimes employed to avoid being trapped in local minima (Fang, et. al., 2003; Mridha et al., 2014). Neural networks, on the other hand, model directly the state variables as a (non-linear) function of the spectral reflectances (Duveiller, et al. 2011; Verger, et al. 2011; Fang, et. al., 2014; Mridha et al., 2015)

Bayesian principle has been implemented in RTM inversion to incorporate information derived from multiple sources; the state variables are inferred from a posterior probability distribution. Mousivand, et al. (2015) verified the good performance of the Bayesian approach by retrieving LAI, fCover and leaf chlorophyll content using multi-temporal/ multi-sensor EO data. The accuracy was improved by using multisource data instead of using a single sensor. Other Bayesian techniques such as Bayesian networks have also been tested and yielded good results (Qu, et al. 2008; Zhang, et. al., 2012). Moreover, hybrid approaches have been implemented seeking to exploit the synergies between different inversion techniques (Liang, et al., 2015).

Variational approaches, implemented frequently in meteorology and hydrology, have been also tested in RTM inversion. The variational cost function is composed of two components; a background error related to model trajectory and an observational error which measures the similarity between observed and simulated state variable in a time window. Multiple constrains can be included in the variational cost function when some data is available, for instance, model parameter distributions, observation uncertainty or the temporal evolution of state variable(s). For instance, Lewis et al. (2012) tested a variational data assimilation system using *a priori* information, aiming to merge information from satellites with different sun-sensor geometries, wavebands and spatial scales. Observational, dynamic model and distribution state constrains were considered in the cost function. A reduction in state variable uncertainty was verified.

2.4.4. Model inversion and ill-posedness.

One of the main drawbacks of estimating biophysical variables by inverting a RTM is the equifinality - also called ill-posed problem - in which different sets of parameter values result in similar spectral signatures. The reasons for this problem are manifold (Combal et al., 2002a; Atzberger, 2004; Duchcheim, 2008; Baret and Buis, 2008; Jacquemoud et al., 2009):

- the limited information content in the radiometric signal compared to the high number of unknown variables and parameters which influence the canopy reflectance,
- the model-inherent simplification, and
- the reflectance measurements uncertainties.

Zurita-Milla et al (2015) presented an approach to visualize the ill-posed problem using self-organizing maps (SOM), which are a type of unsupervised neural network. The approach was performed using SLC-based simulations (Verhoef and Bach, 2007) of synthesized Sentinel-2 data (10 bands). Their results showed that leaf area index, canopy cover and leaf chlorophyll, water and brown pigment content are less confused in the inversion than the rest of variables.

Different types of error and bounding conditions affect the estimation of biophysical variables independently of the approach implemented; for instance:

- measurement errors such as calibration and atmospheric errors, cloud contamination, view-illumination geometry effects (Liu et al., 2014b);
- canopy architecture and leaf optical properties (Haboudane, 2004);
- model structure and parameterization errors (Liang, 2007);
- canopy density (e.g. effects related to and saturation of reflectance in dense canopies or soil brightness effects in low density canopies) (Curnel, et al. 2011);
- temporal and spatial measurement scale (Liu et al., 2014b).

2.4.5. Coping with the ill-posedness of the model inversion.

The most effective way to minimize the ill-posed problem is by reducing the number of free variables during the inversion procedure using prior knowledge such as ancillary data measured on site or provided by another sensor, information about canopy architecture and canopy biophysical variables distribution among others (Combal et al., 2003). For instance, Danson et al., (2003) reduced sugar beet LAI estimation uncertainty using site- and experiment-specific soil reflectance, canopy architecture (ALA) and solar position information to train an artificial neural network (ANN). Combal et al. (2002b) create a specific Look up table (LUT) based on vegetation type map, thereby reducing the range of model input parameters and consequently the ill-posed problem. Atzberger (2004) presented an object-based approach taking into account spatial information. The improved performance of the object-based approach, as compared to a standard inversion, was verified by Atzberger & Richter (2012) using synthetic Sentinel-2 data. Another approach to reduce ill-posed inverse problem was suggested by Lauvernet et al. (2008) who implemented a multi-temporal patch inversion technique to estimate simultaneously aerosol optical thickness and canopy characteristics such as LAI, chlorophyll concentration and leaf inclination angle. Again using multi-temporal data, Koetz et al. (2005) exploited the coupled use of structure dynamics and RTM to estimation bio-physical canopy characteristics. A good review of the ill-posed inverse problem and possible solutions are presented in Baret & Buis (2008).

2.4.6. Pros and cons of different inversion methods.

The main disadvantage of optimization algorithms is the computational demand. To speed up the inversion process, most research groups favor the use of look up tables (LUT). In this approach the spectral signatures are pre-computed for a large range of parameters combinations, being the database generation the most demanding computational step (Liang, 2007). The RTM inversion then consists in identifying the best fitting signature(s) and its corresponding parameters. As an alternative, other teams favor the use of neural nets or other models linking spectral signatures (inputs) to

corresponding biophysical parameters (outputs) (Fang, et. al., 2014; Fang, et. al., 2003; Zhang, et. al., 2012).

As demonstrated recently, the inversion process can be sped up by replacing the original RTM models by some "emulator models". Emulator are surrogate functions able to approximate full RTM retrievals with a certain degree of uncertainty (Verrelst, et al. 2015c; Gómez-Dans, et al. 2016). Rivera et al., 2015, for example, developed an "Emulator toolbox" which approximate a RTM with low demand of computational resources. The main attribute of Emulators are their computational efficiency and excellent accuracy and flexibility for extrapolating spectral profiles. For instances, Gómez-Dans et al. (2016) verified the excellent performance of a Gaussian Process emulator compared to the original (coupled) 6S-PROSAIL outputs.

A few comparisons between competing inversion techniques have been performed in recent years. For instance, Pragnère, et al. (1999) compared three model inversion techniques to estimate four main biophysical variables (LAI, Cab, fcover and fPAR). The iterative optimization approach showed a better performance compared to artificial neural networks (ANN) and look up tables (LUT). Estimation errors for fPAR and fcover were lower compared to LAI and Cab estimations. Vohland, et al. (2010) assessed the performance of numerical optimization, LUT and ANN to estimate LAI, canopy chlorophyll, water and dry matter contents. The numerical optimization provided the best results for the three biophysical variables, followed by LUT and ANN. Vuolo, et al (2010) compared the suitability of empirical and RTM approaches to estimate LAI, canopy chlorophyll content (CCC) and leaf chlorophyll content (LCC) using RapidEye data. Two vegetation indices and two inversion methods (LUT and NN) were used. The best performance was achieved using LUT. However, the NN method had a similar performance to LUT while being much faster. Mridha et al (2015) contrasted look-up table, genetic algorithm and artificial neural network to retrieve soybean leaf area index, leaf chlorophyll content, canopy chlorophyll content, and equivalent leaf water thickness using PROSAIL model. The genetic algorithm and LUT had a similar performance, while artificial neural network had a poor performance.

Gómez-Dans et al. (2016) tested three inversion approaches: Hamiltonian Markov Chain Monte Carlo (MCMC), variational data assimilation and particle filter to inverted LAI, leaf chlorophyll content and equivalent leaf water thickness from a time series of observations from Sentinel-2/MSI, Sentinel-3/SLSTR and Proba-V observations. They found that the variational and particle filter showed smaller uncertainties and better estimation performance than MCMC.

2.5. Overview of retrieval of vegetation bio-physical variables using EO data

Empirical models based on experimental data are a practical choice to retrieve bio-physical variables. However, the main disadvantage is its poor transferability to other conditions. This makes them unsuitable for multi-temporal, multi-site, multi-crop or multi-sensor conditions. Semi-empirical models, based on a few spectral bands combined in a VI, are more flexible but underuse available spectral information from most current (multi-spectral) sensors (Atzberger, et al., 2015).

Considering the requirement of high-quality and consistency of biophysical estimations as inputs in crop models, radiative transfer models are probably the most suitable approach to retrieve bio-physical variables. RTMs, unlike empirical models, are able to analyze EO data acquired with multiple configurations. However, they demand high computational resources due to their complexity and the inversion process to retrieve bio-physical variables is affected by ill-posed problem.

In recent years, numerous strategies have been developed to overcome these drawbacks. To minimize the ill-posed inverse problem have been implemented model inversion algorithms which

use *a priori* information from different sensors and/or spatial neighborhood. For instance, Lewis et al. (2012) proved the efficiency of Bayesian inference to combine multi-spectral data acquired by different sensors over time. Moreover, Atzberger & Richter (2012) found that spatial context of a given pixel provides useful information for constraining the inverse RTM process (Atzberger & Richter, 2012).
Regarding computational demand, emulators, which are able to approximate full RTM retrievals, have been proposed as a good alternative to run RTMs more efficiently. In particular, with regards to the operational mapping of vegetation bio-physical variables for regional and global applications, emulators seem very well suited (Rivera et al., 2015; Gómez-Dans et al, 2016).

3. Assimilating remotely retrieved biophysical variables in crop models.

3.1. Introduction

Crop growth models (CGMs) simulate the temporal evolution of state variables (for instance biomass, leaf area index or soil moisture) as a function of (Mansouri et al, 2014):

- external driving variables such as meteorological data;
- further input variables such as soil and crop characteristics;
- management practices.

The models thereby summarize and formalize current knowledge of the main processes determining crop yield, update model state variables in regular updating intervals (daily, weekly, monthly) and ensure a consistent evolution of crop development (phenology) and growth variables (Delécolle et al., 1992). Using CGMs it is for example possible:

- to analyze and interpret current crop status and forecast crop yields (Spitters, 1990);
- to simulate the effect of weather conditions such as El Niño/Southern Oscillation (ENSO) on crop production (Shin, et al., 2009; Ferreyra et al., 2001);
- to evaluate innovative management strategies in different productive situations thereby achieving a sustainable production system along the years (Faivre et al., 2004);
- to identify underperforming areas with the aim to determine and close yield gaps (Lobell, 2013).

Historically, crop growth models were implemented as a research tool within experimental frameworks (Spitters, 1990, Boote, et al. 1996). Since, they have been increasingly used at regional scale aiming to estimate crop state (e.g. dry mass and yield) over larger areas. The use of crop models at regional scale (e.g. as distributed models) is however hampered by their high input requirements, which are practically impossible to obtain over large areas with a sufficient degree of confidence. Obviously, inaccurate parameterizations and drivers introduce errors and uncertainties, which limit the predictive accuracy of crop models (Launay and Guérif, 2005). For example, inputs like hydraulic soil properties or management practices such as planting, irrigation, and fertilization are in most cases not available with enough accuracy, detail and confidence at regional scale. Consequently, default inputs or mean values are used for model parameterization, causing an underrepresentation of the natural heterogeneity of agricultural systems and adding uncertainties in the model outputs (Machwitz et al, 2014; Jiang, et. al. 2014a). Simpler crop growth models have fewer parameters - and therefore are in principle less data demanding - but often fall short to model all processes at the required level of detail (Murthy, 2003).

Earth Observation (EO) data offer several cost-efficient means to parameterize and constrain crop models. The mapping of crop variables provides the necessary link between remote sensing and crop growth models. The close link between EO and CGM results from the fact that crops are essentially light-harvesting entities (Jones & Vaughan, 2010). Indeed, EO data in the optical domain are related to the same biophysical variables that determine crop growth, such as fraction of absorbed photosynthetically active radiation (fAPAR) and Leaf Area Index (LAI) (Padilla et al. 2012). For the purpose of data assimilation at field scale, optical sensors such as Landsat-8 or Sentinel-2 generate freely available data with wide spatial coverage and high revisit frequency (Immitzer et al., 2016). The sensors deliver synoptic, objective and homogenous data that can be geographically and temporally registered (Tsiligirides, 1998). The potential of optical remote sensing for monitoring large scale vegetation dynamics, vegetation anomalies and crop growth is well documented (Rouse et al. 1974; Bala e Islam, 2009; De Wit, 2012; Li et. al, 2014), as is the use of EO data to characterize intra-field

variability, thereby becoming an information source in precision-farming applications (Thenkabail, 2000b).

Recognizing the close link between EO and CGM led to the early work of Maas and co-workers successfully combining remote sensing data and crop models to reduce the errors and uncertainties in crop growth simulations at regional scale (Maas, S.J., 1988; Maas, S.J. 1993; Delécolle et al., 1992). Combining remote sensing and crop modeling takes advantage of the synergy of the two techniques (Delécolle et al., 1992);

- the capability of remote sensing imagery to provide inexpensive data of the earth's surface at discrete temporal scale and high spatial resolution, and
- the capability of growth models to provide a continuous description of crop status (including phenology) during the growing season.

This chapter is divided in nine sections. In section 3.2 we describe various approaches to model crop growth. We thereby subjectively cluster crop growth models by degree of complexity, approximately proportional to the number of (unknown) parameters in the respective model. For completeness, we also cover approaches for biomass/yield estimation not making use of CGMs. In section 3.3 we briefly introduce the three main techniques to assimilate remotely retrieved bio-physical variables in crop models: forcing, calibration and updating. The topics are covered in more detail in sections 3.4, 3.5 and 3.6, respectively. We put special emphasis on the most widely used approaches such as re-parameterization approaches, Kalman filter and particle filters. Hybrid assimilation approaches are described in section 3.7. In section 3.8, we discuss the main aspects related to the assimilated EO data. Additionally, we present a list of assimilation techniques which we believe are not yet sufficiently exploited in the context of crop growth modeling. Finally, in section 3.9, we present an overview regarding crop growth modeling and monitoring combining CGMs and EO data.

3.2. Crop biomass and yield estimation

In the following, we distinguish three groups of EO-based modeling approaches for estimating crop biomass and yield, according to the excellent review of Delécolle (1992). The models are presented in the following sub-chapters according to their degree of complexity, starting from simple empirical models to complex crop growth models. A good review is also given in Rembold et al. (2013), which however mainly focused on the use of coarse resolution data. It has also to be noted that the techniques presented in §3.2.1 and §3.2.2 are independent means to estimate crop yields/biomass without using assimilation techniques and crop growth models *sensu stricto*. They are nevertheless presented to give the reader a more complete view of yield prediction techniques. Readers solely interested in data assimilation can therefore skip these parts.

3.2.1. Empirical models

Empirical yield models use spectral information such as vegetation indices or accumulated radiometric data as independent predictor variables to estimate biomass and yield (Delécolle, 1992; Guérif, et al 1985). In empirical models is assumed that conditions indicating increased or reduced crop's biomass production, can be captured through spectral measures (Becker-Reshef, et al. 2010). The models are "empirical" in the sense that the model calibration requires suitable reference data.

Different approaches have been proposed over the past four decades using a wide range of vegetation indices and mathematical functions either solely based on EO data or in combination with other (not remotely sensed) variables. Some examples of empirical models are presented in Table 2.

Table 2. Examples of empirical yield models directly estimating crop yield/biomass from remotely sensed variables

Approach	Crop	R^2	Reference
NDVI and monthly rainfall data	Wheat	0.98	Manjunath et al. (2002)
GYURI[1] index	Corn	0.75	Ferencz et al. (2004)
VCI[2] index	Wheat	0.86/0.92	Salazar et al. (2007)
NNSI[3] index	Wheat	0.815	Lin, et al. (2008)
VCI[2], TCI[4] and VHI[5]	Rice	0.61/0.62	Rahman et al. (2009)
NDVI, LAI and FAPAR	Potato	0.84	Bala and Islam (2009)
WDRVI[6]	Corn	0.86	Guindin-Garcia (2010)
WDRVI[6] and crop phenological stages	Corn	0.83	Sakamoto et al., (2013)

[1] General Yield Unified Reference Index, [2] Vegetation Condition Index, [3] Normalized Near-infrared Spectral Index, [4] Temperature Condition Index, [5] Vegetation Health Index, [6] Wide Dynamic Range Vegetation Index.

One of the main advantages of empirical models is their simplicity and the fact that most (statistical) software handles the required (regression) problem. However, some constrains should be considered:

- empirical models relate to specific crop cultivars, in a particular crop growth stage, and within a specific geographical area. As a result, transferability of empirical models to other crops and regions is often low (Ma et al, 2013a). In other words "established relationships are … to some degree, good fortune and rarely operational" (Baret et al., 1989);
- the predictive accuracy is directly related to the size of the reference dataset (Atzberger et al., 2015). To avoid extrapolations beyond the range of values found in the data base, the experimental set-up has to ensure that the dataset is well balanced, including the full range of biomass and yield. Often large time series are required to capture the entire range of growing conditions that can be experienced by a particular crop in a particular region (Padilla, 2012);
- empirical models implicitly assume a constant relationship between yield and biomass in both space and time. However, it is well known that the relationship between the two variables (e.g. the harvest index) might vary for instance by presence of high-yielding (irrigated) crops which do not have a linear relationship with biomass (Meroni et al., 2013).
- the relation between crop yield and spectral data is only indirect (Baret et al., 1989: Hayes & Decker, 1996) and remote sensing provides only little means to assess the harvest index (Meroni et al., 2013; Lobell et al., 2003).

To test model transferability, Lyle et al. (2013) analyzed the predictive capability of a simple NDVI-Yield model across three farms over a period of five years and under a range of different rainfall conditions. The study demonstrated good model performance in years with low and high rainfalls, but not in years with average (medium) rainfall. The research proved that for deriving robust regression functions, large time series and good references samples are needed to capture the variability present in the study area. Sakamoto et al., (2013) obtained an accurate estimation of corn yield at state-level in the United States of America using the WDRVI index. However, the model tended to underestimate corn yield in irrigated regions while overestimating yield in the outlying regions of the U.S. Corn Belt. Rudorff & Bastista (1990) observed that the relationship between vegetation index and corn yield depends on the data acquisition time with respect to the crop phenology. It was demonstrated that the best correlation between spectral data and crop yield was obtained at the booting stage. Afterwards, the correlation decreases caused by crop maturation and senescence. Many other studies quoted similar restrictions.

3.2.2. Semi-empirical models

EO data in the visible and near infrared part of the electromagnetic spectrum are closely related to the fraction of incident photosynthetically active radiation (PAR) absorbed by the canopy (fPAR) (Sellers, 1987). Monteith (1977) demonstrated that the total biomass production is directly proportional to the amount of PAR absorbed over the course of the growing season. The theory is also well supported by experimental data (Steinmetz, et al., 1990; Cannel, et al., 1988; Asrar, et al., 1985).

To mimic conversion of absorbed energy into biomass, Monteith developed the so-called Light Use Efficiency concept (LUE); the yield is derived from accumulated biomass using a classical harvest index (HI) (Eq. 2):

$$\text{Yield} = \sum_{t=1}^{n}(\text{PARt x fPARt}) \text{ x LUE x HI} \quad (2)$$

The summation in (Eq.2) is performed over the growing season, often using a daily time step. PAR (t) is the incident photosynthetically active radiation at time t (often from meteorological stations), and fPAR (t) is the fraction of PAR absorbed by the crop canopy at time t (estimated from EO observations). Some examples of semi-empirical yield models based on the LUE concept are presented in Table 3.

Under favorable conditions, LUE and HI can be relatively stable for a given crop, as assumed in Eq.2. However, in reality both LUE and HI may vary in space and time. This can be easily seen from the fact that different yields can be found for the same amount of aboveground biomass (Meroni et al., 2013). The main factors which cause variations in LUE and HI are:

- high temperatures;
- different management practices;
- insufficient water and nitrogen availability.

Obviously, such variation will violate the assumed uniformity in Eq.2 and will lead to differences between modeled and true yield/biomass. Another problem relates to the necessity to provide temporal profiles of fPAR using EO observations with sometime large data gaps (Nightingale, et al., 2009).

Table 3. Example studies using Monteith's semi-empirical LUE concept with remotely retrieved fPAR to estimate crop yield

Crop	R2	Error	Reference
Wheat		4 %	Lobell at al. (2003)
Maize	0.72		Liu et al. (2010)
Maize	0.89		Peng et al. (2011)
Wheat	0.80		Meroni et al. (2013)
Wheat		0.25-0.35t/ha	Patel (2006)
Maize and Cotton	0.82-0.98		Alganci et al. (2014)

3.2.3. Crop simulation models

Crop simulation models can be defined as a set of mathematical equations which simulate phenological development and physiological processes (light interception, carbon assimilation, respiration, evapotranspiration, dry matter partitioning and organogenesis) in response to environmental factors (soils, weather) and management (Bouman et al., 1996). Dry biomass, leaf area and storage biomass are important model state variables and model outputs. Depending on the

complexity of the CGM, other model state variables refer to the soil compartment (e.g. soil water content and nitrogen pool) or the plant's phenological stage.

The main strength of crop models are (Delécolle et al., 1992):

- the ability to model crop growth in a continuous way by updating the model state variables in a computational loop (usually daily);
- the capacity to model assimilate partition and crop organ development based on phenological routines;
- the flexibility to adjust the physiological and phenological mechanisms for different plant species using model parameters;
- the possibility to integrate soil properties (e.g. soil hydraulic properties), weather data (e.g. air temperature, precipitation, PAR) and management information (e.g. sowing date, fertilizer application and irrigation).

Crop growth models mainly vary in the way they integrate and formalize the above sub-compartments, as well as the time step in which the (computational) updating is performed. (Murthy, 2003). For the sake of simplicity and to optimize the discussion of various models, we grouped crop models in simple models (few processes and parameters) and complex models (more detailed modeling and parameterization).

3.2.3.1-Simple crop simulation models

GRAMI (Maas, 1992) is an example of simple crop growth model able to mimic essential physiological crop process while demanding only a reduced number of parameters and input/drivers variables. Only two drivers, air temperature and PAR, usually available for agricultural production areas, are required.

In GRAMI, the daily crop growth is simulated through four processes (1) calculation of growing degree days (GDD) for determining the actual phenological phase, (2) absorption of incident radiation energy by leaves according to actual leaf area, (3) production of new dry mass by the leaf canopy, and (4) partitioning of new dry mass for production of new leaves and/or grain filling according to the actual phenological phase (Ko et al, 2005). Leaf senescence is modeled using the concept of leaf lifespan (LLS). The model operates from the sowing date to the day of complete leaf senescence and considers three cardinal growth stages: emergency, anthesis and maturity. The leaf extension period lasts from emergency to anthesis and the grain filling period from anthesis to maturity.

A simplified flowchart of GRAMI model based on the description above is presented in Figure 5. In each model loop, state variables such as phenological stage, biomass and LAI are updated. The two drivers, air temperature and incident PAR, have to be provided for each modeled spatial entity (e.g. individual pixel or field) and time step.

The simplicity of this model is compensated by its capacity to easily use/assimilate remotely sensed data (in particular LAI observations) to adjust the values of certain model parameters (Maas, 1992). Moreover, the model is generic and does not need to be "developed" for the region to which it will be applied, nor to the specific crop studied (Padilla, 2012). Soil properties do not need to be specified as it is assumed that processes such as water stress can be amalgamated in crop specific parameters – resulting in changes of the modeled LAI profile.

Simple crop growth models such as GRAMI have been widely used due to their capability of integrating remote sensing data depicting - in high spatial resolution - the spatial-temporal variation of crop growth status as reflected in the LAI of the observed crops (Liu et al. 2010; Meng et al. 2013). A

number of example studies are listed in Table 4 which also includes studies conducted with a similarly simple CGM named SAFY (Claverie et al., 2012).

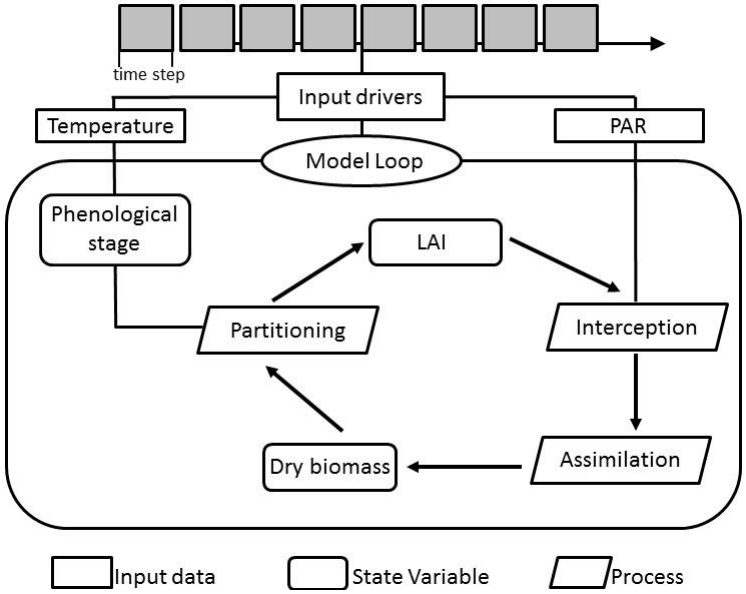

Figure 5. GRAMI model flowchart (adapted from Delécolle, 1992 and Ko et al, 2005).

Table 4. Examples studies using EO data and simple crop growth for yield modeling. Accuracy statistics are indicated and refer to the simulated yield

Model	Crop	R^2	Error %	Reference
GRAMI	Wheat	0.63/0.29		Atzberger el al. (2001)
GRAMI	Cotton	0.63/0.67		Ko et al (2005)
GRAMI	Wheat		6.7	Padilla et al. (2012)
GRAMI	Rice		8.1	Yeom et al. (2015)
SAFY	Wheat	0.48		Duchemin et al (2008)
SAFY	Maize/ Sunflower	0.97/-0.81		Claverie et al. (2012)
SAFY	Barley and wheat	0.45		Chahbi et al, (2014)

Three important drawbacks of simple CGMs have to be mentioned (Duchemin et al. 2008; Claverie et al. 2012):

- dry biomass is usually more accurately modeled than yield. To reduce the number of parameters necessary to model the (complex) grain filling process, it is often assumed that the yield can be calculated using a simple harvest index. This neglects the fact that the prevailing environmental conditions have a strong impact on this process;
- the effects of management factors such as fertilization are mostly neglected. This reduces the number of required parameters and input/driving variables but oversimplifies the modeled processes;
- often it is assumed that all parameters (e.g. LLS and biomass conversion factor) have a constant value during the crop cycle and are not impacted by phenological stage and/or environmental conditions.

Self-evidently, all the above mentioned issues can in principle be addressed by adding further controls. Alganci et al. (2014), for example, proposed some modifications in the LUE equation to

mimic the effect of water stress. However, this automatically leads to more complex CGMs having necessarily higher requirements in terms of parameters and input fields.

3.2.3.2 Complex crop simulation models

Complex crop growth models are composed of subroutines which are for example able to simulate the (combined) effects of nitrogen shortage and soil water shortfall on photosynthesis, as well as pathways of carbohydrate movement in plants, among many other processes (Hoogenboom, et al. 2000; Brisson et al., 2003). As a result of their complexity, such models are in principle suitable to assess the effects of management techniques and to simulate the impact/effects of different environmental scenarios (Faivre et al. 2004).

Some of the most widespread (complex) crop simulation models are SUCROS (Spitters et al. 1989), DSSAT (Jones et al. 2003), STICS (Brisson et al. 1998), CERES (Jones and Kiniry, 1986) and EPIC (Williams et al. 1989). A coupled HYDRUS (Šimůnek, J., 2005) - WOFOST (Diepen, et al., 1989) model is depicted in Figure 6 as an example of a complex crop simulation model. The coupled model is able to simulate the crop growth as well as the atmosphere-crop-soil water balance.

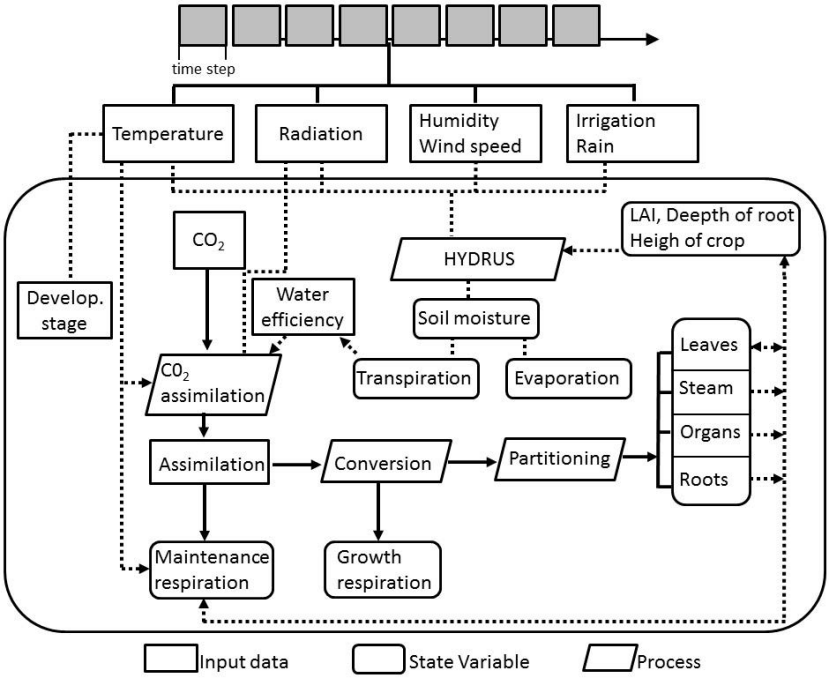

Figure 6. Flow chart of coupled HYDRUS and WOFOST model (adapted from Zhou, et al., 2012)

The complexity of crop models is directly related to the demand of input data in response to the increment of processes and state variables to be modeled. In general terms it can be stated that the number of required parameters increases with the complexity of a model. Detailed information can potentially be made available at local scale or at farm level. For large areas, however, the necessary data is generally not obtainable. As the accuracy of crop simulation models depends on the degree of uncertainties inherent in input data and parameters, the upscaling from a small support unit (a field) to a bigger one (region) is a challenge (Nearing, et al. 2012). Environmental drivers such as climatic variables (temperatures, precipitation and radiation) and model parameters such as soil properties are not always available at larger scales. Additionally, management data such as crop species (genetics parameters), sowing date and density, irrigation, fertilization and soil tillage information are discontinuously distributed in space and vary from year to year (Hoogenboom et al., 2000).

Operatively, this limitation might be reduced by using prior information or by fixing some parameters values. However, such strategies come at the expense of reducing the predictive model capacity (Wallach et al., 2002). A way to identify simplification strategies is to run tools such as PYGMALEO (Cournède et al. (2012). The platform permits implementing different steps along modelling process such as sensitivity analysis, uncertainty analysis, parameter estimation, model selection or data assimilation.

3.3. Main approaches for assimilating EO data in crop growth models

The aim of EO data assimilation is to combine knowledge incorporated in crop models with independently derived, multi-source (EO) information and thereby minimizing uncertainties in the estimation of a given system state (Zhu et al, 2013; Lahoz, et al, 2014). The feasibility to integrate different (direct and indirect) observational data with model simulations results in an increased consistency of the modeled processes in time and space, and across various bio-physical (state) variables (Guérif and Duke 1998).

Assimilation of remote sensing data in crop models permits an improved description of the simulated state variables through space and time. Obviously, the performance of data integration depends strongly on the assimilation protocol, the chosen model and the number, timing and uncertainty of the assimilated observations (Pellenq & Boulet, 2004). Assuming that remote sensing observations can reflect objectively the crop status variables linking CGM and EO, assimilation strategies represent a valuable tool to accurately simulate the impact of management as well as of phenomena such as meteorological disasters and pests, achieving more realistic outputs (Zhao et al, 2013).

The assimilation of remote sensing data in crop models can be realized using one or several model state variables which can be retrieved remotely. In most cases, however, the crop's leaf area index (LAI) is used as link. The LAI is the most natural variable to be assimilated in CGM as the LAI is directly related to crop growth factors such as water stress, nitrogen nutrition, or plant population density. Therefore, most assimilation strategies assume that factors which condition the crop production are reasonably well simulated within the model, when the estimated LAI is closely matching the observed LAI (Maas, 1988). For the very same reason, in the first part of our review (chapter 2), we specifically address EO-based mapping methods for LAI.

Remotely sensed observations can be integrated and assimilated in CGM using:

- forcing,
- calibration (re-initialization /re-parameterization), and
- updating

The three approaches are described in more detail in sections 3.4 to 3.6 based on the concepts introduced by Maas (1988), Delécolle et al. (1992), Plummer (2000) and Duchemin (2008).

In a nut-shell, forcing is a relatively simple assimilation strategy which consists in replacing simulated stated variables in the model using observed data (Figure 7a). After replacing the simulated value by its observed value, the model has a new starting point from which onwards the simulation continues. The forcing is repeated whenever new observations become available.

Calibration (re-initialization and re-parameterization) uses iterative numerical optimization techniques to ensure (in a least-square sense) that the remotely sensed observations available at the time of calibration are optimally "fitted" by the CGM simulations. To achieve a good "fit", values of uncertain – but important – model parameters and/or initial conditions of state variables are optimized by minimizing the difference between the state variable estimated by the model (mostly

LAI) and observed by remote sensing. After calibration, the model is re-executed to produce a new set of simulated values (Figure 7b).

Updating is based on the individual integration of new observations in the crop model taking into account model and observation errors (Figure 7c). Unlike calibration, the updating allows to model state variables directly, without requiring that all remote sensing observations are taken into account.

The three assimilation strategies are schematically portrayed in Figure 7. For simplicity, it is assumed that only one EO observation is available. Obviously, the use of multiple observations is recommended and common standard. In the following, the three approaches will be described in more detail.

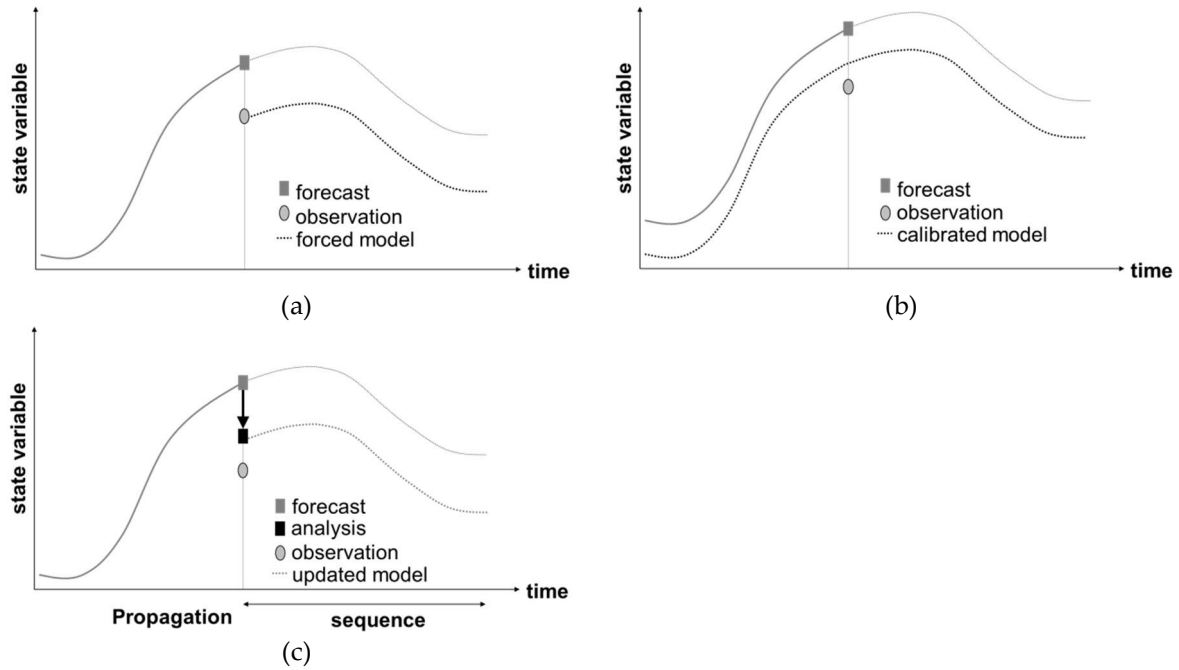

Figure 7. Assimilation strategies: a) forcing, b) calibration, c) updating (adapted from Pellenq & Boulet, 2004).

3.4. Forcing

The forcing approach consists in replacing simulated stated variables in the model using observed data whenever they become available. A list of studies using the forcing strategy is provided in Table 5. Clevers et al (2000), for example, estimated wheat yield by forcing LAI from SPOT data into the ROTASK crop growth model. Two forcing methods were implemented (1) a "reset method" in which the LAI was replaced by LAI-SPOT estimations when an image was available, and (2) a "continuous forcing method" in which an interpolated LAI-SPOT series replaced the LAI model estimations. The study could not demonstrate an improved grain yield simulation compared to the unconstrained ROTASK simulations, albeit both methods, and in particular the continuous forcing method, significantly reduced the RMSE between simulated and observed LAI. The authors attributed this finding to the fact, that the LAI estimates were well estimated at the beginning of the growing season, while for yield formation, the LAI values at the grain filling period are more important.

Chaudhari et al. (2010) compared a regression model and a reset-forcing approach to estimate wheat yield. The EO data was forced in WOFOST capturing the spatial yield variability. However, the regression model showed lower estimation error compared with the official statistics at district level.

Tripathy et al (2013) carried out a similar experiment using WOFOST model and SPOT data. A unique LAI observation was forced in the model near the peak vegetative stage using a correction factor. The simulated growth rate, weight of leaves, stem, storage organ and total above-ground biomass estimated by the model after the date of forcing were reduced and the resulting wheat yield estimation had an error less than 5% with respect to the reference data.

Being computational simple, a main drawback of the forcing strategy is that the model accuracy is strongly conditioned by the accuracy and number of remote sensing observations. Importantly, the intrinsic error level of the model is not reduced since all model parameters are kept at their original values. This also leads to internal inconsistencies between the various model state variables, as only the observed model state variable is modified as well as those state variables directly derived from it. Therefore, other assimilation strategies seem more suitable than the forcing method (Delécolle, 1992; Li et al., 2011).

Table 5. Example studies using the forcing approach for assimilating EO data in crop growth models

Crop model	Crop	Error %	RMSE	Reference
ROTASK	Wheat		0.97/0.81 t ha-1	Clevers et al. (2000)
WOFOST	Wheat	25.4-9.2		Chaudhari et al. (2010)
STICS	Wheat		2.4 t ha-1	Casa et al. (2012)
WOFOST	Wheat	5.0		Tripathy et al (2013)
MOSICAS	Sugarcane		12.2 t ha-1	Morel et al. (2014)

3.5. Calibration: re-initialization and re-parameterization

In the calibration approach, it is supposed that the CGM is formally correct but not well calibrated (Delecolle et al., 1992). Hence, one assumes that the modeling errors are only due to errors in the selected model parameters and initial states (Evensen, 2009). Using observed state variables as references, one or several model parameters and initial states can be optimized so that the newly calibrated model better "fits" the observations. The number of parameters that can be calibrated increases with the number of available observations and the number of (different) state variables observed (e.g. LAI and soil moisture). If successful, calibrating parameters and initial states will result in more reliable simulations of the entire system.

3.5.1. Sensitivity analysis

To identify the parameters and initial states that should be calibrated, it is recommended to first run a sensitive analysis (Cournède et al. 2012). In this way, it is possible to identify parameters with major impact on the observed state variable(s) (Wallach, et al. 2001; Wöhling, et al. 2004). A sensitivity analysis (SA) also provides useful information regarding the model structure and allows identifying parts of the model which could be further improved (Confalonieri et al. 2010). Examples of SA implemented in crop models can be consulted in Wöhling, et al. (2004), Confalonieri et al. (2010) and Richter, et al. (2010).

Considering the sensitivity analysis and calibration of CGMs, Tremblay and Wallach (2004) classified CGM parameters in three groups:

- parameters which could potentially be extracted from experiments;
- parameters which are preferentially be calibrated as a result of their strong influence on the model simulations;
- parameters which should be fixed because of their low impact on the model simulations.

The focus of any calibration should be on those (hopefully) few parameters having the strongest impact on the CGM simulations. Note that in this context, model sensitivity refers to those state variables which are potentially available for assimilation. For example, a model parameter could have a strong impact on the final yield, but without (strongly) influencing the (observed) LAI. Hence, using LAI observations for assimilation would in this case not be successful in retrieving a correct value of that parameter.

To calibrate the best parameter combination, several algorithms have been developed and used. The various approaches are summarized in Table 6. A probably stronger impact on the final modeling accuracy can be expected from the following factors, which are below further discussed:

- EO data availability (e.g. number and timing)
- Errors in the remotely-retrieved state variables
- Erroneous parameterization of fixed parameters
- Number of (free) parameters to be calibrated
- Ill-posedness of the calibration problem

Table 6. Examples of calibration techniques

Technique	Abbreviation	Reference
Shuffled Complex Evolution	SCE	Huang et al (2015a; Ren et al. (2009) ; Ma et al. (2013b); Duan et al, (1992)
Fortran program for calibration and uncertainty analysis of simulation models	FSEOPT	Ma et al. (2013a); (Stol et al. (1992)
Shuffled Complex Evolution POWELL	SCE_AU vs POWELL	Tian et al. (2013)
Particle swarm optimization	PSO	Wang et al. (2014); Li et al. (2015; Kennedy and Eberhart, (1995)
Levenberg–Marquardt	LM	Chandran et al. (2005)
Genetic algorithm	GA	Soundharajan and Sudheer (2013)
Markov Chain Monte Carlo	MCMC	Dzotsi et al. (2015)
Error minimization	EM	Trombetta, et al. (2016)

3.5.2. Remote sensing data availability

Generally, the calibration improves with more EO observations being available, in particular if those observations are well distributed along the crop cycle. In gramineous crops, gaps at the beginning of heading stage and/or at the end of stems elongation have a critical impact on parameter calibration (Fang et al. 2008; Dente 2008). Nevertheless, compared to empirical approaches for yield prediction (§3.2.1), the exact timing of EO acquisitions is less important.

3.5.3. Errors in the EO-retrieved state variables

Obviously, the better the quality of the remotely retrieved state variables, the more efficient is the model calibration approach. To avoid cumulating errors along the processing chain, it is also possible to couple a CGM with an appropriate canopy reflectance model, thereby omitting the need for RTM inversion and estimation of crop state variables such as LAI. For instance, Guérif and Duke (1998) calibrated SUCROS parameters using reflectance data in a coupled SUCROS-SAIL model, thereby avoiding the error-prone LAI estimation. To further minimize the negative impact of soil reflectance

on canopy reflectance in large scale applications of SUCROS, Guérif and Duke (2000) later converted the spectral reflectance into TSAVI vegetation index. Similar approaches were implemented by Moulin et al. (1995), Launay and Guerif (2005), Doraiswamy et al (2003) and Atzberger (1997).

3.5.4. Effect of fixed parameters and number of parameters to be calibrated

When a calibration is performed, usually a group of parameters are optimized while the rest remain at their default values. This can potentially lead to unrealistic values of the calibrated parameters since the calibration tries to compensate for any possible error within the group of fixed parameters. Of course, calibrating all model parameters is practically impossible. Any over-parameterization has even the potential of strongly reducing the prediction quality of the model (Tremblay and Wallach, 2004). Therefore, the recommended strategy is to calibrate relatively few parameters and to constrain their allowed parameters ranges avoiding excessively large intervals (Curnel, et al. 2011).

3.5.5. Compensation between parameters and ill-posedness of the calibration

The calibration of CGMs is often ill-posed. This holds especially for complex CGMs with many parameters. For instance, similar LAI time profiles can be simulated using quite different parameter combinations which may strongly affect other state variables in dissimilar ways. As a result, errors in retrieved state variables such as dry mass and yield can strongly increase (Duchcheim, 2008).

Other factors have also a strong influence on the calibration performance under ill-posed conditions such as (1) the complexity of the model, (2) the criterion used to calculate the calibration error, (3) the algorithm used to fit the optimum parameters values (Table 6), and (4) the criteria used to compare different algorithms (Wallach, et al. 2001).

It is important to highlight that re-initialization and re-parameterization techniques have some constrains such as the omission of uncertainties in input, output and model structure. Using these relatively simple techniques it is also not possible to add information from new observations without re-running the entire calibration procedure again. Since one assumes that the parameters are time-invariant, a lack of flexibility has been observed (Moradkhani et al, 2005).

3.6. Updating

Crop growth models contain errors due to a simplified representation of complex natural processes as well as uncertainty in input parameters. In a similar way, remotely derived information is negatively affected by factors such as atmospheric distortions, geo-location errors and pixel mixing, among others (chapter 2). Updating is a technique in which both sources of error, from remote sensing and the crop growth model, are considering during the assimilation process to provide optimum estimations (Vazifedoust et. al. 2009).

Important advantages of the updating strategy are:

- it can be used without altering model structure;
- state variables are periodically updated within the growing season using EO observations;
- two or more model state variables or a combination of parameters and state variables can be assimilated (e.g. the assimilation of LAI and surface temperature) (Montzka et al. 2012)
- model and observational errors are taken into account.

In the context of EO, the CGM provides the forecasted state variable while remote sensing observations serve as external forcing (Ines et al. 2013; Dongwei et al. 2008). The (multi-variate) observations are sequentially updated during the assimilation procedure.

Updating techniques have been developed and widely used in weather and earth system models. Table 1 lists use cases of updating outside the agricultural application covered in the present review. Ruiz et al. (2013), for example, present a valuable review of ensemble technique applied in weather forecast. A sketch of the updating process is shown in Figure 7c. A review of methods for approximating filter distributions is presented in Künsch (2013). The historical evolution of filters described in the following sub-chapters is depicted in Figure 8.

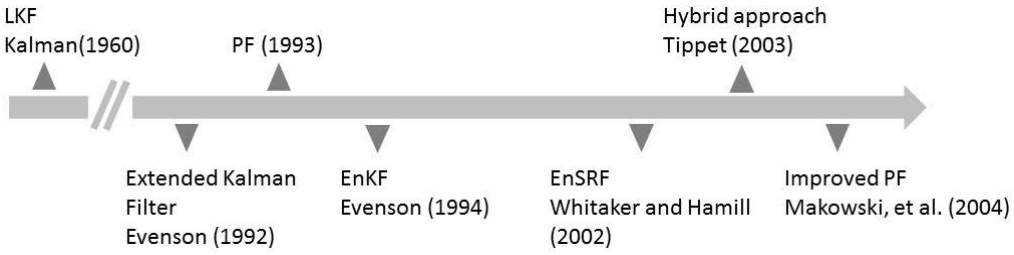

Figure 8. Chronology of some filters.

3.6.1. Linear Kalman filter (LKf)

Most techniques to update model state variables by measured data are based on the Linear Kalman filter (LKf) (Kalman, 1960). This filter is a sequential data assimilation method initially used in control engineering and space/aircraft navigation. The algorithm is able to integrate and control the model forward in time. Whenever measurements are available, the state variable is updated before the integration continues. The algorithm is based on Bayes theorem and calculates the state of a system based on linear equations for the time evolution of the system and noisy measurements of quantities related to the state variables. The error distribution is assumed as Gaussian. The result of data updating, where observational and model information and their errors are combined, is termed "analysis." The filter algorithm can be summarized as follows (Evensen, 2003) (Eq. 3):

$$A_a = A + P_e H^T (H P_e H^T + R_e)^{-1} (D - HA) \quad (3)$$

where A and A_a are the model forecast and analysis (updating) state, D the measurement, H is the measurement operator, P_e, P_a, and R_e are the forecast, analysis and measurement covariance respectively.

In Eq 3 three main components can be identified; A which is the state value at time t-1, the component PeHT (HPeHT + Re)-1 called Kalman gain (K) which provides information about the measurements and (D-HA) which represents the innovation vector. The larger Re (measurement covariance) the lower K, consequently, the impact of the measurement D in the Aa calculation is smaller. No assimilation will be performed when K value is 0. In contrast a K value equal 1 implies that EO observation will be directly assimilated. In this way, model and measurements are validated during the sequential updating (Eskes, et al, 1998).

The Linear Kalman filter equation using a simple example is sketched in Figure 9. The measurement operator H is not implemented because the simulated LAI is updated using estimated LAI values, without transformation. This simplified equation is:

$$A_a = A + (P_e / (P_e + R_e)) (D - A) \quad (4)$$

In Figure 9 is indicated the innovation component (D-A); the weight of the innovation is calculated as ratio between model uncertainty (P_e) and total uncertainty ($P_e + R_e$).

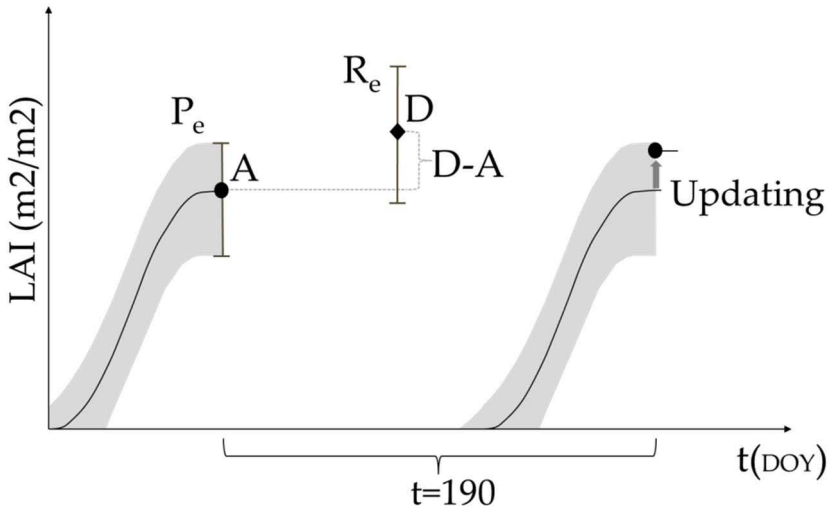

Figure 9. Schematic illustration of LAI updating in a CGM.

3.6.2. Extended Kalman filter (EKF)

The prerequisite of linearity assumed in the LKf is violated in non-linear systems. In the case of a highly non-linearity, the filter diverges from optimality and may become unstable (Evensen, 1994). The linearity restriction and the high computational cost to run the LKf algorithm impede its implementation in real systems (Tippett, et al. 2003). This first drawback has been overcome by developing a family of filters based on the principle of LKf but which are able to use non-linear systems in the state prediction.

To overcome some restrictions of the original Liner Kalman filter, a tangent linear operator is added in the error covariance equation to linearize the error prediction equation (Evensen, 2003). This approach assumes that the corrections are sufficiently small so that the model can be locally linearized (Aubert, et al. 2003). However, when the system is strongly non-linear, and the linear approximation no longer holds, a statistical approach known as the Ensemble Kalman Filter is preferred (Pellenq & Boulet, 2004).

3.6.3. Ensemble Kalman filter (EnKF)

The EnKF was proposed by Evensen in 1994 and is based on the generation of Monte Carlo ensembles. The main difference between EKF and EnKF is the approach to calculate the error covariance. The EKF uses a linearized equation to propagate the error covariance while the EnKF propagates a finite ensemble of model trajectories. The ensemble forecasted members are individual model realizations generated by mutually independent and temporally uncorrelated perturbations (Crow, W. T and Van Loon, E. 2006). Burgers et al. (1998) suggested an improvement of EnKF adding random perturbations to the observations in order to generate an ensemble of observations which will be used in updating the ensemble of model states avoiding filter divergence. Reichle et al. (2002a) compared both approaches while assimilating soil moisture data in a hydrologic model and found that the EnKF achieved a better accuracy than EKF. In particular, a more robust performance of the EnKF was demonstrated, while offering more flexibility in covariance modeling.

The updating procedure of EnKF is presented in Figure 10. The state variable ensemble is forecasted by the model from t_{k-1} to t_k. At time step t_k each particle is updated based on Eq 3 and the ensemble observations. The mean of the updated ensemble represents the updated sate variable at

time K_t (bold arrow). This value is forcing the crop model which is running independently of the updating process. Then, the updated particles are forecasted to t_{k+1}.

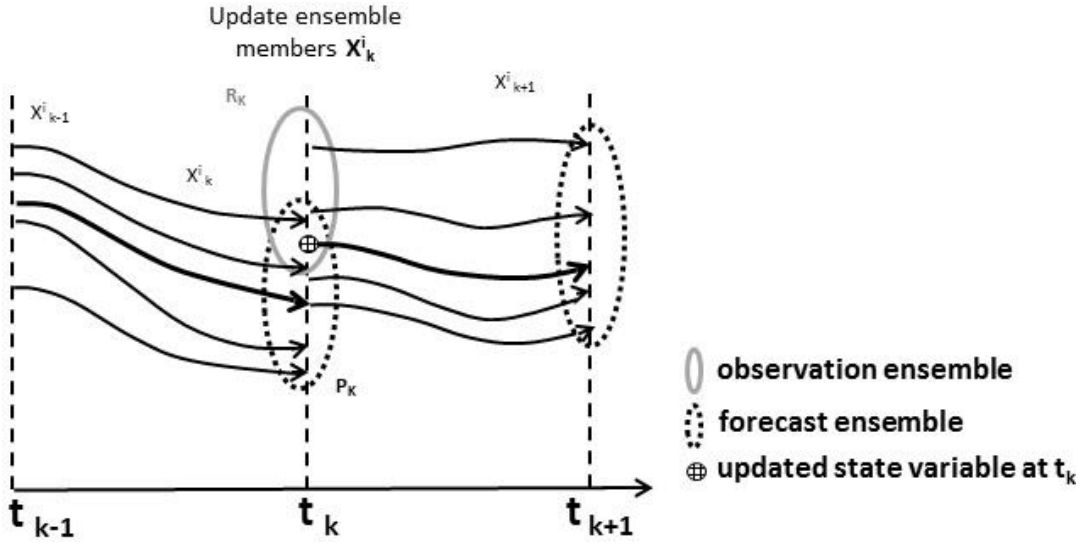

Figure 10. Illustration of updating steps in Ensemble Kalman Filter (EnKF); X^i_k (state vector), P_k (state error covariance), R_k (observation error covariance) (adapted from Reichle et al., 2002a).

The procedure to assimilate LAI in a crop model is further depicted in Figure 11. In a first step, the EnKF generates an ensemble of state variables for time (t). A white Gaussian noise from Monte Carlo simulations is added to the state variables. If an observation for time (t) is available, a Gaussian perturbation-ensemble with mean equal to zero and covariance equal to the observational error covariance matrix is added to the observation in order to create the observation ensemble. In a third step, the state ensemble and the observation ensemble are assimilated based on the linear equations used in the LKf (Eq. 3). The mean is the best estimation of the state variable. The ensemble dispersion is the best estimation of the error variance. This process is repeated until all the observations are assimilated (Ma et. al., 2013a).

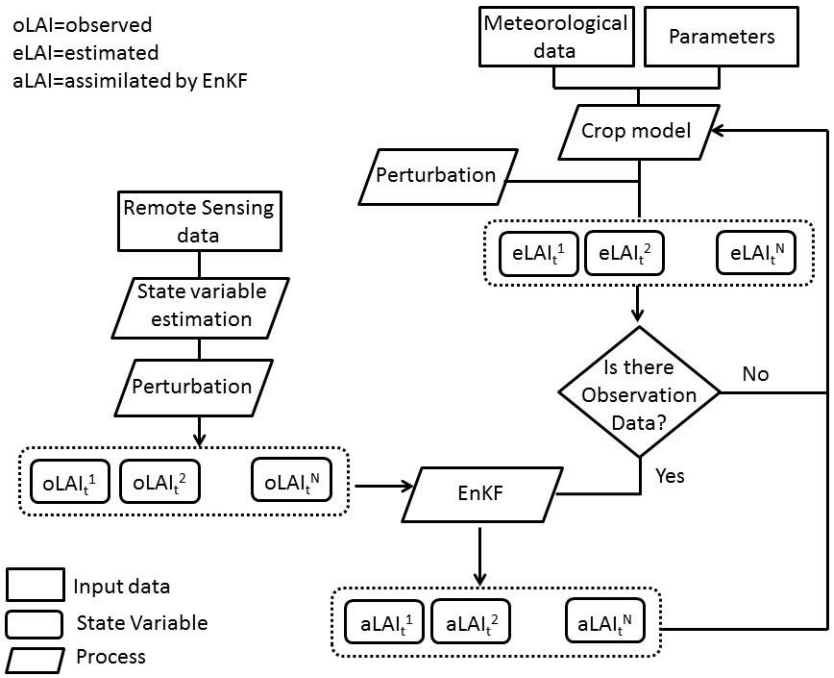

Figure 11. Assimilation of LAI in a crop model using EnKF (adapted from Ma et. al., 2013a).

A consistent EnKF has to fulfill the assumptions stated in the Lineal Kalman filter (LKF) (Kalman, 1960). This includes a forecast error with Gaussian distribution as well as temporally and spatially uncorrelated innovations. These assumptions can be evaluated by looking at the distribution of the normalized innovations. An excessive spread in the distribution of normalized innovations indicates that the sum of the variances on observations and forecasts is under-estimated (De Wit and van Diepen, 2007).

Within the EO community, the Ensemble Kalman filter has been extensively used to update crop growth state variables (or a combination of parameters and state variables) using EO observations. Some examples are presented in Table 7.

Table 7. Example studies using the Ensemble Kalman filter (EnKF)

CGM	Assimilated state variable(s)	Crop(s)	Reference
WOFOST	Soil water	Wheat and Maize	De Wit and van Diepen (2007)
SWAP	LAI+ Evapotranspiration	Wheat	Vazifedoust et. al (2009)
CERES+PROSAIL	LAI	Wheat	Li, et al. (2011)
DSSAT	LAI+Soil moisture	Maize	Ines et al. (2013)
WOFOST+ACRM	LAI	Wheat	Ma et al. (2013a)
PyWOFOST	LAI	Maize	Zhao et al (2013)
WOFOST+ACRM[1]	LAI+Phenology	Maize+Wheat	Zhu et al. (2013)
WOFOST+HYDRUS-1D	LAI	Maize	Li, et al. (2014b)
Dynamic model+ACRM[2]	LAI	Grassland/Forest	Liu et al. (2014a)

[1] multi-resolution data, [2] multisource data

3.6.4. Ensemble square root filter (EnSRF)

Although the most widespread updating technique is the Ensemble Kalman filter, other filters have been developed aiming to overcome some drawbacks. The use of perturbed observations to create an observation ensemble in EnKF increases the probability to under-estimate the analysis-error covariance. To solve this problem (Whitaker and Hamill, 2002) developed the ensemble square root filter (EnSRF). The EnSRF is a deterministic algorithm, which does not use perturbed observations. Instead, two Kalman gains are used; one to update the ensemble mean and a second to update the deviations from the ensemble mean. The latter gain only depends on the observation and background error variance.

An improved performance of EnSRF with respect to EnKF was verified by Huang, et.al (2013). They compared both filters integrating remotely sensed information (ASD spectral, HJ-1 A/B CCD and Landsat-5 TM data) in the WheatGrow model. A good performance of EnSRF filter was also found by Wang, et al. (2014). They applied a coupling method based on a parameterization of the RiceGrow model at regional scale using the Particle Swarm Optimization (PSO) algorithm and EnSRF to update leaf area index (LAI) and leaf nitrogen accumulation (LN).

Another aspect to consider about the EnKF is the assumption that the posterior density of the ensemble at every time step is Gaussian, parameterized by mean and covariance. This assumption hampers the application of the filter in non-linear and non-Gaussian dynamic system (Arulampalam, et al. 2002; Jiang et al, 2014c). Considering that crop models such as EPIC, WOFOST, and STICS

among others, describe the biophysical processes as a non-linear approximation of the state variables, a filter able to manage nonlinear and non-Gaussian effects seems more suitable (Mansouri et al. 2015).

3.6.5. Particle Filter (PF)

Particle Filters are based on Monte Carlo simulations to estimate state variables using a set of random drawn samples and their weights. PF methods approximate the posteriori probability ensemble distribution by a set of weighted samples, called particles. No matrix operations are necessary and no pre-assumptions with respect to the model characteristics (e.g. linear or nonlinear) as well as the noise probability distribution (Gaussian or non-Gaussian). Therefore, particle filters are able to handle any form of the probability distribution (Han and Li, 2008). For that reason the PF algorithm appears to be a better choice for crop-growth models which operate in nonlinear and non-Gaussian systems (Arulampalam, et al. 2002; Lahoz, et al, 2014).

A drawback of PF is the filtering divergence produced after several iterations in which very few particles have significant weights. Consequently, the filter efficiency is reduced demanding computational resources to update particles with low importance (Han and Li, 2008; Makowski et al 2004). A possible approach to reduce this effect is to increase the number of particles or to use a resampling technique. A widespread resampling techniques called Sequential Importance Resampling (SIR; Arulampalam, 2000) consists of sampling the particles with replacement n times, being n the ensemble size. In this process, particles with high weight have the chance to be selected more than one time while particles with low weight are more likely to be dismissed (Han and Li, 2008). The main drawbacks of resampling are the loss of diversity and the difficulties to parallelize the data processing because the particles are combined along the updating process (Arulampalam et al., 2002). A possible solution is introducing Markov Chain Monte Carlo (MCMC) steps on each particle cancelling the resampling drawback and keeping the ensembles independent after resampling step (Montzka et al., 2012). A discussion about filter divergence and resampling among other related topics are described in detail by Van Leeuwen (2009).

Although, EnKF and PF are both Bayesian filters, some important differences are highlighted in Table 8 according to Evensen (2009) and Han and Li (2008).

Table 8. Comparison Ensemble Kalman Filter (EnKF) and Particle Filter (PF).

Item	EnKF	PF
Model type	Linear model	Linear or non-linear
Error distribution	Gaussian error distribution	No assumptions
Resampling	Not required	Advisable to reduce filter divergence
Computational costs	High	Low

The main steps of the PF when an observation is assimilated are depicted in Figure 12. At T=0 the particles are forecasted using the crop model (no observations available). At T=10, an observation becomes available. The observation distribution is calculated considering the observed value and its error. The center of the distribution is assessed using the observation value and a random error which is calculated as the product between the observation error and a random number generated by a normally distributed random number function. The error of each particle with respect to the center of the observation distribution (mean) is calculated. The deviations are expressed as z values (e.g. standard scores). Then, the error is normalized representing the weight of each particle. The updated state variable at T=10 is calculated based on the state value of each particle and its weight. In the two

last steps the particles are resampled to reduce the filter divergence effect and a perturbing process is applied to keep the diversity. Finally, the particles are forecasted to T=20 where the process is repeated.

The performance of PF has been extensively tested and partially improved. For instance, Makowski, et al. (2004) proposed the Improved Particle Filter (IPF), derived from PF, which uses the Kullback–Leibler distance to overcome the filtering divergence. Machwitz, et al. (2014) tested a similar approach but using APSIM+PROSAIL model. Chen and Cournède (2014) applied the Convolution Particle Filtering (CPF) method to update state and parameter of STICS and LNAS models. The filter showed promising predictive capacity for different test configurations (different years, experimental sites, cultivars, crop densities, levels of water stresses). Mansouri, et al. (2015) compared the performance of PF and IPF for predicting and modeling winter wheat biomass and grain protein content. Several experiments were conducted aiming assessing the effects of measurement noise, number of states and parameters updated in estimation accuracy. The simulation showed a better performance of IPF respect to PF.

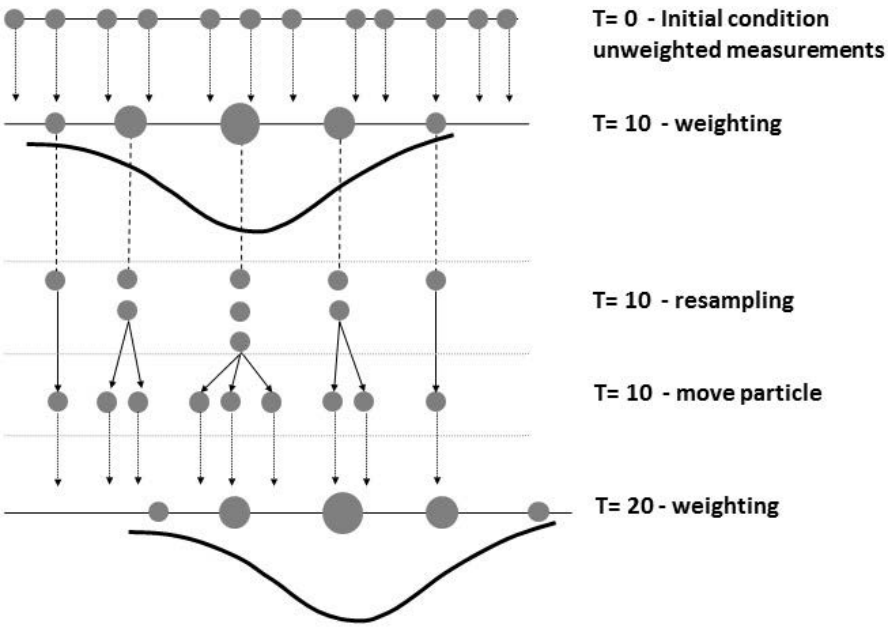

Figure 12. Schematic illustration of the updating steps in PF (adapted from Montzka et al., 2012).

3.6.6. Versatility of updating techniques

Updating technique mostly assume that the parameters are known *a priori* and uncertainties come from the state variables and corresponding observations. However, using updating approaches it is also possible to estimate model parameters that vary with time. These parameters are simply considered as state variables during the updating process. The inclusion of parameters in the state vector generally can cause linear systems to become nonlinear. Additionally, considering an excessive number of unknown model states and parameters render the estimation unstable (Pellenq & Boulet, 2004; Trudinger, et. al. 2008). Moradkhani et al (2005) presented a dual state–parameter estimation approach based on the EnKF for sequential estimation of parameters and state variables of a hydrological model. The approach had a reliable and effective performance to forecast streamflow.

3.6.7. Important aspects for implementing ensemble updating filters

Aspects of ensemble-based Kalman filtering such as ensemble size, filter divergence, treatment of non-Gaussianity and nonlinearity among other related topics have been addressed by Ehrendorfer (2007). The most important aspects will be summarized below in more detail.

3.6.7.1. Ensemble size

The ensemble size defines the space from which the update is computed at each time step of the analysis. The ensemble size choice requires a compromise between the computational costs and the accuracy of the covariance matrices (Trudinger, et al. 2008). An inappropriate ensemble size (e.g. a too small ensemble) can degrade the forecast error covariance representation, causing a filter divergence (Evensen, 1994; Evensen, 2009; Tippet, et al, 2003). For that reason, a preliminary study is usually recommended to find the minimum ensemble size, which assures an optimal performance of the updating data (Pellenq & Boulet, 2004). Such a preliminary study allows also adding some restrictions in the random perturbations process to ensure the values of the state variables to fall within their reasonable physical intervals (Han and Li, 2008).

3.6.7.2. Time step

The assimilation step size is another factor which affects the stability of the assimilated profile. Liu et al (2014a) assessed the effect of assimilation period testing different updating intervals (2, 4, 8 and 16 days). It was shown that the larger the assimilation step sizes, the greater the fluctuation of the assimilated profile. In their study, an interval of 4 days was considered appropriate. The updating interval of EO data depends on technical satellite characteristics (e.g. revisit time) and atmospheric conditions (e.g. cloudiness). A reduction of the assimilation step size is possible by assimilating multisource EO data.

3.6.7.3. Normality of the residuals

A potential downside for the EnKF is the presence of skew in ensemble model forecasts, which could (negatively) affect the optimal updating of ensembles via the Kalman filter approach (Crow, W. T. 2003). To avoid a systematic bias, it is recommended to test the degree of non-linearity of the function used to forecast the state variable.

3.7. Hybrid approaches

In recent years, hybrid techniques have been implemented, combining variational and sequential approaches (Dong et al. 2013; Jiang, et al. 2014a). Prominent examples are the Four Dimensional Variational Data Assimilation (4DVAR), a variational algorithm extensively used in meteorology, and POD4VAR which combines 4DVAR algorithm and EnKF.

The 4DVAR (Le Dimet and Talagrand, 1986) is a variational algorithm which calculates the model state analysis value by minimizing a cost function J (Eq. 5). The function is compound by a first term, Jb, which quantifies the misfit of the state variable (x_o) and the background state (x_b) and a second term, Jo, which quantifies the misfit between the model trajectory $H(x(k))$ and the observation $y(k)$ in the assimilation windows from K=1,2…, S (Lahoz, et al. 2014; Jiang, et al. 2014a). The algorithm searches for an optimal set of free parameters that minimizes the discrepancies between the simulated and observed state variable. The minimization process within the 4DVAR algorithm requires an estimation of the cost function which can be provided by adjoint modelling (Dong et al., 2013).

$$J(x) = J_b + J_o \quad (5a)$$

$$J(x) = (x_o - x_b)^T B^{-1} (x_o - x_b) + \sum_{K=1}^{S} (y_{(k)} - H(x_{(k)}))^T R_{(k)}^{-1} (y_{(k)} - H(x_{(k)})) \quad (5b)$$

$\mathbf{x_o}$ initial condition at the beginning of the assimilation window

$\mathbf{x_b}$ background value

B background error covariance matrix

R observation error covariance matrix

H is the nonlinear observational model

K observational time

The errors in the model (background) B and observational information are uncorrelated.

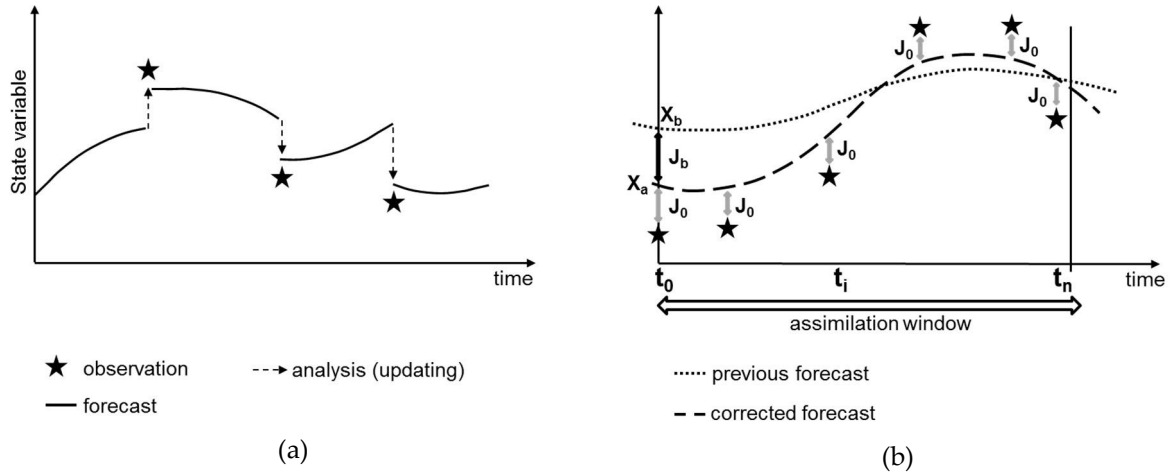

Figure 13. Schematic illustration of (a) sequential and (b) variational assimilation (adapted from Lahoz, et al. 2014).

The sequential updating of observations through time is depicted in Figure 13 (a), whereas (b) shows the variational assimilation in a temporal window. Variational procedures start by choosing a time interval [t_0, t_n]. Initially, a first-guess model trajectory is computed by running the model in the time window selected. The mismatches between the model and the available measurements in the interval are recorded. Then, a second model which translates the mismatches backwards in time is implemented (the "adjoint" model). The error at time t_0 is used to improve the analysis at time t_0. From this new start an improved trajectory is computed by the model. The procedure is repeated several times to converge to the most likely actual state variable distribution. All measurements in the interval [t_0, t_n] are taken into account in a single analysis (Eskes, et al, 1998). Consequently, variational algorithms have a reduced computing cost in comparison with sequential assimilation algorithms working as a smoother (Jiang et al., 2014a; Lahoz et al., 2014). Huang, et al. (2015b) applied 4DVAR algorithm to predict regional-scale winter wheat yield obtaining reliable estimations at county scale. He et al (2015) estimated aboveground dry biomass of grass with a satisfactory accuracy level (R^2= 0.73 and RMSE = 617.94 kg ha^{-1}).

Although 4DVAR often shows a good performance, a disadvantage of the algorithm is the requirement of using the adjoint or tangent linear model. To cope with this disadvantage, methods have been proposed which combine variational and sequential algorithms. POD4DVAR is such a hybrid approach which merges Monte Carlo and proper orthogonal decomposition technique (POD) into 4DVar. In POD4DVAR, the initial condition $\mathbf{x_o}$ is perturbed at the start time of the assimilation window generating a four-dimensional ensemble trajectory. Then, POD technique is applied to

capture the spatial structure and temporal evolution of the state. The use of the adjoint or tangent linear model is avoided increasing the assimilation precision and reducing computational costs with respect to EnKF (Tian, et al., 2008)

Jiang, et al. (2014a) compared the performance of the POD4DVar and EnKF to assimilate LAI in CERES-Wheat model. The POD4DVar provided improved yield predictions at plot and regional scale. In addition, the computing time required to run the POD4DVAR was seven times lower than the time required by EnKF.

Based on the work of Dong et al., (2013), Arulampalam, et al. (2002), Lahoz, et al. (2014) and Reichle, et al. (2002b), Table 9 summarizes some characteristics of EnKF and variational approaches.

Table 9. Comparison of Ensemble Kalman Filter (EnKF) and variational approaches.

Item	EnKF	Variational
Number of free parameters	Single free parameter	Multiple free parameters
Observations used	Only past observations	Past and future observations
Updating procedure	Sequential (real time)	Batch processing
Linearization	No linearization required	Linearization required
Use of adjoints	No adjoint function needed	Adjoint function needed
Assumed error type	Additive, multiplicative, state dependent and in model structure	Additive
Assumed error distribution	Gaussian assumption	No Gaussian assumption
Computational costs	High	Low

3.8. Aspects related to the assimilated EO data

A number of factors related to the quality of the assimilated EO data affect the accuracy of data assimilation in crop models. In the following we briefly discuss the most important factors.

3.8.1. Spatial resolution

The spatial resolution of the EO sensor does not always match the required (fine) resolution of the crop growth modeling and also introduces mixed pixel effects. The mixed pixel problematic depends on the spatial resolution of the remote sensing data, its geometric/spatial accuracy, its point spread function (PSD) and the degree of fragmentation of land use (Jiang, et. al. 2014b). A practical strategy to reduce the effect of mixed pixels is to select only those pixels that have a high fraction of a single crop. However, the main drawback of this approach is the requirement of a detailed crop type map, available early enough in the growing season (De Wit, 2012). Regarding the availability of remote sensing data with different spatial resolutions, Montzka et al. (2012) suggested two methods to minimize mixing/scale effects:

- Using an observation operator. In this approach, an observation operator at fine scale uses the modeled state variables to simulate the coarse resolution observation. The simulated coarse signal (one single value) is then used to update the parameters of all fine-scale model pixels inside the large grid. Weights can be assigned to each fine model pixel according to the distance to the center of the (large) grid cell. In this way, pixels closer to the center of grid cell will have higher weight and will receive a larger update than pixels with a lower weight far(er) from the center cell (e.g. similar to the PSF).
- Rescaling the observations prior to data assimilation. This approach consists in resampling all remote sensing data to a specific spatial resolution according with the goal of the research – in

most cases from coarse resolution to a finer cell size. After resampling, the assimilation procedure is run in the usual way. In this case, it is necessary to define a downscaling/resampling algorithm and to quantify the measurement uncertainty on the fine scale. This approach is very practical when multiple data sets at different spatial resolutions need to be assimilated.

3.8.2. Temporal resolution and timing of observations

The effective temporal resolution of an EO system is the product of the revisit frequency of the sensor and cloudiness during the growth period (Jiang, et. al. 2014b). Hadria et al. (2006) found that the model accuracy was directly related to the satellite revisit frequency and suggested an optimal satellite revisit time of 10 days. Dente et al (2008) noticed that the number of remote sensing observations is not the main factor responsible for the simulation accuracy; they pointed out that the observation timing is much more critical. Atzberger (1997) found that the timing is most critical when only few EO observations are available. In the study of Dente et al (2008), the error in the simulated yield increased significantly when no observations were available during the period of maximum development of the crop such as stem elongation and heading stage in case of gramineous. The assimilation after the heading stage of wheat was not as important as before the heading. De Wit (2012) found that the tuning of CGM parameters improved with increasing availability of remote sensing data (even with different technical configurations). A positive effect was also noted if crop masks were available to identify crops of interest minimizing mixed pixel problems (De Wit, 2012). Launay and Guérif (2005) observed that the yield estimation did not improve, and even decreased in performance, when late season remote sensing data were assimilated after LAI decrease.

3.8.3. Combining data from several sensors

Simultaneous assimilation of remotely sensed data from various sensors (optical and radar) into a crop model is feasible and reduces the effect of the cloud cover (Prèvot, et al. 2003). The fusion of remote sensing observations from different sensors is another alternative to tackle spatial and temporal data constrains. Algorithms such as the spatial and temporal adaptive reflectance fusion model (STARM; Gao et al., 2006) have been developed to combine fine and coarse resolution images (e.g., Landsat and MODIS) to generate high temporal resolution data at the finer spatial scale. A related approach was implemented by Zhu et al. (2010) labelled enhanced STARFM (ESTARFM). Meng et al. (2013) combined NDVI images from high resolution HJ-1 CCD and MODIS satellites to generate a NDVI dataset with high spatial and high temporal resolution using STAVFM (Spatial and Temporal Adaptive Vegetation index Fusion Model). A review of spatial and temporal remote sensing data fusion techniques is presented by Zhang (2015).

3.8.4. Assimilation of reflectances instead of bio-physical variables

The assimilation of biophysical products such as LAI and FAPAR is operatively convenient. Assimilation of LAI and FAPAR can also handle observations from different sensors as both variables are sensor independent and scale linearly. However, the assimilation of crop bio-physical variables also carries some disadvantages such as uncertainties related to the atmospheric correction and the radiative transfer model inversion (chapter 2).

To reduce the effects of uncertainties in the (retrieved) LAI/FAPAR observations, the assimilation of surface reflectance in the CGM is a possible alternative (Guérif and Duke, 1998). In this case, both the atmospheric model and the canopy reflectance model are solely run in direct mode. No inversion is needed and the observed reflectances are directly assimilated into the combined CGM + canopy +

atmosphere model (Atzberger, 1997; Machwitz et al, 2014). As the combined model simulates the spectral (ToA) reflectance over the full optical domain (e.g. 400-2500 nm), potentially any sensor with a suitable spatial resolution can be assimilated. In a similar way, instead of assimilating spectral reflectances it is also possible to assimilate vegetation indices to avoid effects of errors in the LAI/FAPAR retrieval prior to the assimilation (Ma et al, 2013b).

3.8.5. Identification and modeling of key phenological events

In CGMs, many state variables such as LAI are directly related to the crop's phenological stage. Therefore, phenological events must be estimated with high accuracy to achieve a realistic crop growth simulation (Moulin et al., 1995). Curnel et al (2011) proved the importance of crop phenological synchronization through an experiment in which EnKF was compared with the performance of the recalibration/re-initialization strategy. A "phenological shift" of the EnKF members was detected since the ensemble was generated by perturbation of two model parameters directly related with crop phenology. The performance of the EnKF was even worse compared to the crop model run with default parameters.

These results proved the importance of rigorously calibrating crop growth cycles refining the estimation of emergence, anthesis and maturity dates (Machwitz et al, 2014). Unfortunately, RS contributes only very little to the observation of plants phenological stages (Delecolle et al., 1992). Regarding the effect of the growing season assessment, it is important to highlight that in real conditions (e.g. at regional scale) the uncertainties about phenological stages are large since sowing and emergence date never occur at the same time for all the fields and moreover vary from year to year due to the different climatic conditions and management decisions (Yuping et al. 2008).

3.8.6. Developments in geophysics

The updating approaches described in this document have been originally implemented in research areas such as meteorology, climatology, oceanography and hydrology. Considering that in geophysics new approaches are developed continuously, we encourage the remote sensing community testing these innovations in EO data assimilation. In Table 10 some innovative algorithms are presented which are potentially interesting for crop growth modeling. Aware of the influence of resampling in PF performance, Van Leeuwen (2009), for example, presented and discussed different resampling techniques in the context of geophysics.

Table 10. Innovative assimilation approaches in geophysics.

Approach	Reference
Ensemble smoother with multiple data assimilation (ES-MDA)	Emerick (2013)
Iterative ensemble Kalman smoother	Bocquet and Sakov (2014)
Modified Ensemble Kalman particle filter	Shen and Tang (2015)
Improvement of ensemble smoother with SVD-assisted	Kang, et al. (2016)
Efficient Kernel-Based Ensemble Gaussian Mixture Filtering	Liu, et al. (2016)

3.9. Overview of the assimilation of retrieved EO data in CGMs

The most widespread approaches to estimate crop biomass and yield are empirical, semi-empirical and mechanistic crop growth models. Empirical models establish a mathematical relationship between the EO data and the observed crop yield. They are easy to implement, however, have a low transferability to other crop cultivars or geographical regions (Ma et al, 2013a). On the

other hand, crop simulation models, based on mathematical equations, are able to simulate phenological development and physiological processes in response to environmental factors and management (Bouman et al., 1996). Therefore, they have a high transferability to crop cultivars and geographical regions. The main drawback of complex crop growth models is its high demand of input data, which hampers its use at regional scale.

To reduce estimation uncertainties at regional scale, crop growth models have been integrated with EO data. The integration allow combining the capability of remote sensing imagery to provide data of the earth's surface with the capability of growth models to provide a continuous description of crop status during the growing season (Delécolle et al., 1992). The most widespread assimilation techniques are: forcing, calibration and updating.

Forcing is a relatively simple assimilation strategy. However, its accuracy is strongly conditioned by the error and number of remote sensing observations. Calibration uses iterative numerical optimization techniques to ensure that the remotely sensed observations are optimally "fitted" by the CGM simulations. The efficiency of calibration depends on the availability of EO data, the error of the retrieved state variables, the value of fixed parameters and number of parameters to be calibrated, among others factors. Finally, updating is based on the individual integration of new observations in the crop model taking into account model and observation errors. The parameters are known a priori, thus, the assimilation is implemented without altering model structure. Updating is a versatile technique which allows assimilating two or more model state variables or a combination of parameters and state variables (Montzka et al. 2012).

A number of factors related to the quality of the EO data affect the accuracy of data assimilation in crop models. For instance, a mismatch between the spatial resolution of the EO sensor and the crop model requirement affect the accuracy of the estimations by the mixed pixel effect. The timing of the EO data is another important factor to considering in assimilation. For instance, gaps data during stem elongation and heading stages for gramineous affects strongly the accuracy of yield estimations (Dente et al., 2008). The fusion of remote sensing observations from different sensors is an alternative to minimize spatial and temporal data constrains (Prèvot, et al. 2003). Finally, another error source is related with the retrieval of bio-physical variables. A strategy implemented to reduce the error effect consists in assimilate the surface reflectance in the CGM. The observed reflectances are directly assimilated into the combined CGM + canopy + atmosphere model (Guérif and Duke, 1998; Atzberger, 1997; Machwitz et al, 2014).

Regarding the innovation in assimilation techniques, we highlight updating which has been boosted in the last years thanks to its flexibility. The Ensemble Kalman filter (EnKF) is the most widely used updating technique; however, new filters have been proposed aiming overcoming known EnKF restrictions, such as the Particle filter which operates in nonlinear and non-Gaussian systems. Additionally, the combination of updating with variational approach has yielded promising results. Moreover, high potential is also seen in the joint combination of multi-source remote sensing data with fusion algorithms. Such techniques allow matching the CGMs spatial and temporal scale with user demands.

4 Materials and Method

A. Materials

4.1 Study area

The study area is localized in Marchfeld region, one of the most important agricultural production areas of Austria, located in the north-eastern (NE) of the country (Figure 14). The area is flat (around 900 km²) with minor variations in elevation, ranging from 143 to 178 m. The dominant soil types are Chernozem and Fluvisol (FAO-World Soil Classification) characterized by a humus-rich A horizon and a sandy C horizon, followed by fluvial gravel from the former river bed of the Danube. The region is influenced by a semi-arid climate; winters are usually cold with frequently strong frosts and few snowfalls, and summers are hot and intermittently dry (Müller 1993). The annual average temperature is around 9.8°C and the annual precipitation sum is 550 mm, corresponding 200–440 mm to the growing season (April–September). The most important summer crops are sugar beet, maize, soybean, sunflowers and vegetables.

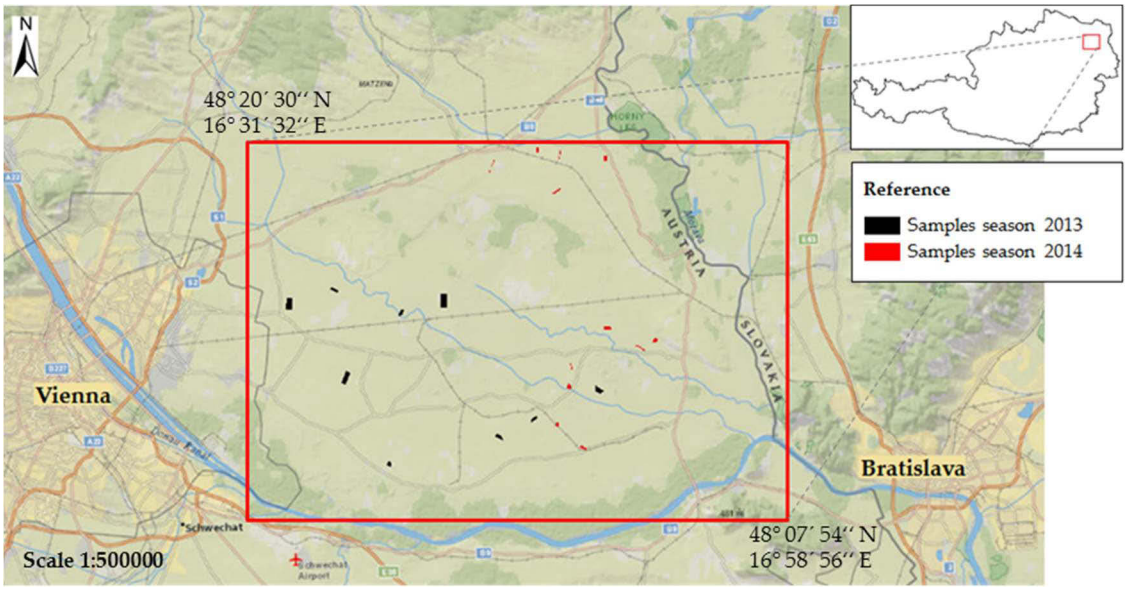

Figure 14. Study area and maize samples for seasons 2013 and 2014.

4.2 Meteorological data

The meteorological data used in GRAMI and SAFY models were daily average temperature (°C) and global solar radiation (MJ/m²) obtained from meteorological station Zwerndorf (Zentralanstalt für Meteorologie und Geodynamik-ZAMG). In Figure 15 are presented the daily average temperature (°C) and global solar radiation (MJ/m²) for seasons 2013 and 2014.

4.3 Satellite Data

The used satellite images were obtained by Landsat 5 TM, Landsat 8 OLI and DEIMOS sensors. DEIMOS images were provided orthorectified to sub-pixel accuracy (~10 m) using ground control points and the elevation model of the Shuttle Radar Topography Mission (SRTM v3). The atmospheric correction was carried out using ATCOR (Richter, 2004) model. A reference image from the data series was atmospherically corrected using the model and reference measurements of ground spectral reflectance collected at the acquisition date of the reference image. The rest of the images were

corrected by cross-checked of pseudo-invariant targets between the reference image and the image to be atmospherically corrected. This procedure was carried out by Vuolo et al. (2013).

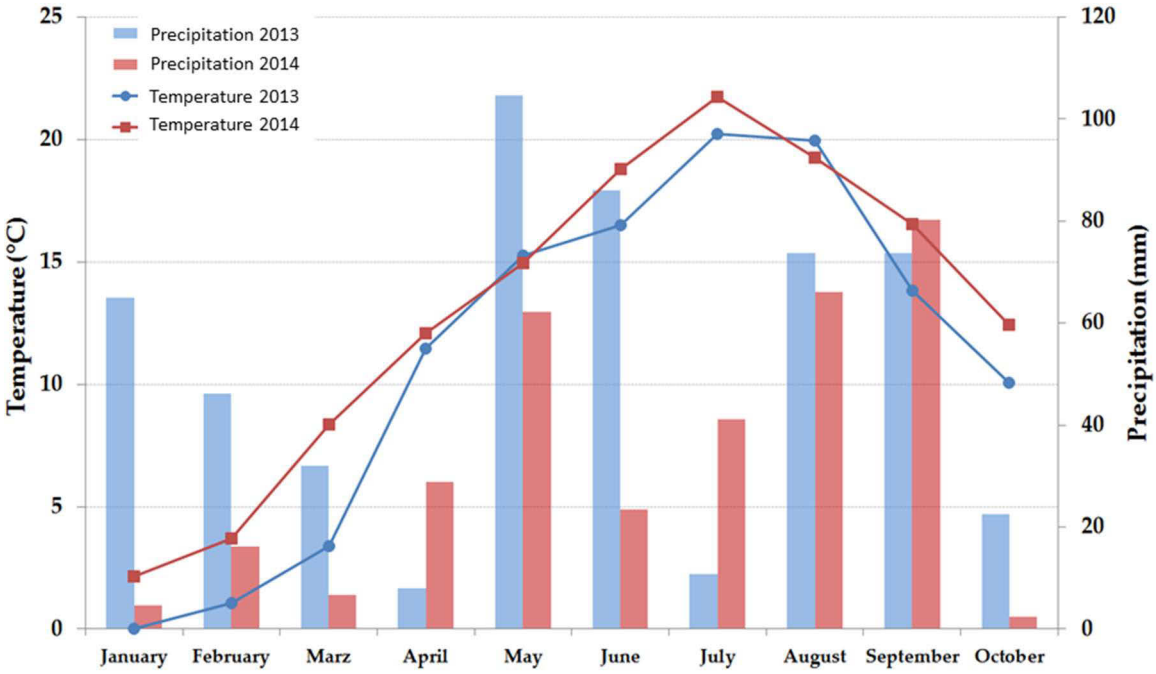

Figure 15. Meteorological data from station Zwerndorf (ZMAG) seasons 2013 and 2014.

4.4 Field measurements

A weekly ground data survey was carried out in twelve maize plots in the growing season of 2013. The selected plots were bigger than 3.5 ha with a nearly squared shape to avoid the mixed pixel effect in LAI estimations. The measured variables were LAI, crop height, phenological stage, agronomic crop condition (plagues, diseases, and damages). Moreover, corn samples as well as measured yield components were collected in twelve plots in season 2013 and eight plots in season 2014. The measurements were carried out one month before harvesting. The following section describes the different types of measurement in detail.

The plots sampled in the season 2013 can cluster in two groups: plots to seed and to grain production. The management of seed production plots is sharply different from grain production. The plant density of seed plots is larger till anthesis, then, the masculine plants are eliminated. Additionally, 1/3 of the female plants are chopped. Consequently, the biomass is reduced drastically. The fertilization is also different between groups. We noticed a stronger fertilization with nitrogen for seed plots.

4.4.1 Leaf Area Index measurements

We used the instrument LAI-2200 to estimate LAI, which is a non-destructive method, based on radiation measurements obtained with a "fish eye" optical sensor. The measurements made above and below the canopy are used to determine canopy light interception at five angles. Then, LAI is computed using a model of radiative transfer for vegetative canopies (LAI-2200C Plant Canopy Analyser, Instruction Manual, 2016). It is important to point out some limitations of the instrument. Estimations of LAI by LICOR 2200 are affected, mainly, by two types of errors; underestimation because of the non-random positioning of canopy elements and overestimation due to the incapacity

of the instrument to distinguish photosynthetically active leaf tissue from other plant elements (stems, flowers, senescent leaves). The effect of non-random positioning of canopy elements is maximized at the beginning of the plant growth, specially, for crops such as maize with a relatively large row space.

To minimize error measurements, some precautions were implemented: (a) the instrument was operated maximal two hours after sunrise or before sunset under diffuse radiation conditions to reduce multiple scattering on the measurements, (b) the sensor field of view was limited with 180° view-cap to prevent interference caused by the operator's presence and the illumination condition, (c) the measurements were azimuthally oriented opposite to the sun azimuth angle.

A sampling strategy was drawn up for each plot based on a soil map and high spatial resolution images available in Google Earth. Homogeneous plots had a unique sampling area along the crop season, while heterogeneous plots had two sampling areas, for instance low and high zone depending of the plot topography. In each sampling area, the LAI was calculated from the average of three replications of one above-canopy and nine below-canopy measurements. This procedure was repeated along the crop season for all the plots.

4.4.2 Yield crop estimation in field

The method used to forecast yield in field was based on the premise that one can estimate grain yield based on the measurement of crop yield components (Lauer, 2002). The yield components considered in the experiment were the number of ears per ha, the number of kernel per ear and the weight of kernel. The first and second components were measured in field while the last one was estimated by weighting 1000 seeds extracted from average ears.

We applied a systematic sampling scheme with a sampling distance of 10 m, representing altogether at least 0.1% of the total row extension of the plot. Moreover, additional samples were localized in heterogeneous areas detected by visual interpretation of high resolution images from Google Earth to increase the representativeness of the sampling.

In each sample, the number of ears was counted and two ears were selected to estimate the number of kernel per ear as well as the weight of the kernel. The samples were collected when the maize kernel began the phenological stage of milk grain. Details of field measurements can be consulted in Appendix A.

The reference data used at regional scale was provided by Statistics Austria (Statistik Austria, Feldfruchternteerhebung). The methodology used is based on information from special harvest reporters on municipality level in combination with sample survey after harvest time at provincial level.

B. Method

We used SAFY and GRAMI crop models as well as EO data to estimate maize yield. The assimilation of the EO data in the crop models was done in two ways: calibration and calibration + updating. We introduced an innovative scenario with a maximum number of free parameters, which corresponds to around 80% of the total number of model parameters. Figure 16 gives an overview of all implemented procedures in the experiment. The following sub-sections explain the individual components in detail.

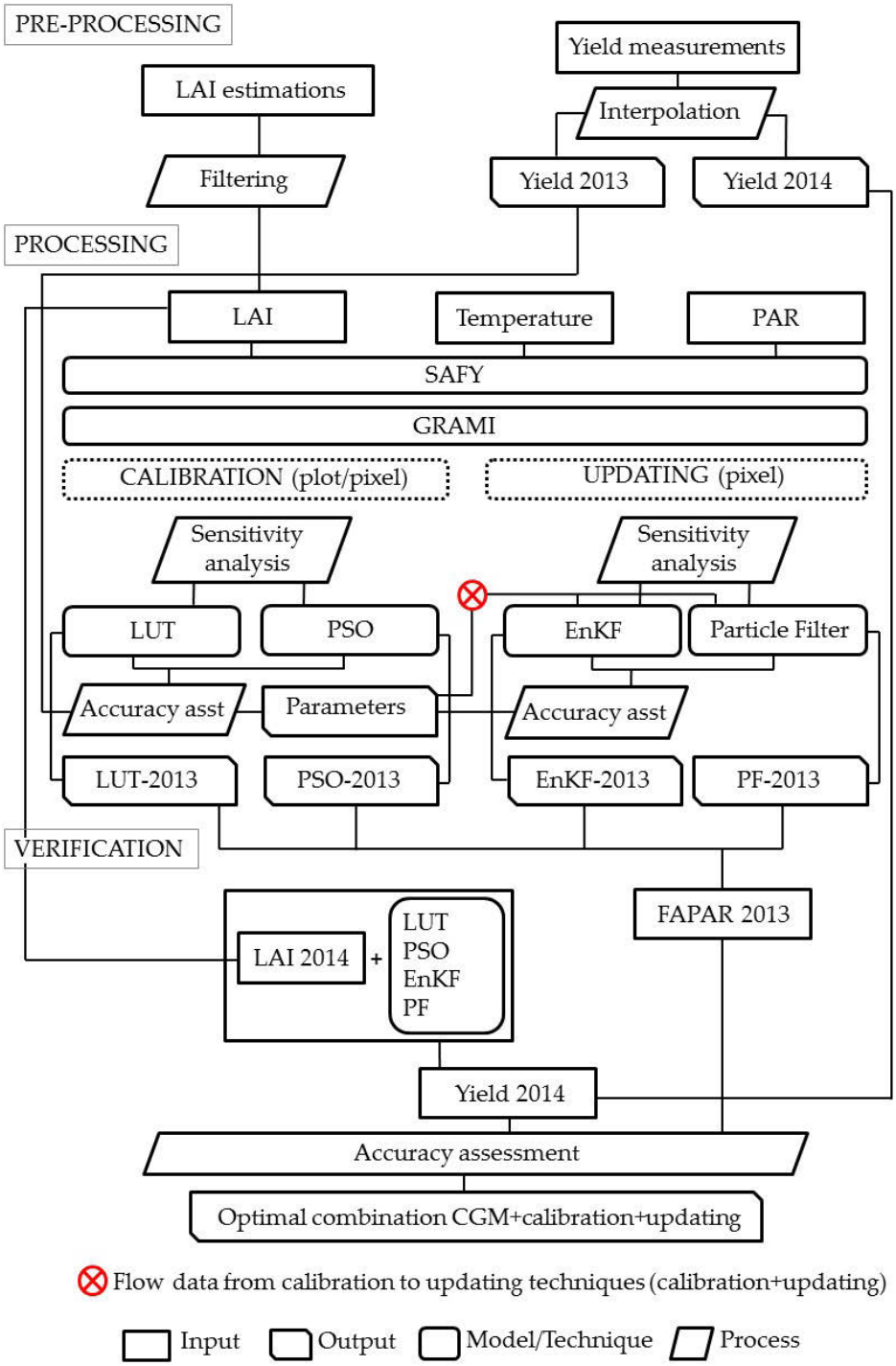

Figure 16. Flowchart of the procedures implemented in the experiment

LUT: Look Up Table;
PSO: Particle Swarm Optimization;
EnKF: Ensemble Kalman filter;
PF: Particle Filter;
Asst: Assessment;
FAPAR: Fraction of Absorbed Photosynthetically Active Radiation.

4.5 GRAMI and SAFY crop simulation models

GRAMI and SAFY models use the Monteith (1977) theory to simulate crop growth at daily time steps. The daily crop growth is simulated through four processes: (1) calculation of growing degree

days (GDD) for determining the actual phenological phase, (2) absorption of incident radiation energy by leaves according to actual leaf area, (3) production of new dry mass by the leaf canopy, and (4) partitioning of new dry mass for production of new leaves and/or grain filling according to the actual phenological phase (Ko et al, 2005). A representation of GRAMI model is depicted in Figure 17.

The models operate from the sowing date to the day of complete leaf senescence and consider three cardinal growth stages: emergency, anthesis and maturity. The leaf extension period starts from emergency to anthesis and the grain-filling period from anthesis to maturity. The model conception considers that cereals have an initial period in which most of the aboveground dry mass consists of leaf tissue. Then, the percentage of non-leaf tissues (stem and reproductive organs) increases along growing season. Prior to flowering, the production of new leaf tissue ceases and the photoassimilates are routed to grain growth. The leaf senescence is modelled by assuming that leaves appearing on a given day have a specific lifespan expressed in degree-days.

The data required to run these models are daily average air temperature and daily total solar irradiance. Input data such as soil physical properties, water content, fertility and management data are not required. It is assumed that the effects of these factors, related with canopy growth, are mimicked globally when the LAI simulation is "fit" to the observed LAI data by tuning a group of model parameters.

Moreover, it is assumed that Light Use Efficiency (LUE), which represents the efficiency to convert absorbed PAR into biomass, captures in a simple manner a global level of all agro-environmental crop stresses integrated together. Therefore, it could be an indicator of the performance of agricultural practices, such as the irrigation and fertilization.

In the experiment, the grain yield was calculated using the total biomass estimated along the crop season times a constant harvest index which value was 0.48.

The formulae of both models are presented in Appendix B.

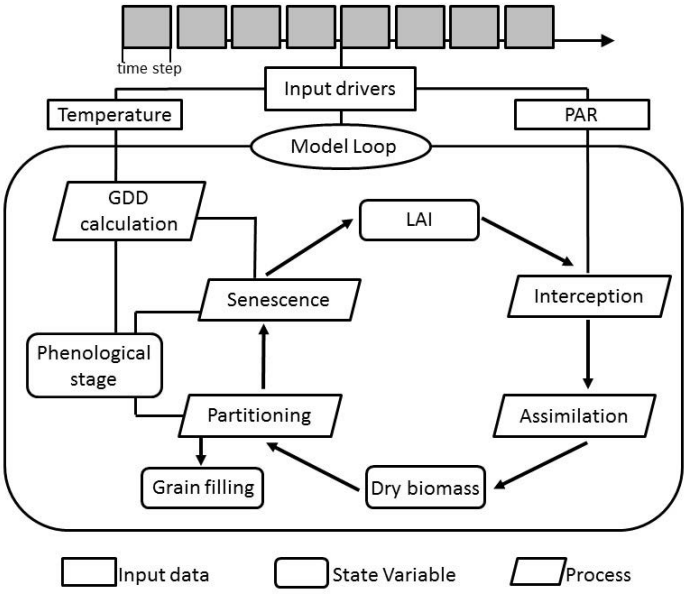

Figure 17. GRAMI model flowchart (adapted from Delécolle, 1992 and Ko et al, 2005).

4.6 LAI estimation

The Leaf Area Index was estimated based on CLAIR model (Clevers, 1989). The model states an exponential relationship between LAI and the soil-line based Weighted Difference Vegetation Index (WDVI). The equations are defined as follows:

$$WDVI = \varrho_{nir} - (\varrho_{red} * \varrho_{s\ nir}/\varrho_{s\ red}) \quad (6)$$

where ϱ_{red} and ϱ_{nir} represent the reflectance in the red and near infrared channels respectively. The ratio $\varrho_{s\ nir}/\varrho_{s\ red}$ is called soil line slope, a linear relationship of red and near infrared reflectance of bare soils, which represents the effects of the soil background on the calculation of the vegetation index.

$$LAI = \frac{1}{\alpha} * \ln\left(1 - \frac{WDVI}{WDVI\infty}\right) \quad (7)$$

where α is the extinction and scattering coefficient which depends on canopy architecture, crop type and leaf angle distribution. WDVI∞ is the asymptotically limiting value for the WDVI.

In the present study, the WDVI∞ was estimated for each image (maximum WDVI value for vegetated areas), while, the coefficient α assumed a constant value for all the crop coverage types along the season.

The LAI estimations were obtained by processing 10 LANDSAT and DEIMOS images for season 2013 and 12 images for season 2014. A detailed description of this methodology can be found in Vuolo et al. (2013).

4.7 Sensitivity analysis

Sensitivity analysis techniques have been developed to determine how sensitive model outputs are to changes in model inputs such as parameters or input variables, focusing mainly on the measurement and calibration of those parameters (Wöhling, et al. 2004). Additionally, this kind of analysis provides useful information about the model structure and allows identifying parts of the model which could be further improved (Confalonieri et al. 2010). Examples of sensitivity analysis for crop models can be consulted in Wöhling, et al. (2004), Confalonieri et al. (2010) and Richter, et al. (2010).

In this study, we carried out three experiments: a univariate sensitivity analysis, a correlation analysis between model parameters and a test of robustness for Look up Table (LUT) and Particle Swarm Optimization (PSO) techniques.

4.7.1 Generating a reference simulation

Reference model parameter values were extracted from an initial Look up Table approach (fully explained in section 4.9.1). The combination of parameters which yielded the best fit between observed and simulated LAI values for the 8 maize plots were used to create a dispersion distribution for each parameter. Then, the median values of each distribution were assumed to be representative for the group of analyzed plots. Reference curves for each state variable were obtained using reference parameters and both crop models GRAMI and SAFY.

4.7.2 Univariate sensitivity analysis

The univariate sensitivity analysis was carried out in both models to determine which parameters have the most significant effect on biomass and LAI simulation. The goal was to state a priority calibration's parameters list. The rate of change in respect to reference values was ± 15 %. The biomass and LAI differences were expressed in percentage.

4.7.3 Parameter correlation analysis

A correlation analysis between parameters regarding biomass estimation was carried out to identify possible ill-posed problems in model calibration. The two parameters analyzed assumed

values in a broad range of possibilities, the rest of them kept fixed values. A correlation matrix and a multi-parameter analysis chart were obtained.

4.7.4 Sensitivity analysis of LUT and PSO to LAI data

The robustness of the LUT and PSO approaches to calibrate accurately GRAMI and SAFY models was tested using synthetic LAI data. We tested different levels of random error, frequency and gaps data. The sensitivity was assessed by comparing the reference yield and phenology against the estimations obtained by SAFY and GRAMI calibrated by LUT and the PSO.

The goal of the sensitivity analysis was simulate the effect of error in EO data such as presence of clouds, atmospheric noise or inaccuracy of the inversion algorithm to retrieve LAI in the calibration of the CGMs. The experiment was integrated for two steps:

1. A "LAI observation" data series was obtained by running GRAMI and SAFY model using reference parameters (item 3.3.1).
2. A set of synthetic LAI observations was generated using the reference LAI data series and adding noise to the reference curve by the Monte Carlo approach. The type of errors and levels considered are detailed in Table 11.

Table 11. Type and level errors used along the sensitivity analysis

Item	Levels	Constant value
random error (%)	10,15,20,25 and 30	frequency 10 days
frequency (days)	10,15,20,25 and 30	random error 20%
gaps observation (crop stage)	emergency, anthesis, senescence	random error 20%

4.8 Filtering of Leaf Area Index estimations

LAI estimations by CLAIR model were filtered using Whittaker filter. The filter is based on the penalized least squares approach (Eilers; 2003). The basic algorithm integrates two components, which measure the fit of the smoothed series in respect to the original data series (8) and the roughness of the smoothed data series (9):

$$S = \sum_{i} (y_i - z_i)^2 \quad (8)$$

$$R = \sum_{i} (\Delta z_i)^2 \quad (9)$$

The combination of both components is defined as:

$$Q = S + \lambda R \quad (10)$$

where y is the original data series, z the smoothed data series and λ the smoothing parameter which represents the influence of the roughness component in the global function (5). In the formula, R is expressed as a first order difference but it could be considered a second or third order.

The goal of the penalized least squares approach is to find the smoothed data series which minimize Q. The larger is λ the stronger is the component R in the global equation. Consequently, the series will be smoother but less fit in respect to the original data series.

In our study, λ was tuned considering two criteria: the visually comparing the smoothed curve and the LAI series (estimated by EO data) and the error between the measured LAI in the field and the smoothed LAI values. The λ tested were 100, 300, 1000.

The Whittaker filter was chosen because it is easy to implement, it is able to process large amounts of data and it is controlled by a unique parameter (λ) which can be calibrated visually or by a cross-validation approach (Atzberger and Eilers, 2011).

4.9 Calibration of CGM parameters

Two calibration approaches, iterative Look Up Table (iLUT) and Particle Swarm Optimization (PSO), were tested with the aim of calibrating 10 out of 12 parameters of the GRAMI model and 11 out of 16 parameters of the SAFY model. As already mentioned in chapter 1, the main goal of calibration was to obtain accurate yield estimation using as little input data as possible.

4.9.1 Iterative Look up Table (iLUT)

LUT is a simple approach in which a range of parameter combinations are executed to create a pre-computed table of modeled state variables. The parameter levels are selected by minimizing a cost function which calculates the error between the state variable estimated by EO and the modeled one corresponding to a LUT record.

a) Parameters range for the first LUT

The range of parameters considered to build the initial LUT for GRAMI and SAFY were based on existing agronomic data and bibliographical references (Duchemin et al., 2008; Claverie, et al., 2012). Table 12 details the parameter ranges and Table 13 presents values of fix parameters and size of the LUTs for each model. A combination of levels for each parameter represents a record in the LUT and hereinafter will be called treatment.

Table 12. Initial Look up Table for GRAMI (G) and SAFY (S) models

Parameters	Model	Symbol	Min	Max	Pace	N° classes
Initial LAI	G-S	LAIin	0.05	0.15	0.05	3
Efficiency light use	G-S	LUE	2	6	1	5
Extinction coefficient	G-S	K	0.3	0.9	0.2	4
Specific leaf area	G-S	SLA	0.012	0.036	0.008	4
Leaf partition fraction	G-S	A	0.05	0.5	0.15	4
Leaf partition fraction	G-S	B	0.0006	0.0054	0.0016	4
Sowing date	G-S	SW	100	120	5	5
GDD emergency	G-S	GDDem	100	260	40	5
GDD maturity	G-S	GDDmt	1180	1580	100	5
Leaf span	G	LLS	700	1300	200	4
Senescence factor A	S	SenA	700	1300	200	4
Senescence factor B	S	SenB	3000	9000	3000	3

Table 13. Fix parameter values and LUT size for GRAMI and SAFY models

Item	GRAMI	SAFY
Minimum temperature	8	8
Optimal temperature		30
Maximum temperature		40
Power stress function		2
Parameters calibrated	10	11
LUT size record	1,920,000	5,760,000

The original names of the GRAMI and SAFY parameters have been modified with the aim of simplifying the comparison between models. For a detailed description of the models refer to Mass, 1992 (GRAMI) and Duchemin et al, 2008 (SAFY).

In Figure 18 are represented some of the parameters introduced in Table 12. The figure is complementary to the concepts presented in section 4.5 and the formulas detailed in Appendix B.

As showed in the equation 11 a determined amount of biomass is synthetized by the crop every day t (ΔDMt). The amount of biomass assimilated daily depends on the photosynthetically active radiation absorbed by the crop (APAR) and the efficiency of the plant to convert this energy in biomass (LUE). The APAR is calculated using the photosynthetically active radiation (PAR) and the Beer's Law which assesses the fraction of PAR absorbed by the plant. The Beer's Law includes the LAI and the coefficient K. The LAI indicates the total area of the leaves. The coefficient K represents the proportion of the incident light extinct through the crop canopy. The value of K is directly related with leaf structure and canopy architecture. The allocation of the biomass to the leaves and stem as well as the length of the leaf growing period depends on the parameters A and B. When the plant reaches the anthesis the biomass is accumulated only in the grain and the stem. The beginning of the leaf senescence is determined by Lls in GRAMI and Sen A in SAFY. Additionally, for SAFY the speed of the senescence is mimed by the parameter Sen B. The LAI at the end of the day is calculated considering the LAI of the day before (t-1), the new biomass accumulated in the leaves in the day t and the senescence in case the GDD is larger than the senesce threshold. The biomass accumulated in the leaves is converted to LAI using the parameter SLA.

The brown curve represents the total cumulated biomass synthetized along the crop season.

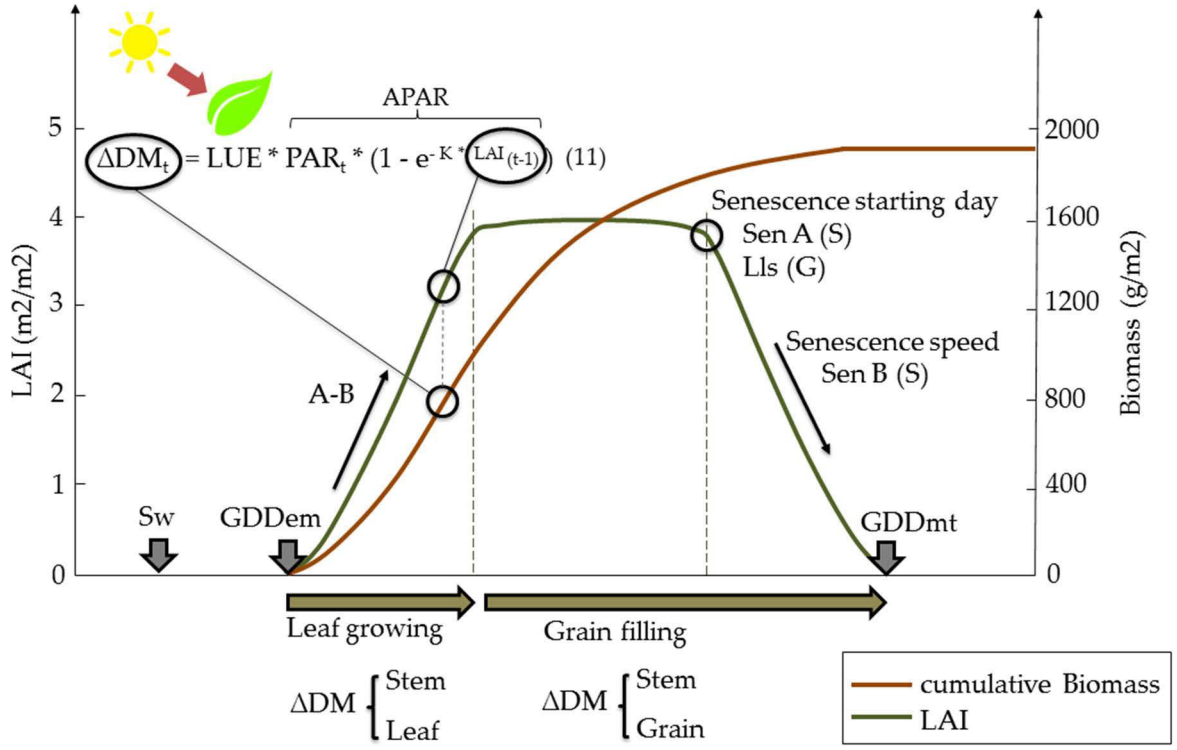

Figure 18. Representation of LAI and cumulative dry biomass along the crop season for GRAMI (G) and SAFY (S) models.

b) Cost function

Four cost functions were built considering factors such as phenology and LAI observation uncertainties. The functions tested were: "simple cost function", "weighted cost function by

phenology", "weighted cost function by LAI uncertainty" and "balanced cost function". The formulation of each cost function is described in detail in Appendix C.

c) Criteria to select LUT treatments

Two criteria were tested: (1) maximum number of treatments and (2) threshold tolerance expressed in error percentage.

(1) 100, 1000 and 1% of the best treatments.

(2) 20, 15, 10, 5 %

Finally, the iterative LUT (iLUT) was carried out using the best cost function and the best extraction criteria. The biomass was calculated as the average of the simulations obtained by the selected LUT records.

d) Iterative LUT

The iterative approach consists of a successive selection of parameters levels by analyzing the frequency distribution of treatments with lowest global LAI calibration error. The process was repeated till a minimum number of 100 LUT records were selected. The perceptual global error threshold to select the treatments ran from 20 % (first iteration) to 5 % (fourth iteration). The logical rules using to extract the parameters levels are presented in Appendix C.

In Figure 19 is represented the iterative procedure. The LAI, retrieved from EO data, was used to assess the error of each LUT record in each iteration. The state variable most relevant for our experiment was biomass. The logical rules were used to select the levels of each parameter and generate a new LUT for the next iteration.

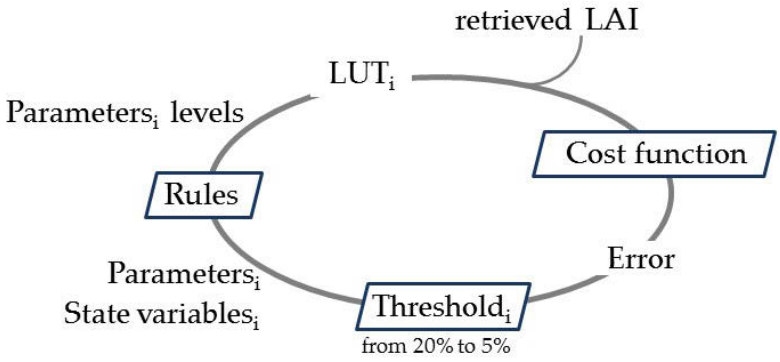

Figure 19. Representation of iterative LUT procedure.

4.9.2 Particle Swarm Optimization algorithm

PSO is a stochastic optimization technique, developed in 1995 by Kennedy and Eberhart. The algorithm, inspired by social behaviors of bird flocking or fish schooling, simulates the flying of n particles in a D-dimensional search space (Wang (2014) and Bazargan, 2011). The optimization algorithm is initialized with a population of random solutions and a searching process is carried out along the updating generations. The particles change their location along the generations based on their own best search point in the history of the search process (personal best; pbest) and the best search for all the particles in the swarm (global best; gbest). The position and velocity of a particle are updated in each generation according to the following equations:

$$\underbrace{v_i^{t+1}}_{\text{Velocity t+1}} = \underbrace{w.v_i^t}_{\text{current motion}} + \underbrace{c_1.rand_1.\ (pbest_i^t - x_i^t)}_{\text{particle memory influence}} + \underbrace{c_2.rand_1.\ (gbest_i^t - x_i^t)}_{\text{swarm influence}} \quad (12)$$

$$\underbrace{x_i^{t+1}}_{\text{position t+1}} = x_i^t + v_i^{t+1} \quad (13)$$

where i indicates the particle number, t is the generation number; c1 and c2 are cognitive and social constants which modify the velocity of particles toward the previous best position and the global best position respectively. Then, w is the inertia weight, rand1 and rand2 are random numbers uniformly distributed within the range [0-1]. Finally, v_i^{t+1} and x_i^{t+1} are the velocity and position of the particle i at time t+1 respectively (Kim et al, 2013). From the velocity formulation emerges that the updated particle velocity depends on: the previous velocity plus its inertia weight, the randomly weighted difference between the particle and the particle best position and the randomly weighted difference between the particle and the global best position. The incorporation of a randomly uniform component weighting the differences allows a good exploration of the state space and reduces the probability to get stuck at a local minimum (Trelea, 2003).

In the PSO procedure, it is recommended to confine the particles position to a feasible search space, in case, there is information about the parameters available beforehand. Then, the velocity of a particle should be limited to a maximum to prevent its departure from the search space. A rule of thumb states that the initial maximum velocity is equal to 50 % of the search range for each dimension (Evers, 2011). With respect to the inertia weight (w), it is recommended to apply a decreasing value from 0.9 in the first velocity update to 0.4 in the final velocity update (Bouallègue, et al.,2012). Moreover, the acceleration coefficients C1 and C2 should assume similar values giving stability during the searching process. A high value of C1 respect to C2 can produce a more erratic flight of the individual particles through the problem space, while a low C1 respect to C2 produces a prematurely convergence toward local minima. A value of 2 for both coefficients outperforms the previous versions (Kennedy and Eberhart). In Figure 20 depicts the PSO algorithm for one particle in a two dimensional space at time t (generation).

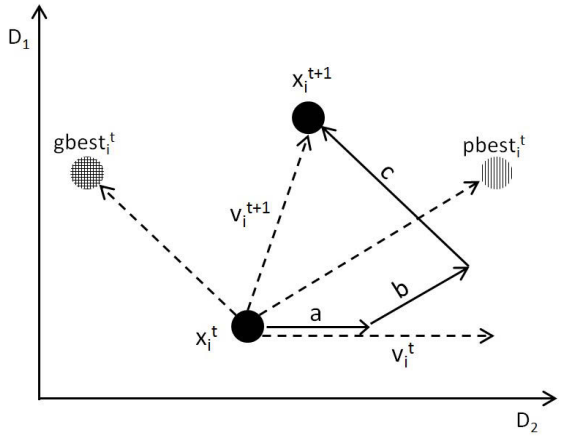

Figure 20. Particle Swarm Optimization; a: current motion influence, b: particle memory influence, c: swarm influence (adapted from Hanrahan, 2011).

The strength of PSO is its simplicity and capacity for optimizing a wide range of functions. The velocity adjustment by a combination of pbest, related with the particle "experience", and gbest related with group knowledge ensures diversity of response and at the same time stability to the system (Kennedy and Eberhart, 1995).

A sensitivity analysis was performed considering three important aspects of PSO algorithm: the value of the PSO parameters, the number of GRAMI/SAFY parameters to be optimized and the effect of LAI errors.

The PSO optimization function implemented in our experiment is driven by 12 parameters. A sensitivity analysis was carried out considering five parameters with large impact on the function performance. A range of ± 50% with respect to the default values was implemented (Table 14). The remaining PSO parameters assumed default values. Moreover, the number of parameters to be optimized was tested aiming to assess the effect of the ill-posed problems in the PSO algorithm. Then, a fixed value, extracted from iLUT approach, was assigned to the non-optimized parameters.

Finally, the effect of the LAI random error, gaps and frequency was tested using the same procedure as depicted in section 4.7.4.

Based on the results obtained in the sensitivity analysis, a strategy was developed to estimate biomass using the "Simple cost function" and "Weighted cost function by LAI uncertainty". Additionally, we tested the above mentioned cost functions using an emulator of 4DVAR approach. The main goal was assess the feasibility to incorporate restrictions in parameters optimization using ancillary data (Appendix D).

The PSO algorithm was implemented in Matlab using the code developed by Evers (2011).

Table 14. PSO parameters and range values used in the sensitivity analysis

Item	GRAMI	SAFY
N° parameters to be optimized	5: LUE, K, SLA, LAIin, LLs 7: LUE, K, SLA, LAIin, A, B, LLs 10: 7 + Sw, GDDem, GDDmt	6: LUE, K, SLA, LAIin, SenA, SenB 8: LUE, K, SLA, LAIin, A, B, SenA, SenB 11: 8 + Sw, GDDem, GDDmt
GRAMI/SAFY range parameters	defined in Table 12	
Maximum velocity	range parameter * factor (0.25-0.5-0.75)	
Max. n° iterations	500-1000-1500	
Number of particles	12-24-48	
Acceleration	1-2-3	
Final inertia	0.2-0.4-0.6	

4.10 LAI updating approach

Updating approach takes into account model and observation errors in the assimilation process. Two updating techniques were tested in combination with calibration: Ensemble Kalman filter (EnKF) and Particle filter (PF).

4.10.1 Ensemble Kalman filter

The EnKF is based on the Linear Kalman filter method proposed by Kalman (1960). It was developed by Evensen (1994) with the objective to overcome the requirement of model linearity of Kalman's algorithm. The EnKF generates an ensemble of observations and model which are used to update the variable of interest using the Linear Kalman filter equation:

$$A_a = A + k\,(D-A) \quad (14)$$

where A and A_a are the model forecast and analysis (updating) state, D the observation and K the Kalman gain which depends of the forecast and measurement covariance errors.

The assimilation of LAI using EnKF was conducted in the following manner. GRAMI and SAFY models began running at sowing date. Gaussian noise, based on random sampling of LUE, was added to shift the simulated LAI. In this way, the ensemble of forecasted LAI state was generated also called model ensemble. The rest of model parameters remained constant during the experiment. In case an observation was available at time t, we added a Gaussian perturbation to generate the observation ensemble. The forecast and observation ensembles were assimilated using the formulae described above (12). Then, the updated LAI at time t was forced into the crop model. The process was finalized when all LAI observations were assimilated. In Figure 21 is depicted LAI updating using EnKF.

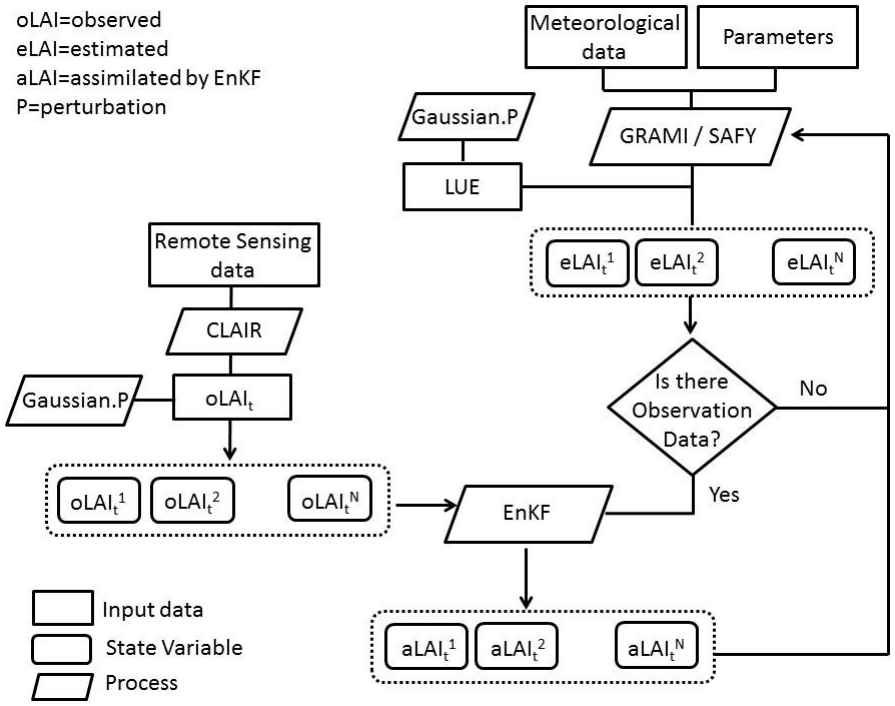

Figure 21. Assimilation of LAI observations in GRAMI and SAFY models by EnKF.

To generate the model ensemble, one can apply Gaussian perturbations in state variables, drive variables or model parameters. We decided to generate the model ensemble by adding Gaussian noise only in LUE parameter. Our decision was based on two reasons. First, if Gaussian noise is added to a correlated group of parameters, repeated particles are obtained because different parameters levels combinations yield same LAI values. Therefore, the efficiency of the process is reduced. Second, considering that it is advisable using few or only one non-correlated parameter; LUE seems more suitable because it is directly linked to the effect of environmental and management conditions on crop growing. Then, a special focus of our analysis is to test the ability of updating techniques to capture the spatial variability in each plot using EO data at pixel scale.

A sensitivity analysis of EnKF was performed to test the effect of the number of particles of observation and model ensembles as well as model and observation error. In Table 15 are detailed the ranges of value used in the sensitivity analyze.

The GRAMI and SAFY models used in the iLUT and PSO sensitivity analysis were implemented. A synthetic LAI data series was generated by adding a maximum random error of 20% in the LAI values obtained by the reference CGMs. Then, the error of the CGM was simulated by

replacing the LUE parameter for a value 20% larger than the reference (CGM "to update"). The rest of parameters kept the same values. Finally, 12 observations from the synthetic LAI data series were extracted to carry out the updating simulation. The model and observation errors were calculated by comparing the LAI values with the LAI data series from the reference CGMs. The sensitivity of EnKF regarding overestimation and underestimation errors in observations and the model was tested using a range of ± 50 % of reference error values. The observation and model uncertainties were assumed to be constant throughout the experiment.

Table 15. Variables and value range tested in the sensitivity analysis of EnKF

Observation and Model ensemble size	from 50 to 500 particles
Observation error	0.5-1.5 % of observation reference error
Model error	0.5-1.5 % of model reference error

4.10.2 Particle Filter

Particle filter is an approach based on the Monte Carlo simulation, which is able to estimate state variables using a set of random samples (particles) and their weights (Lahoz, et al, 2014). The main advantages of PF are the non-pre-assumption regarding the model characteristics and the noise probability distribution (Han and Li, 2008). These characteristics represent a benefit respect to other filters considering that crop-growth models operate in nonlinear and non-Gaussian systems (Arulampalam, et al. 2002). However, the main drawback of PF is the filtering divergence produced after several iterations in which very few particles have significant weight. (Makowski et al 2004).

For this reason, two approaches, suggested by bibliography, were implemented in this study: a resampling routine called Sequential Importance Resampling (SIR; Arulampalam, 2000) and a non-resampling technique consisting of using a larger particles ensemble. In Figure 22 is depicted the PF procedure to updating LAI in GRAMI and SAFY.

A sensitivity analysis of the PF was implemented to test the effect of: the size of the model ensemble, the model and observation errors. The ranges of values used in the sensitivity analysis were the same as in the EnKF. It is important to highlight that no observation ensemble is implemented in the PF is to update the state variable. Instead, a unique random value is introduced as observation considering a Gaussian distribution with a standard deviation equal to the observation error.

Based on the results of this analysis, it is the objective to find the optimal strategy to estimate yield using the best updating technique in combination with the best calibration technique.

Both methodologies EnKF and PF have been implemented in Matlab based on the work of Evensen (2003) and Arulampalan, et al. (2002) respectively.

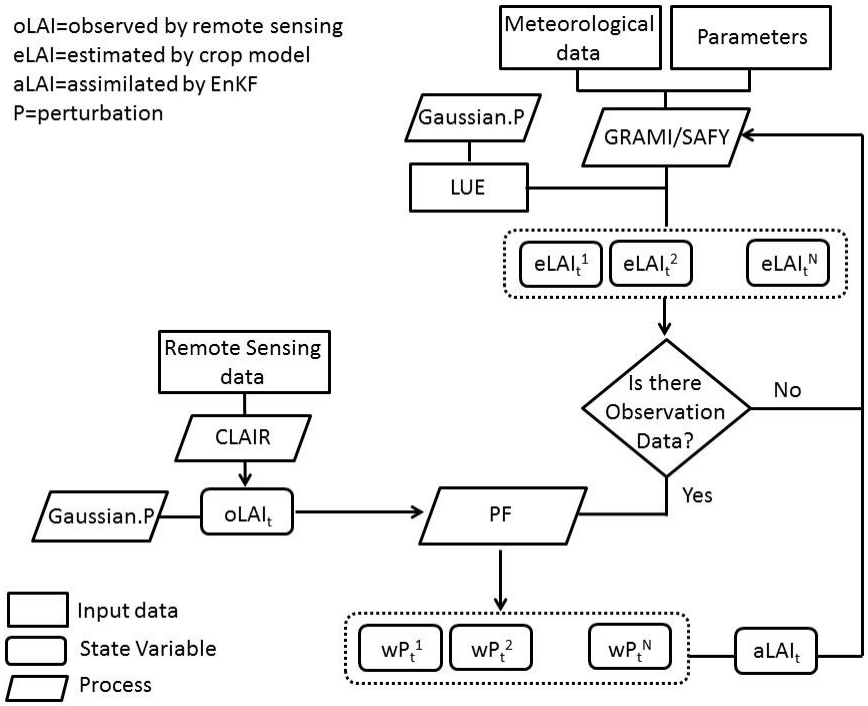

Figure 22. Assimilation of LAI observations in GRAMI and SAFY models by PF.

4.11 Validation of GRAMI and SAFY models

To further validate the performance of the calibrated GRAMI and SAFY models, a base-line approach is applied which derives yield data independently based on a remotely sensed FAPAR dataset and the well-known Monteith equation (Monteith, 1977). The Monteith approach well-known states that the produced total biomass is directly proportional to the accumulated absorbed photosynthetically active radiation (APAR) and the capability of the plant to convert this energy in biomass (LUE). Then, the yield is calculated as a percentage of the total biomass defined by the harvest index (HI). In this approach no computational loop was implemented in comparison with SAFY and GRAMI models.

$$\text{Yield} = \sum_{t=1}^{n} \text{APARt} \,.\, \text{LUE} \,.\, \text{HI} \tag{15}$$

The performance of the estimation depends greatly on the accurate determination of the biomass accumulation interval defined for cardinal points. Three different cardinal points extracted from iLUT approach, filtering approach (Atzberger et al. 2014) and field data observations were tested. Moreover, two groups of LUE values for each calibration technique were evaluated; the regional average LUE value and the calibrated LUE values at plot scale.

The FAPAR data series was derived from gap-free LANDSAT images series with a temporal resolution of 15 days provided by Vuolo, et al. (2016). The daily FAPAR resolution was obtained by implementing the approach suggested by Atzberger et al. 2014.

4.12 Verification

The calibration and updating techniques were run in a group of well spatially distributed maize plots identified in the field for season 2014. The resulting average modeled yield represented the average regional yield estimation and was compared with the official statistics for county Gänserndorf. Then, the yield estimations at plot scale were compared with field estimations.

4.13 General considerations

The Normalized RMSE (NRMSE) is used hereafter because facilitates the comparison between datasets or models with different scales. The NRMSE expresses the RMSE as a percentage with respect to the mean value of the dependent variable. It can be interpreted in a similar way to the variation coefficient.

Four goodness-of-fit parameters have been used to compare the performance of the calibration and updating techniques along the experiment. Three parameters have been used at plot scale: R2, NRMSEf and EEP and one at regional scale, EER.

The determination coefficient (R2) indicates the proportion of yield variability explained by the regression model. The normalized root mean square error for the regression function (NRMSEf) represents the mean error expressed in percentage between the estimated yield by the regression function and the observed yield. Additionally, the estimation error at plot scale (EEP) between yield observed and estimated by the CGM is included. This error is calculated using the same equation as NRMSE, however, without considering the regression function. Finally, EER measures the agreement between regional yield estimation by the official Austrian Institute of Statistics (Statistics Austria) and the average yield simulated by the CGM.

Finally, the maize yield is expressed, hereafter, in quintals per hectare (q/ha) with 0 % of grain humidity (1q = 0.1 tons). The commercial humidity of the maize is 14%.

5 Results and Discussion

The chapter is divided in three parts. In the first part, the results of calibration and updating of GRAMI and SAFY models regarding yield observations of the season 2013 are presented and discussed (§ 5.1 to § 5.8). Then, we introduce in section 5.9 the results of the verification of the techniques using yield observations of the season 2014. Finally, we present an overview discussion about the most relevant points of our experiment and a comparison the results obtained for both seasons with findings from similar previous research (§ 5.10).

5.1 Yield estimation by field sampling

The fitting function between yield informed by farmers and estimated in field using the procedure described in Appendix A is presented in Figure 23. The black bars indicate the variability of yield estimations (mean ± standard deviation).

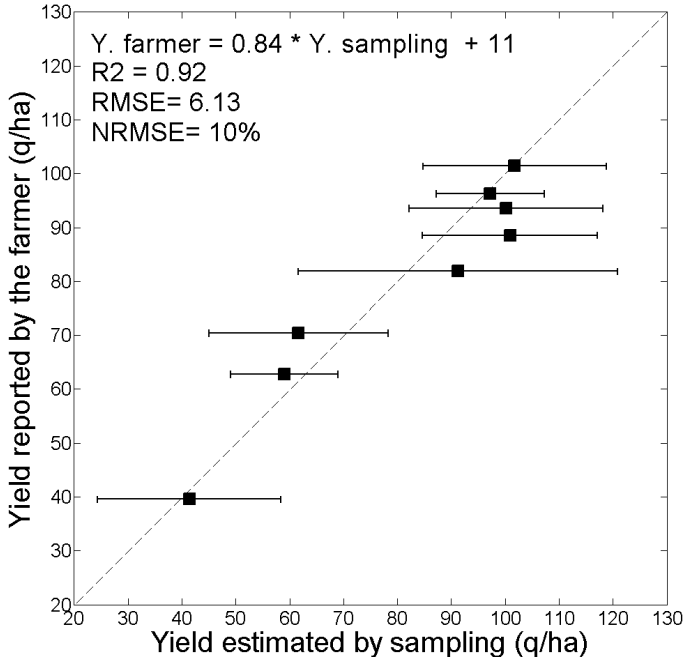

Figure 23. Regression function between yields reported by farmer and estimated in field by sampling for season 2013.

The function shows a good fit between the average yield estimated by sampling and the yield reported by the farmers. However, the variability of the estimations for some samples is markedly large. The main sources of spatial variability observed in field were the size of the maize cob and the number of ears per 10 meters (Appendix A).

The sampling covered a broad range of maize yield. As introduced in section 4.4, a sub-group of samples with a special management corresponds to seed production. In Figure 23, these observations are localized on the left side of the chart. If the analysis only considers the plots for grain production the R^2 is reduced to 0.54.

The official average yield estimation by Statistics Austria for the county of Gänszendorf expressed as dry grain (0% humidity) was 75 q/ha and 90 q/ha for seasons 2013 and 2014 respectively. Then, the yield estimation error at regional scale, calculated as the average of the measurements in field, was 2.2 % for season 2013 and 10.7 % for season 2014.

5.2 LAI estimation using EO data

The fitting between LAI measured in the field for season 2013 and LAI estimated by the semi-empirical model described in section 4.6 is depicted in Figure 24. A total of 71 LAI observations were compared with the estimations by the CLAIR model based on Landsat 5TM and DEIMOS observations. The regression function shows the underestimation of LAI with respect to the field measurements. This mismatch is expressed by the slope of 1.2.

In a more detailed analysis of the scatter plot it is possible to identify a range between 0.75 and 1.5 (m2/m2) in the Y axis with larger variability with respect to the rest of the distribution. This mismatch between LAI observations and estimations could be explained by the overestimation of field measurements by LICOR 2200. This type of error is maximum during senescence due to the fact that the instrument is not able to discriminate green tissues from senescence vegetation.

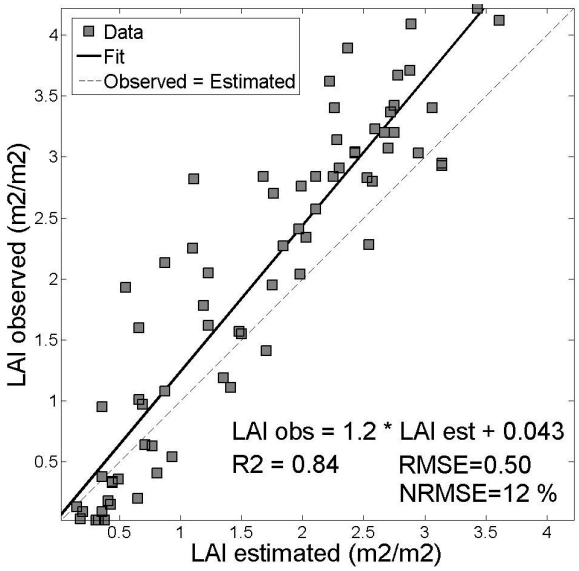

Figure 24. Scatter plot between LAI measured in field and estimated by the CLAIR model using Landsat 5TM and DEIMOS imagery.

5.3 Sensitivity analyses of crop growth modelss

5.3.1 Univariate sensitivity analysis

The effect of parameters variation on biomass and LAI simulation for GRAMI and SAFY models is represented in Figure 25. The bars indicate the percentage of change of biomass (a) and LAI (b) for a variation range of ±15 % of reference parameters. This percentage of variation was chosen to keep the parameter in a realist range of values.

The parameter with the largest effect on the simulated biomass for both models is Light Use Efficiency (LUE). Then, parameters such as SW and GDDmt showed an unbalanced effect in biomass simulation because they are affected by daily mean temperature. For instance, a very early sowing date could produce no modification in biomass simulation, because the temperature is lower than the optimum growth temperature. On the other hand, the biomass simulation is affected notably if a late sowing date is set because of the reduction of the crop season.

An important difference between the models is observed in senescence parameters. Senescence has a higher impact on biomass simulation for GRAMI. This can be explained by differences in the formulas of the models (Appendix B). In GRAMI the age of the biomass produced at time t is calculated along the crop season in each loop step. Consequently, this specific amount of biomass dies

when the lifespan threshold is reached. There is a link between senescence and the biomass produced in the period between emergency and anthesis. In SAFY the leaf daily senescence is calculated as a percentage of the biomass synthetized the day before the current loop. Therefore, the senescence is decoupled from the leaf growing period.

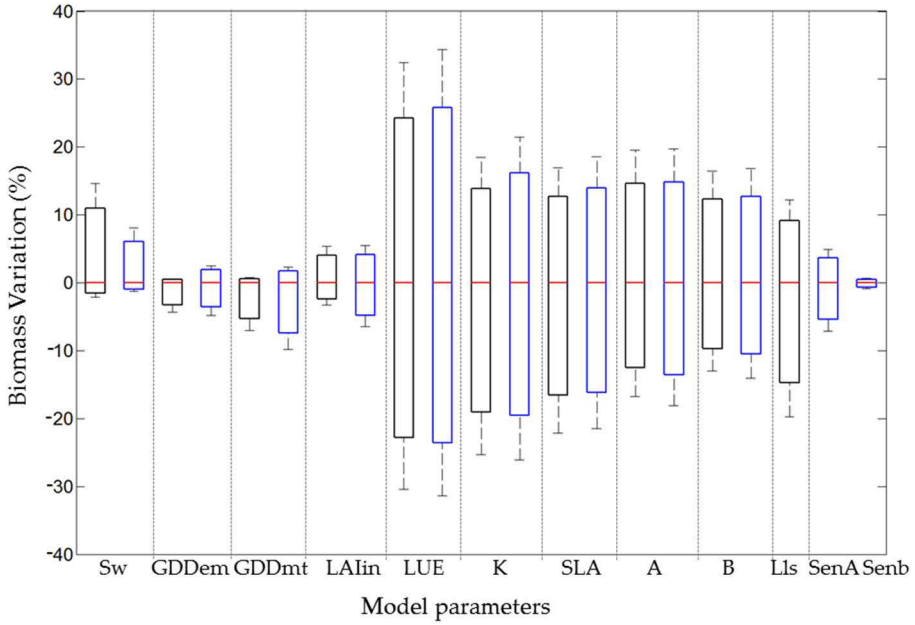

(a)

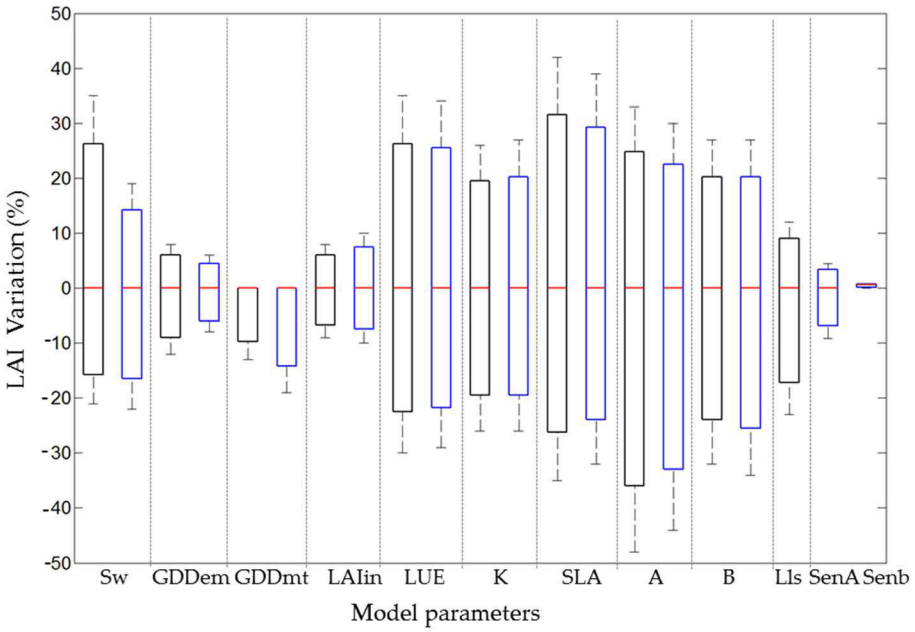

(b)

References:	**LAIin**: LAI initial	**LUE**: Light Use Efficency
Sw: sowing date	**K**: extinction coefficient	**SLA**: Specific Leaf Area
GDDem: cumulative degree days to emergency	**A**: Leaf partition factor	**B**: Leaf partition factor
GDDmt: cumulative degree days to maturity	**Lls**: Leaf lifespan	**SenA** and **B**: Senescence factors

Figure 25. Univariate sensitivity analysis, a) biomass and b) LAI. The black bars correspond to the GRAMI model and the blue to the SAFY model.

Regarding LAI simulation, the parameters with a higher impact are SLA, A and B. These last two parameters are related with the slope and maximum value of the LAI curve (Figure 18). Then, phenological parameters such as SW, GDDem, GDDmt showed proportionally more influence on LAI simulation than on biomass simulation. This is due to phenological cardinal points define the crop season. Consequently, an inaccurate estimation of these parameters shifts the simulated LAI curve in relation with the reference. We observed also that the differences for senescence between the CGMs are similar to the behavior noticed for biomass simulation. The chart gives a good overview of the complexity of parameters calibration by using LAI data series.

The influence of the fixed parameters on the sensitivity analysis was verified. To define proper parameter values a bibliographical review and an exploratory analysis was carried out.

5.3.2 Parameter correlation analysis

The correlation between CGMs parameters regarding the biomass estimation for a group of LUT records is presented in Figure 26. The records were selected considering a maximum total error between reference and simulated LAI of 20%. For each parameter analyzed, the first column refers to GRAMI and the second one to SAFY. The correlation values in references are expressed in absolute values. The inverse correlation between parameters is identified with (-).

Figure 26. Level of correlation between CGM parameters: first column (GRAMI), second column (SAFY). The inverse correlation between parameters is identified with (-).

The parameters with higher correlation are LUE, LAIin, K, SLA, A and B. These high correlation values indicate restrictions to calibrate them jointly due to similar biomass simulations. Hence, similar estimations might be obtained by different combinations of parameter levels (ill-posed problem). On the other hand, parameters related to senescence and GDDmt have low correlation with the rest of parameters. Sw and GDDem have an intermediate inverse correlation in both models. For instance, a very early Sw could be compensated by a larger GDDem and vice versa.

A complementary plot based on stepwise analysis is presented in Appendix E.

5.4. Yield estimation using calibrated GRAMI and SAFY models by the iterative LUT technique (iLUT)

5.4.1. First step of iterative LUT calibration

In this section we discussed aspects related with the cost function and the criterion used to extract LUT records in the iterative procedure. Additionally, we present some findings about the effect of LAI filtering in parameters calibration.

5.4.1.1 Cost function

As introduced in section 4.9.1 and extensively described in Appendix C, four cost functions were compared: simple, balanced, weighted by phenology and weighted by LAI uncertainty.
The cost function weighted by LAI uncertainty showed the worst performance. Different tolerance thresholds were tested. However, in all the cases the treatments selected yielded simulated LAI curves with little resemblance to the observed LAI series. Therefore, biomass was estimated with low accuracy. The effect of incrementing error tolerance at the beginning of crop season, in a context of large number of free parameters, boosted the selection of a broad range of GDD to emergency and initial LAI parameter levels with the consequently dispersion of biomass estimations.

On the other hand, the weighted cost function by phenology showed the best performance provided the weight for anthesis range was not larger than 50% of the total function weight; otherwise unsuitable combinations of parameters levels are extracted reducing the biomass estimation accuracy.

The calculation of the above mentioned cost functions require additional data to identify the phenological crop stage or to set the LAI uncertainty threshold. The simple cost function showed an acceptable performance without requiring ancillary information. Therefore, aware of the restrictions of data availability at regional scale; the simple cost function was implemented in the iterative LUT technique.

In Table 16 are represented the average biomass estimation error and variation coefficient (CV) for each cost function.

Table 16. Comparison accuracy and CV of four cost functions

Cost function	Average error (%)	CV (%)
Simple	6.7	5.6
Balanced	10.1	3.6
Weighted by phenology	2.6	6.4
Weighted by LAI uncertainty	20.6	15.1

5.4.1.2 Criteria to extract LUT records

We compared two types of threshold criteria: a maximum number of LUT records and a maximum global error expressed as percentage. The threshold expressed as percentage had better performance because allows selecting a representative number of LUT records for each plot. Additionally, this criterion enabled us to compare the global error between plots along the iterative procedure.
The thresholds implemented from the initial iteration to the fourth one were 20, 15, 10 and 5% respectively.

5.4.1.3 LAI filtering

Finally in this first step of iLUT calibration was tested the effect of filtering the LAI observations before calibrating the CGMs parameters. As depicted in section 4.8, it was used the Whittaker filter and were tested three levels of λ smoothing parameter; 100, 300, 1000. The better performance was obtained with λ equal 300. The correlation between LAI measured in field and LAI retrieved from EO data was optimized with a reduction of RMSE of 5.5 %. However, the most important improvement was observed in LUT approach. The error of the yield estimation was reduced due to new parameter levels were selected. The smoothed LAI observations data series had a better fitting with the LAI simulations obtained by the calibrated SAFY and GRAMI models. We verified that a λ smoothing parameter equal 1000 does not improved the results incrementing the dispersion of biomass estimations.

5.4.2. Iterative LUT approach at plot scale

The main goal of the iterative iLUT was to select a reduced group of parameter levels which minimize LAI error during calibration.

An example of iterative LUT inversion for GRAMI and SAFY models is presented in Figure 27. The comparison was done for the same maize sample and iteration level. The black lines represent the simulated LAI curves generated by the combination of parameter levels selected in the iLUT process. The LAI values estimated by the CLAIR model are indicated with red points (a-c). The simulation of the cumulative biomass along the crop season is presented in figures (b) and (d).

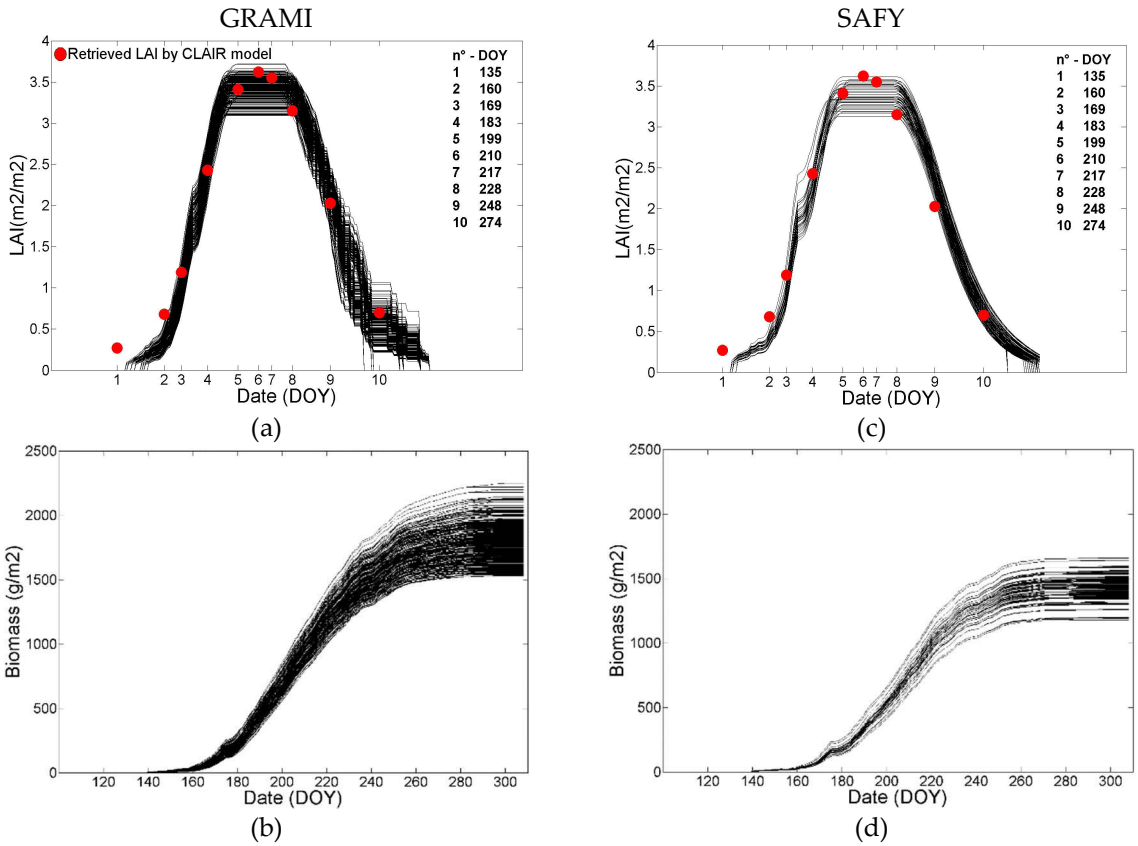

Figure 27. Simulated LAI and cumulative biomass for GRAMI (a, b) and SAFY (c, d) respectively.

The LAI curves simulated by GRAMI (a) and SAFY (c) were extracted from LUT records with a global LAI calibration error lower than 10% (third iteration). GRAMI showed a larger variability of selected LAI curves for the same global error tolerance. The number of LUT records extracted for

GRAMI was 40% larger than for SAFY. The parameters with larger variability were LAIin, LUE, K, SLA and B. On the other hand, phenological parameters were similar in both models. Finally, the maize yield was 5 % underestimated for SAFY and 15 % overestimated for GRAMI. This trend was observed in all the samples analyzed.

The lower number of selected LAI records in SAFY (Figure 27 b) compared to GRAMI (Figure 27 a) could be related with the temperature stress function (Appendix B). This function implemented in SAFY might work as a constraint, reducing the number of simulated LAI curves for a given global calibration error threshold.

Through the iterations the LAI calibration error and parameter variability were reduced for most of the samples. The global LAI calibration error diminished 50% on average for all the plots. Additionally, parameter variability was reduced in a range from 40% to 100% depending on the type of parameter.

The scatter plots between yield simulated and observed for the first and best iteration of LUT for GRAMI (a, b) and SAFY (d, e) are sketched in Figure 28. In this analysis, the best iteration was chosen based on the lowest maximum global error for a given plot. The black bars in Figure 28 depict the variability of the yield estimations considering ±one standard deviation from the mean yield estimation.

A significant improvement is observed by comparing GRAMI performance from the first iteration (a) in relation to the best iteration (b). All the parameters of goodness-of-fit improved. The regional estimation error was reduced by 38% while for EEP the reduction was 16.7 % regarding the first LUT iteration. Moreover, the R^2 was increased and the NRMSEf decreased by 11 %. Additionally, the variability of yield estimations was sharply reduced in response to the reduction of parameter variability. On the other hand, a partial improvement is observed in SAFY. The regression function was enhanced in the best iteration, evidenced by the increase of R^2 and the reduction of NRMSEf by 10%. However, EEP increased and the EER went from 0.6 % (first iteration) to 10.4 % (best iteration). The regional yield was underestimated by SAFY and overestimated by GRAMI.

A complete summary with the goodness-of-fit parameters for both models is presented in Appendix F.

The efficiency of the iLUT approach to calibrate phenological parameters was also analyzed. The variability of phenological parameters such as sowing date, GDDem and GDDmt was reduced, in average, 80% with respect to the first LUT iteration. Moreover, both models showed good accuracy to estimate sowing date and anthesis in relation to field observations collected for season 2013. The average error for sowing date was 3.75 and 3.5 days, whilst for anthesis was 4.63 and 3.27 days for GRAMI and SAFY, respectively.

A lower accuracy was observed for GDDmt estimation. The main reason of these discrepancies is related to the physiology of maize crop. It was verified that after grain maturity LAI can reach values around 1.4 to 1 m^2/m^2 depending on hybrid, stress conditions and agricultural management. Then, there is a time frame of around one month between grain maturity and total plant senescence. Therefore, the estimation of GDDmt by fitting LAI series showed a shift regarding physiological maize grain maturity. Proof of this was the identification of a systematic offset in the estimation of GDDmt regarding field measurements in a range of 20 to 40 days for all the plots. This mismatch between grain maturity and plant senescence has no impact in our estimations because yield is calculated considering the total above biomass, from emergency to senescence, times the harvest index.

The high accuracy of calibrated GRAMI and SAFY phenological sub-models by iLUT is promising since phenology is directly related to partition of photoassimilates among other physiological processes.

It is important to emphasize that the accuracy of phenological estimations depends on the availability of LAI observations during crop season.

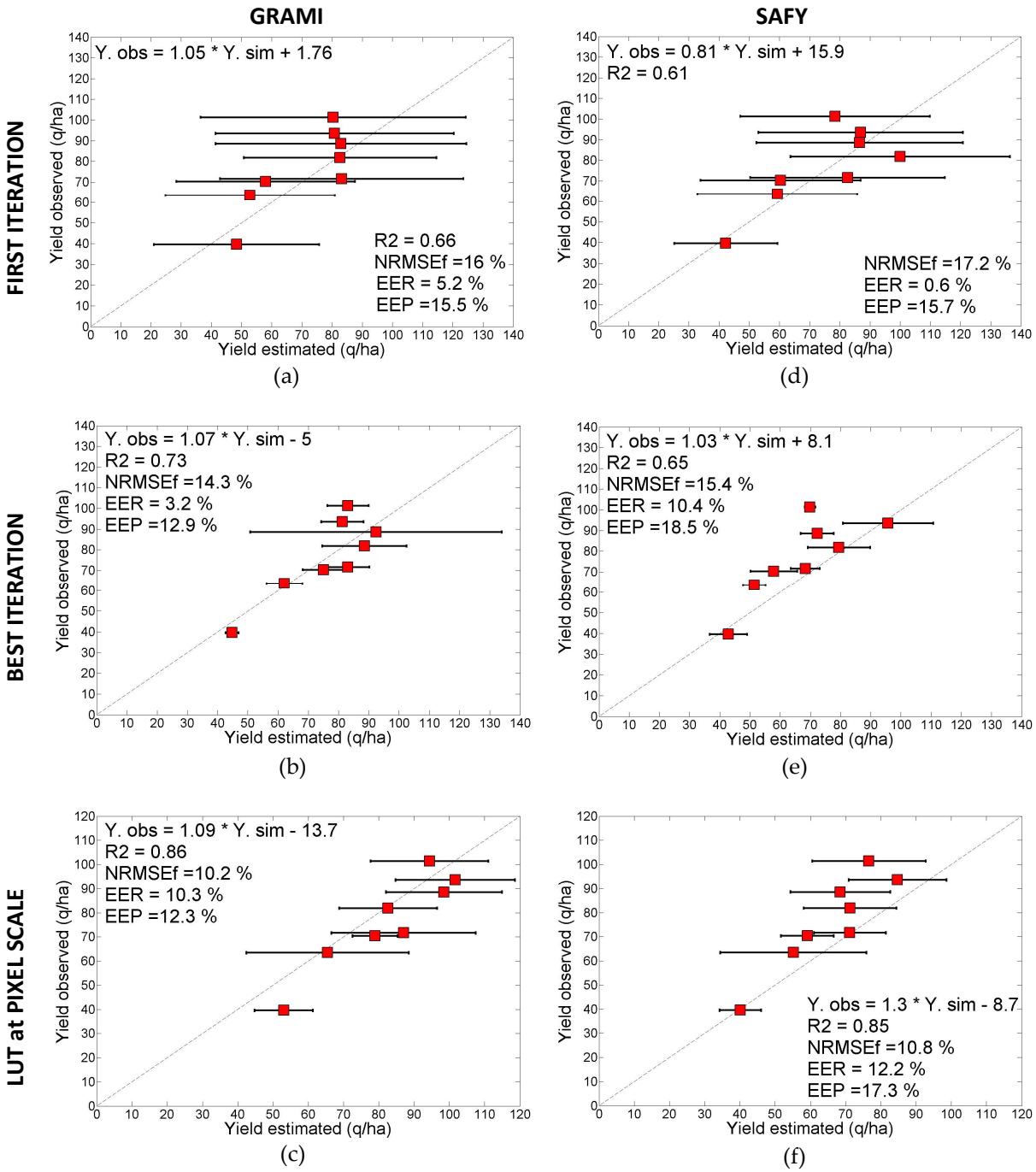

Figure 28 Scatter plots between observed and estimated yield by GRAMI (a,b,c) and SAFY (d,e,f) calibrated by the first iLUT iteration, the best iLUT iteration and LUT at pixel scale respectively.

5.4.3. LUT approach at pixel scale

To further improve yield estimation, a routine was tested using reference plot parameters from iLUT and LAI data of each pixel. We evaluated different combinations of fixed and free parameters as well as ranges of maximum and minimum values for each free parameter in the LUT.

In a first step, the free parameters were reduced from 10 and 11 to 7 and 8 for GRAMI and SAFY, respectively, keeping constant Sw, GDDem, GDDmt. The assumption was that these phenological parameters are constant for each plot depending on the maize hybrid. However, results were not satisfying.

In a second step, we included A and B in the group of fixed parameters. These parameters drive biomass partition from emergency to anthesis (Figure 18). Therefore, the four phenological cardinal points (sowing date, emergency, anthesis and maturity) assumed to be constant for each pixel. In Table 17 are detailed the fixed and free parameters for the first and second step of GRAMI and SAFY calibration at pixel scale.

Table 17. Fixed and free parameters in the first and the second step of GRAMI and SAFY calibration at pixel scale.

		GRAMI	**SAFY**
1° step	fixed	Sw, GDDem, GDDmt	Sw, GDDem, GDDmt
	free	LAIin, LUE, K, SLA, A, B, LlS	LAIin, LUE, K, SLA, A, B, SenA, SenB.
2° step	fixed	Sw, GDDem, GDDmt,A, B	Sw, GDDem, GDDmt,A, B
	free	LAIin, LUE, K, SLA, LlS	LAIin, LUE, K, SLA, SenA, SenB.

The scatter plots for LUT approach at pixel scale for GRAMI and SAFY are depicted in Figure 28 (c) and (f) respectively. In both cases, strong biases are observed. The underestimation observed in SAFY might be related to the temperature stress function. In this function, the LUE is modified according to the daily temperature (Appendix B). On the other hand, in GRAMI, the LUE does not depend on the daily temperature. This could be a reason of the overestimation observed.

The charts also show the strong increase of R2 for the GRAMI model compared to the first and best LUT iteration. Additionally, the EEP was reduced. However, EER increased from 1.4% to 10% reaching a similar value to the first iLUT. In SAFY, the EEP improved with respect to the best iteration, however, with values higher compared to the first iLUT. The regression function was also improved by the same magnitude as in GRAMI.

Finally, the variability of yield estimations increased for all the samples in both models. This can be explained by introducing intra-plot variability and by the fact that correlated parameters such as LAIin, LUE, K, SLA had to be calibrated.

5.5. Yield estimation using calibrated GRAMI and SAFY models by the Particle Swarm Optimization (PSO)

5.5.1. PSO parameters sensitivity

The PSO algorithm is able to select a combination of parameter levels which minimize the error of a given cost function in an iterative process. A sensitivity analysis was carried out to assess the influence of the PSO parameter levels in the performance of the optimization process. Five parameters were analyzed: maximum particle velocity (MPV), population size (n° particles) (PS), maximum number of iterations (MNI), acceleration (Acc) and final inertia weight (FIW). The influence of each parameter was measured as a percentage of variation of the optimized values in relation to the mean value considering all parameter/levels included in the sensitivity analysis.

The range for each parameter is detailed in section 4.9.2. The percentage of variation of PSO optimization value for the five parameters is represented in Figure 29.

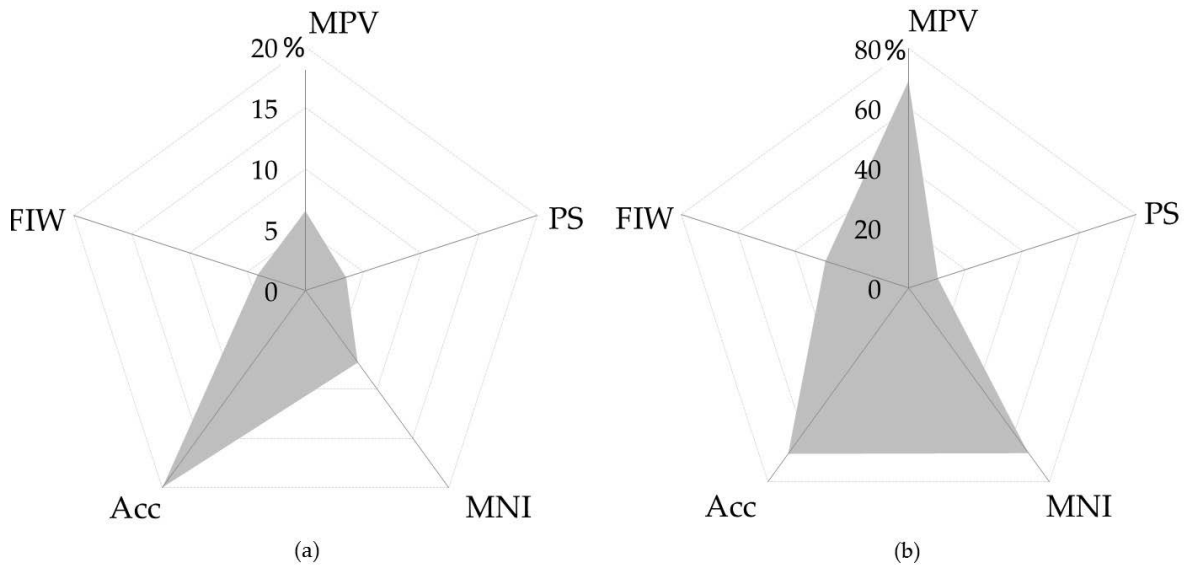

Figure 29. Sensitivity of PSO to MPV, PS, MNI, Acc and FIW implemented in (a) GRAMI and (b) SAFY.

The sensitivity of PSO parameters between both models is markedly different. Overall, SAFY seems more sensitive to PSO parameters. The maximum percentage of variation is around three times higher than for GRAMI. Acceleration has in both models an important influence. For SAFY, the reduction of maximum particle velocity, from 0.5 to 0.25, has a sharp effect on optimization with an error reduction of 80%. Moreover, the optimization value diminished when the maximum number of iterations increased from 1000 to 1500.

These findings express the importance of setting suitable PSO parameters instead of using default values. The procedure used to define suitable PSO parameter levels for the SAFY and GRAMI models is described in the following sub-chapters.

5.5.2. Optimum PSO parameter value

A LUT of PSO parameters was tested emphasizing the three parameters with larger influence in the performance of PSO: maximum particle velocity, maximum number of iterations and acceleration.

The combination of parameter levels 0.25 (MPV), 25 (PS), 2000 (MNI), 2 (Acc) and 0.4 (FIW) yielded the lowest EEP for PSO-GRAMI. The average variation coefficients (CV) for all the combinations tested were about 22 %. The best parameters combination for PSO-SAFY was similar, only the optimal level for MNI was 1000 instead 2000. The CVs were higher than in PSO-GRAMI with an average value of 35 %.

5.5.3. Number of PSO repetitions

The PSO approach includes two random components as described in section 4.9.2. Therefore, when PSO is run more than one time, using same input data, different parameter levels could be selected. This effect is maximized in our experiment since the parameters optimized are ill-posed.

To increase the reliability of the optimization procedure, we assessed the effect of the number of PSO repetitions in the selection of CGM parameter levels and consequently in the variability of biomass estimations by GRAMI and SAFY. The number of repetitions tested was 10, 30 and 60.

The variability of yield estimations was reduced by 10% when the number of repetitions increased from 10 to 30. At the same time, the error reduction from 30 to 60 repetitions was lower (5 %), however, the computational time demand increased significantly. Therefore, PSO was set 30 repetitions for each sample as a good balance between reliability and computational processing time. Moreover, the implementation of repetitions has the additional advantage of allowing calculating biomass estimation variability.

5.5.4. Number of optimized parameters

We tested the performance of PSO according to the number of parameters optimized. The fixed parameter values were extracted from iLUT approach. The NRMSEf, EEP and EER for 5, 7 and 10 optimized parameters in GRAMI (a) and 6, 8 and 11 parameters in SAFY (b) are represented in Figure 30. The upper part of the chart specifies which parameters have been optimized in each case.

A constant reduction of EEP from 5 to 10 optimized parameters is observed in Figure 30 (a). In SAFY (b) the minimum EEP is reached with 8 optimized parameters. After 8 parameters, the error increases sharply by 72%. This increase is due to the inclusion of phenological parameters such as Sw, GDDem, GDDmt in the optimization routine.

Regarding EER, the values for SAFY are lower than 10% for the three cases analyzed. A minimum is obtained for 8 optimized parameters. On the other hand, for GRAMI the maximum is around 14%, then, a strong reduction of 76% is achieved with a 10-parameter optimized model.

Finally, the minimum NRMSEf error is achieved when 7 (GRAMI) and 8 (SAFY) parameters are optimized.

Considering the negative effect of including phenological parameters in PSO-SAFY, it was decided to optimize 7 and 8 parameters from GRAMI and SAFY, respectively. The phenological data were extracted from iLUT approach.

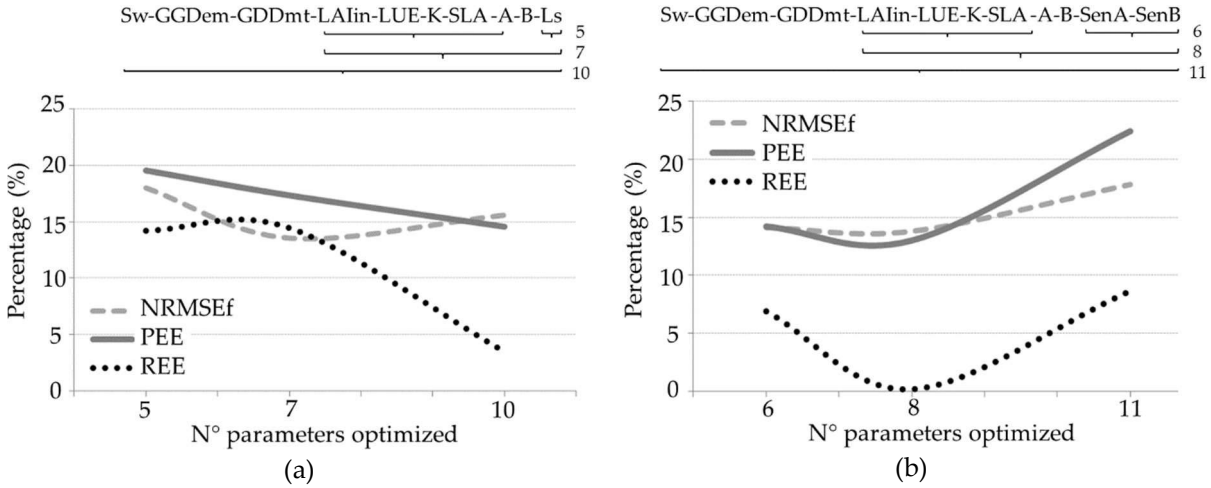

Figure 30. Variation of EEP, EER and NRMSEf according to the number of variables optimized for (a) PSO + GRAMI and (b) PSO + SAFY.

5.5.5. Cost function

The simple cost function and the weighted cost function (Appendix C) were tested in PSO. The weighted cost function showed a low performance with an EEP 90% higher than the simple cost function. A higher error was also registered in regional yield estimation (EER) with an overestimation of 26 % as compared to 3.1 % obtained using the simple cost function.

Additionally, we tested both cost functions using 4DVAR formulation (Appendix D). The background parameter values and standard deviations were extracted from iLUT technique.

The modified cost functions did not overcome the performance of the simple cost function. We observed that PSO was strongly constrained if background parameters, with low standard deviation, are included in the optimization function. The algorithm is "forced" to select a combination of parameter levels, practically, equal to the background parameter values set in the cost function. Therefore, it is recommended to implement this kind of cost function only if there is enough knowledge about the variability of the parameters in the study area.

Acceptable results were obtained when background phenological parameters were included in the cost function. This could be a suitable option if the CGM is implemented in "forward" mode before the crop season is finished. In this way the impact of gaps data on the calibration of parameters related with plant senescence and grain maturity might be minimized.

An alternative of using a cost function based on 4DVAR is to define a more restricted searching range for some parameters based on ancillary data or field observations. Then, the cost function is not altered and only the searching range is modified.

5.5.6. Application of PSO at plot and pixel scale

Based on the results presented, the PSO algorithm was implemented for each sample plot. The number of parameters calibrated were 7 and 8 from GRAMI and SAFY, respectively. The phenological parameters were extracted from the iLUT approach. The PSO parameters set are specified in Table 18.

Table 18. PSO parameters for the GRAMI and SAFY models

Model	MPV	PS	MNI	Acc	FIW	n° of P. calibrated	n° repetitions
GRAMI	0.25	25	2000	2	0.4	7	30
SAFY	0.25	25	1000	2	0.4	8	30

The scatter plots between reference and simulated maize yield using the PSO approach are sketched in Figure 31. At plot scale, the goodness-of-fit parameters of calibrated GRAMI (a) and SAFY (d) are similar. However, for GRAMI a number of observations are overestimated. As a consequence, the average simulated yield has an overestimation error of 14.4% in relation to the official statistics. This error is lower for SAFY model with only 0.2%. The EEP value is also better for SAFY model. The overestimation in GRAMI and underestimation in SAFY confirm the trend already observed and discussed in the iLUT approach.

In a second step, a calibration of a reduced group of parameters using LAI pixel data was implemented. The Sw, GDDem, GDDmt, A and B parameters were fixed to values obtained by PSO calibration at plot scale. We assumed that these parameters, which drive crop phenology, are constant at plot scale.

Two scenarios were tested for each CGM: the calibration of parameters with low inter-correlation and parameters with high correlation to the LUE. In Table 19 the parameters for each scenario and CGM are introduced.

Table 19. Parameters **c**alibrated in PSO pixel approach

CGM	GRAMI	SAFY
Parameters low correlated	LUE, Lls	LUE, SenA, SenB
Parameters high correlated with LUE	LUE, Lls + LAIin, SLA, K.	LUE, SenA, SenB + LAIin, SLA, K.

Figure 31 (b) and (e) shows the scatter plots for GRAMI estimations with two calibrated parameters (LUE and Ls) and SAFY with three calibrated parameters (LUE, SenA, SenB).

A significant reduction in the variability of yield estimation is observed in most of the plots (black bars) for both models. The correlation between simulated and observed yield for the SAFY model improved as shown by a slope close to one (1.03) and a low offset. Moreover, the EEP value is reduced for both models; 23% for GRAMI and 7.2% for SAFY compared with the estimations obtained by the models calibrated using only plot data. Again compared to the plot data results, the Regional error estimation (EER) decreased for GRAMI, while an increase for SAFY was noted. However, the EER for SAFY is still much lower compared to GRAMI.

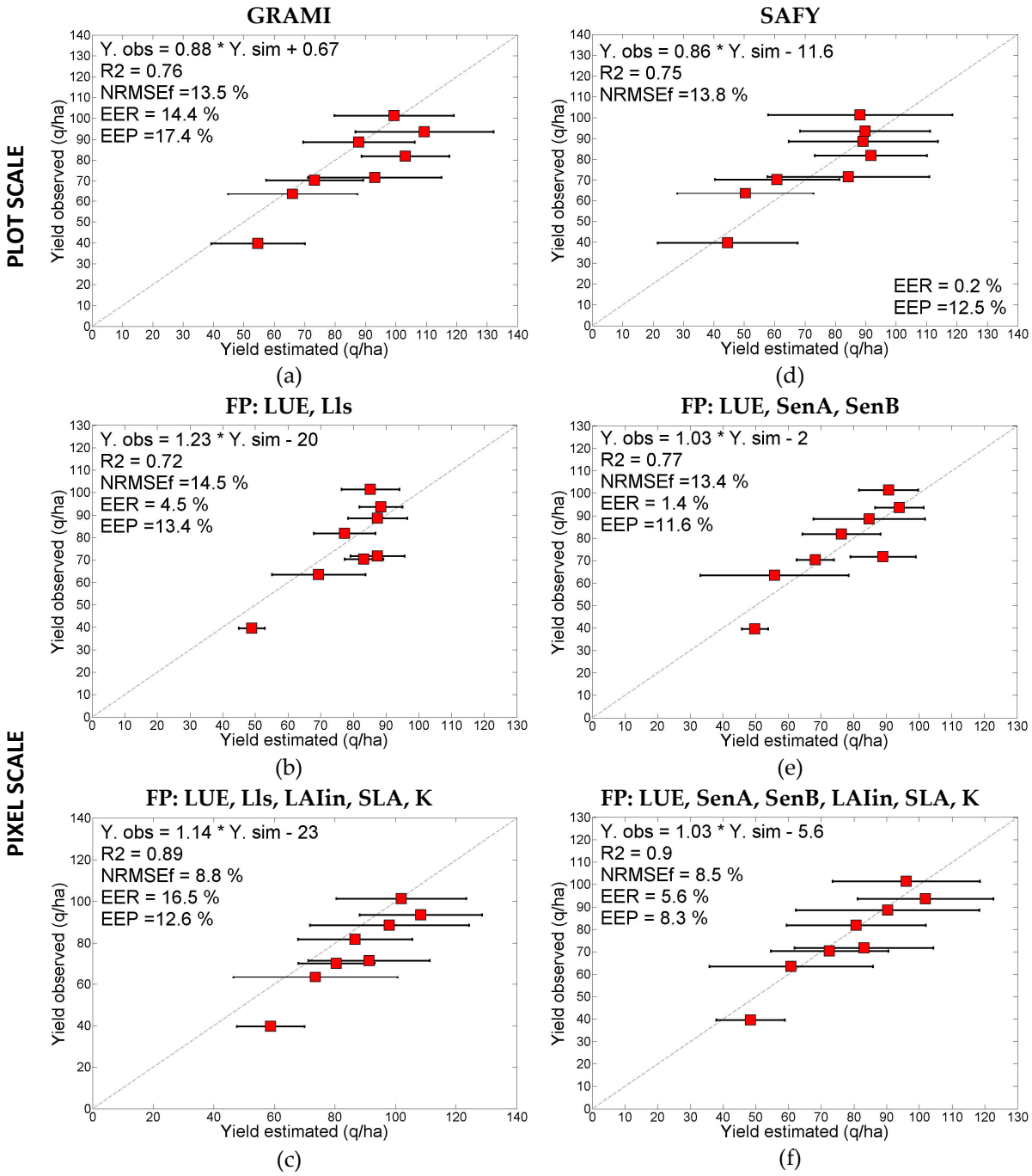

Figure 31. Scatter plots between observed and estimated yield by GRAMI (a,b,c) and SAFY (d,e,f) calibrated by PSO at plot scale and pixel scale respectively (FP: free parameters).

Finally, yield estimations obtained by GRAMI with five calibrated parameters and SAFY with six calibrated parameters are presented in Figure 31 (c) and (f) respectively. The increased number of free parameters has a clear effect on the variability of yield estimations (black bars). This can be explained by the fact that LAIin, SLA and K were included in the calibration. These parameters have a strong influence on the biomass estimation and high correlation with LUE. The average yield variability increased 58% for GRAMI and 90% for SAFY regarding estimations obtained by the PSO with two (GRAMI) and three free-parameters (SAFY). Additionally, the average computational processing time for both models was raised by 50%. The regression functions, in both cases, were improved with higher R^2 and a reduction in NRMSEf of 35% for GRAMI and 38% for SAFY with respect to the calibration at plot scale. The overestimation trend in GRAMI is confirmed by a high negative offset in the regression function. SAFY shows a better performance than GRAMI with lower EEP and EER.

A complete summary with the goodness-of-fit parameters for both models is presented in Appendix F.

5.6 Comparison between calibration approaches regarding yield crop estimation

5.6.1. Sensitivity analysis of LUT and PSO to LAI data

The robustness of LUT and PSO to calibrate GRAMI and SAFY was assessed using synthetic LAI data. We tested different levels of: random error, temporal frequency and data gaps (§ 4.7.4). The sensitivity of both techniques was assessed by calculating the yield estimation error (Figure 32) and the phenological estimation error (Figure 33). These parameters were calculated by comparing reference data with the estimations obtained by the calibrated GRAMI and SAFY models.

In Figure 32, we combined two types of plots: the violin plot which represents the kernel probability density of the data (Hoffmann, 2015) and the box plot which describes the distribution of the data through their quartiles. In each plot, the distribution of the yield error is identified with a black contour line: complete for GRAMI and dashed for SAFY.

In Figure 32 (a) is depicted the effect of LAI frequency in the performance of the LUT technique for a constant random error of 20%. The reduction of the number of LAI observations from 12 (frequency of 10 days) to 5 (frequency of 25 days) showed a steadily increase of the variability of the yield estimation error. This trend was stronger in GRAMI than in SAFY. The increase of the standard deviation of the yield estimation error between the LAI frequency of 10 days and 30 days was 45% for GRAMI and 33% for SAFY.

As mentioned above, SAFY showed less sensitivity to LAI frequency than GRAMI. This behavior was also observed for PSO technique (Figure 32 d). The variability of the yield estimation error for SAFY was, practically, not modified along the first four LAI frequencies tested. On the other hand, for GRAMI the trend of yield error is similar to LUT approach. We observed, in most of the cases, an error distribution more compact for SAFY than GRAMI.

Based on the sensitivity analysis we can state that a LAI frequency no larger than 15 days is suitable to calibrate GRAMI and SAFY by using LUT approach. For PSO the LAI frequency should be no larger than 20 days. The frequencies above suggested are valid as long as the LAI observations are well distributed along the crop season.

The effect of LAI gaps in the calibration of GRAMI and SAFY models is presented in Figure 32 (b) and (e). The largest variability of the yield estimation error was obtained when SAFY and GRAMI were calibrated using a LAI data series with gaps in crop emergency. The lack of LAI observations in the growing period had direct impact in the accuracy of calibration of phenological parameters such

as GDDem and growth parameters such as LUE, A and B. Consequently, the synthesis of biomass from emergency to anthesis was incorrectly simulated.

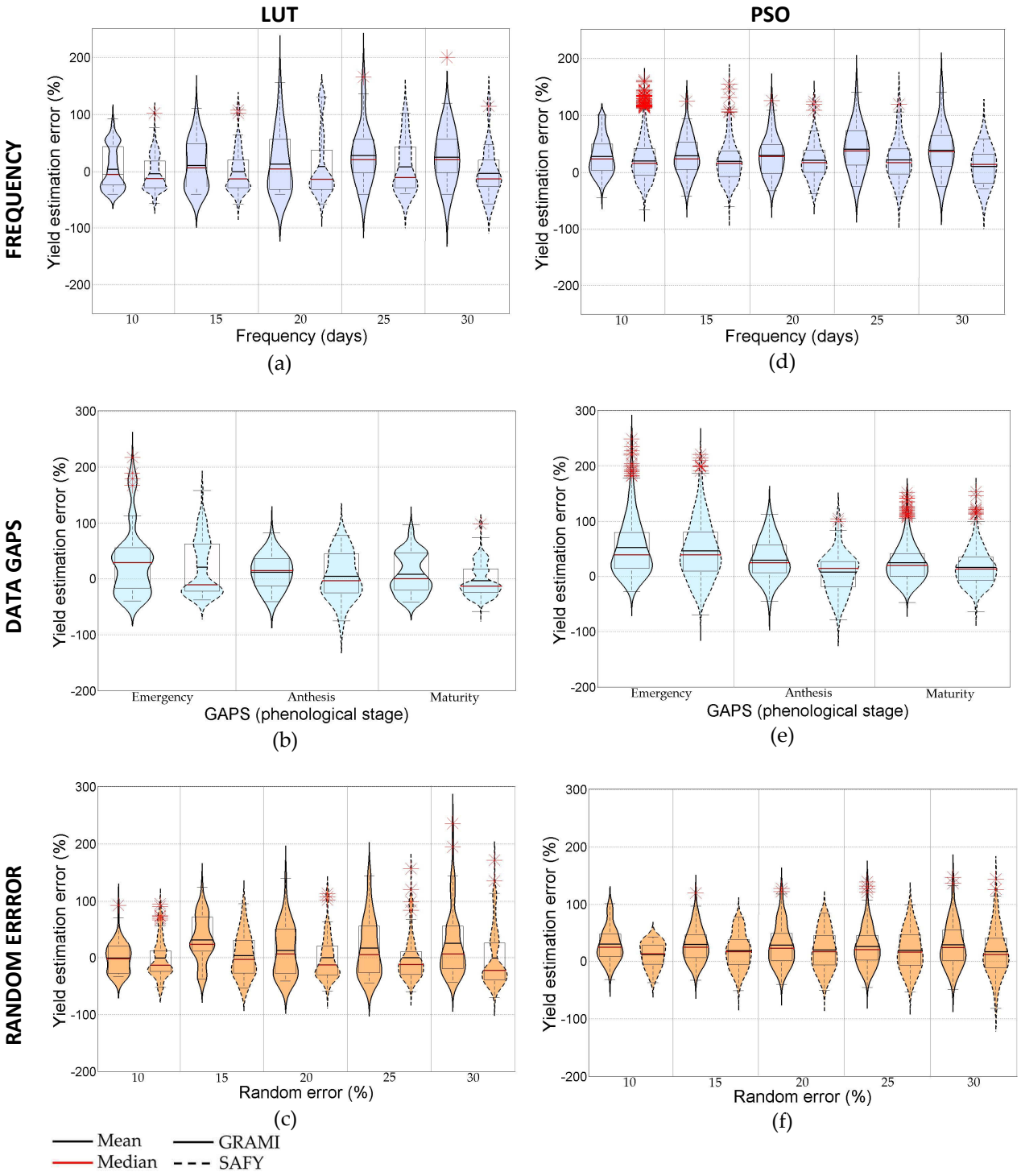

Figure 32. Yield estimation error by GRAMI and SAFY models calibrated using iLUT (a, b, c) and PSO (d, e, f) techniques and LAI with different levels of temporal frequency, data gaps and random error respectively.

The effect of LAI gaps in anthesis and maturity had less impact in yield crop estimation. This trend was observed for LUT and PSO.

Comparing the calibration techniques, we observed that the yield error estimation showed a distribution more symmetric in PSO than in LUT approach. However, a larger number of outliers were noticed in PSO. This difference is related with the calibration technique. In LUT the levels of each parameter are set before the calibration in order to generate a table of simulated LAI data. On the other hand, in PSO the parameter levels are not set beforehand. The combination of parameter levels is only constrained by the maximum and minimum thresholds set for each parameter. This greater degree of freedom might explain the larger number of outliers observed.

Finally, in Figure 32 (c) and (f) is depicted the sensitivity of LUT and PSO to random error of the LAI data. The figure shows a direct relationship between the random error of the LAI data series and the yield estimation error.

A larger variability was noticed for GRAMI model. The mean error showed a tendency to overestimate maize yield for both calibration techniques. On the other, for SAFY the overestimation was only observed in PSO technique. For LUT, the error had a mean value close to 0.

Finally, in Figure 32 (c) and (f) is depicted the sensitivity of LUT and PSO to random error of the LAI data. The figures show a direct relationship between the level of random error and yield estimation error.

A larger variability was noticed for GRAMI model. The mean error indicates the tendency to overestimate maize yield for both calibration techniques. On the other hand, in SAFY the overestimation was only observed in PSO technique. For LUT, the mean of the yield estimation error was close to 0.

Based on the results of our experiment, we suggest as rule of thumb a tolerance of the LAI random error of 20%. This threshold is more relevant when the crop yield is estimated using GRAMI and the model parameters are calibrated by LUT approach.

The robustness of LUT and PSO assessed as phenological estimation error is presented in Figure 33. The phenological error was calculated by comparing the reference value of GDD to anthesis with the estimation obtained by the calibrated SAFY model. This error estimator allowed us to evaluate directly the accuracy of GDD to anthesis estimation and indirectly the accuracy of other parameters such as GDD to emergency and parameters related with biomass partition such as A and B which are directly related with crop phenology.

As showed in Figure 33 some outliers have been registered in our experiment. The value -100% indicates that the estimation of the GDD to anthesis by the calibrated CGM is equal to 0. Then, based on this simulation the crop had only a growing period and did not reach anthesis. On the other hand, a value larger than 100 indicates a strong overestimation of the GDD to anthesis in relation to the reference value. In these cases the calibrated CGM simulates a long growing period followed by an extremely short period of anthesis + senescence which is constrained by the daily temperature at the end of the crop season.

In Figure 33 (a) and (c) is presented the effect of LAI gaps in the calibration of GRAMI and SAFY models. The data series LAI used had a constant random error of 20%.

The maximum variability of the phenological estimation error was reached when SAFY model was calibrated using a LAI data series with gaps in crop anthesis. This trend was observed in LUT and PSO techniques. The number of outliers in LUT technique represented only 8% of the total cases analyzed. On the other hand, in PSO the percentage of outliers reached 14%. This is explained by the greater degree of freedom of PSO technique during the optimization procedure as explained above.

Moreover, regarding the mean phenological error, we verified that for LUT the mean value for the three cases considered was 0, while for PSO a tendency to overestimation of the GDD to anthesis was observed. Overall, PSO showed more sensitivity to LAI gaps regarding GDD to anthesis estimation.

The robustness of LUT and PSO regarding the LAI random error is depicted in Figure 33 (b) and (d). The effect of the random error in the estimation of GDD to anthesis is similar for both calibration techniques. The variability of the error increase gradually along the five levels tested. For LUT the mean of the phenological error estimation is close to 0 for all the cases analyzed.

Regarding PSO technique, we detected a larger number of outliers in relation to LUT. Moreover, the mean of the error has a tendency to overestimate the GDD to anthesis as was observed in Figure 33 (c). The number of outliers increased together with the LAI random error. However, they represent less than 15% of the total of cases analyzed for a LAI random error of 30 %.

Based on the results obtained and aiming to estimate accurately crop phenology, we recommend the calibration of GRAMI and SAFY parameters by using LAI data series with an average random error lower than 20%.

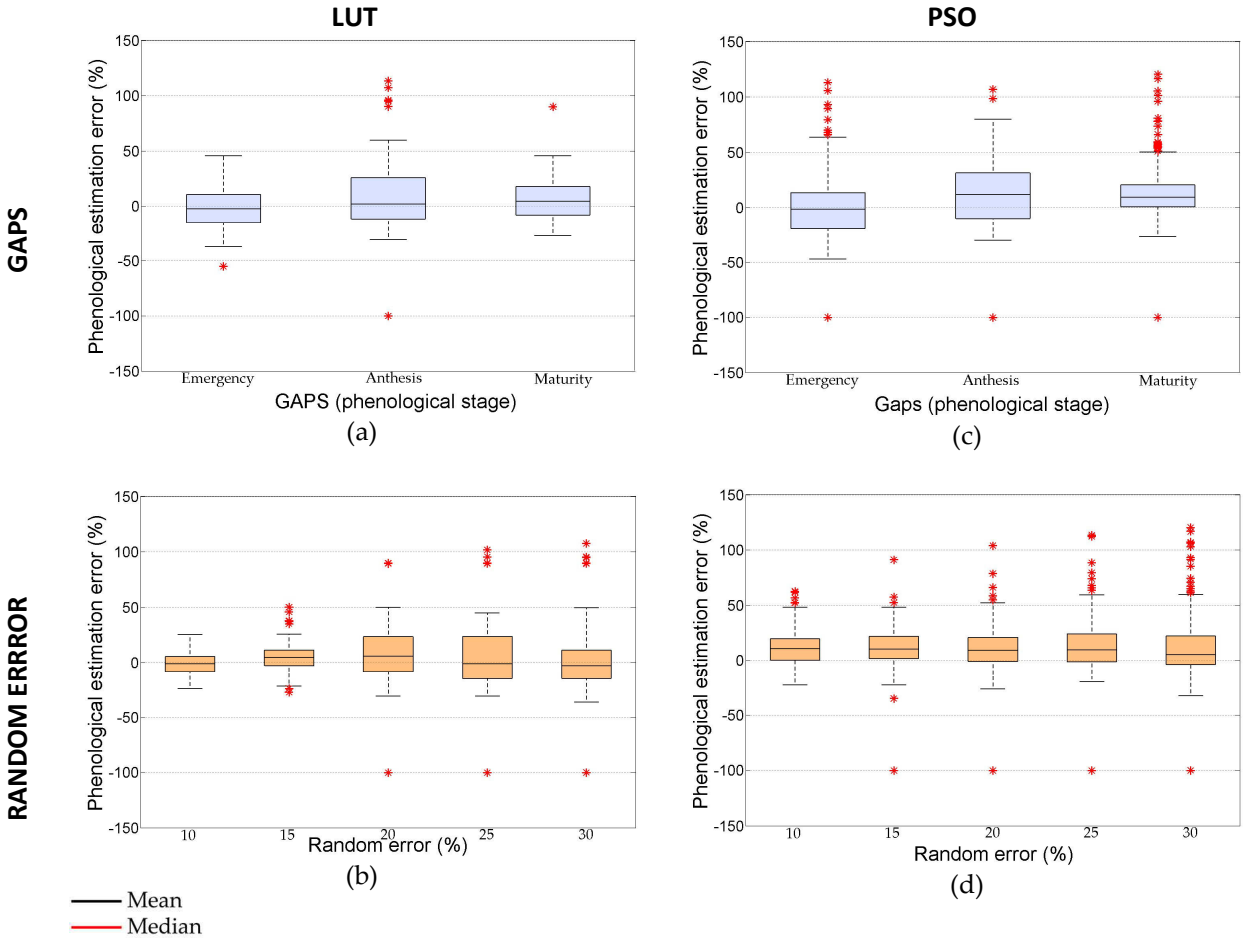

Figure 33. Phenological estimation error by SAFY model calibrated using iLUT (a, b) and PSO (c, d) techniques and LAI with data gaps and different levels of random error respectively.

5.6.2. Crop yield estimation

A summary of the best calibration strategy for each CGM is presented in Table 20. The goodness-of-fit parameters considered for the selection were EEP, EER and NRMSEf (in order of relevance).

The best yield accuracy for GRAMI model was achieved using the iLUT approach at pixel scale with 5 free parameters (Figure 28c). In Table 20 is verified that EEP and NRMSEf values are lower than the

values obtained by the GRAMI calibrated by PSO. On the other hand, the best yield accuracy for SAFY was reached by using PSO at pixel scale with 6 free parameters (Figure 31f).

SAFY + PSO was the best of the four strategies presented in Table 20 with a reduction by 32% of EEP and 46% of EER in relation to GRAMI + iLUT. The regression function was also improved with a reduction of NRMSEf. However, the average time required for running the routine SAFY + PSO is 8 times larger than GRAMI + iLUT. This computational demand might hamper the use of this strategy at regional scale.

Table 20. Goodness-of-fit parameters for the best iLUT and PSO strategy for GRAMI and SAFY models

CGM	**GRAMI**		**SAFY**	
Calibration	**iLUT**	**PSO**	**iLUT**	**PSO**
Scale	**plot + pixel**	**plot + pixel**	**plot**	**plot + pixel**
N° FP plot	**10**	**7**	**11**	**8**
N° FP pixel	**5**	**2**	**-**	**6**
Slope	1.09	1.23	0.81	1.03
Offset	-13.7	-20	15.9	-5.6
R^2	0.86	0.72	0.61	0.9
NRMSEf	10.2	14.5	17.2	8.5
EER	10.3	4.5	0.6	5.6
EEP	12.3	13.4	15.7	8.3

FP: free parameters

5.6.3 Crop yield forecasting

Crop yield forecasting is of high relevance in the agricultural sector. For this reason, the performance of calibrated CGMs by iLUT and PSO techniques was tested to estimate crop yield in two scenarios: two and one month before harvesting. Historical meteorological data (HD) was used to simulate meteorological conditions for both scenarios. Regarding the iLUT technique, the effect of using a complete LUT was assessed (in which all the parameters were free) compared to a reduced LUT in which GDDmt and senescence parameters were fixed to regional average values. This last approach had the goal of assessing the effect of uncertainty in parameter calibration in a scenario without LAI observations at the end of the crop season. In Table 21 the forecasting accuracy of both CGMs calibrated by iLUT and PSO are compared. The lowest EER and EEP values for each category are highlighted.

Table 21. Comparison iLUT and PSO yield estimation accuracy two and one month before harvesting

	EER (%)		EEP (%)	
	GRAMI	SAFY	GRAMI	SAFY
	2 months before harvesting			
iLUT	***6***	17.4	21	29.8
PSO	19	7.13	25	**16.4**
	1 month before harvesting			
iLUT	10.1	4.5	21.5	19.3
PSO	17	**3.03**	23	**15.2**

SAFY shows a good performance in both scenarios when calibrated by PSO approach. The regional yield was estimated more accurately than at plot scale thanks to the errors compensation. For

GRAMI the best performance was obtained using a reduced LUT in which GDDmt and senescence parameters were fixed.

5.7 Yield estimations using updated GRAMI and SAFY models

Updating was implemented using pixel LAI data and the calibrated GRAMI and SAFY models. The updating approaches tested were ensemble Kalman filter (EnKF) and particle filter (PF). The models were calibrated previously using iLUT and PSO techniques as described above.
This section introduces first the sensitivity analysis for both filters. Then, the yield estimations obtained by updating techniques are presented and discussed.

As discussed in chapter 3 (§3.6.7), aspects related to ensemble size, model and observations errors, among others factors have high influence in the performance of updating techniques. We developed an innovative experiment to assess the effect of the above mentioned factors on the updating of LAI in GRAMI and SAFY models.

5.7.1 Parameter sensitivity

The effect of the ensemble size as well as the overestimation and underestimation of model and observation errors were tested in EnKF and PF. Being aware of the filtering divergence drawback, two approaches of PF were implemented: a resampling and a non-resampling technique (§4.10.2).

The influence of ensemble size was measured by assessing the variability of the updated LAI values for different ensemble sizes. The filters were run 100 times for each ensemble size, then, the global variability of the updated data was calculated.
The variability of updated LAI for EnKF according to ensemble size is depicted in Figure 34 (a). A strong reduction in the variability is achieved with an ensemble size of 200 particles. For this ensemble size, the LAI updating becomes more stable for a given model and observation error. On the contrary, a larger ensemble size reduces the updating variability in a lower rate, however, increases unnecessarily the demand of computational resources.

The effect of ensemble size is more erratic for PF (Figure 34 b). The reduction of the global variability for the updated data did not show a relation to the ensemble size. This could be related to the working principle of PF in which only a model ensemble is included. In PF, the observation is represented by a unique random value instead of an ensemble of observations as in EnKF.

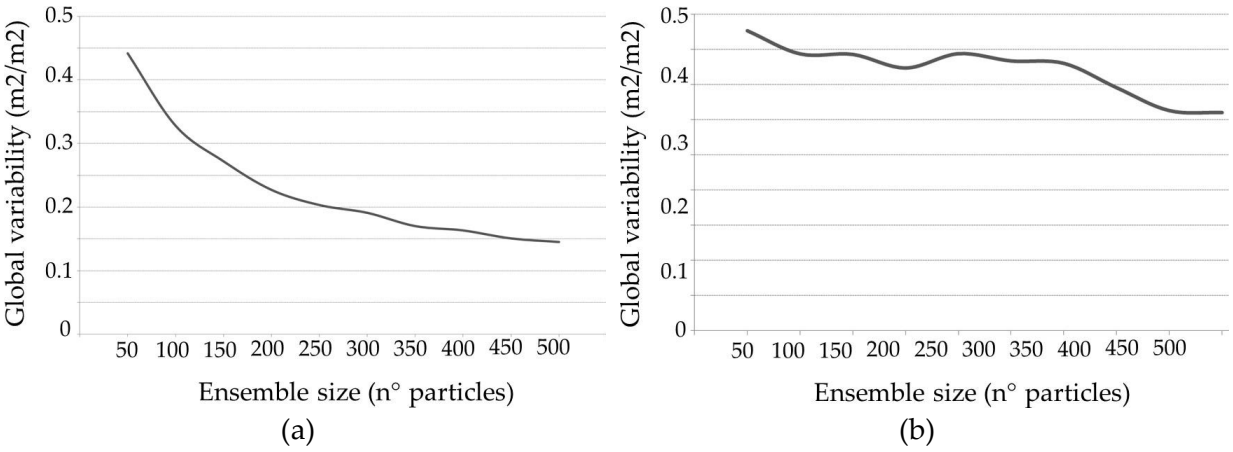

Figure 34. Variability of updated LAI according to the ensemble size of EnKF (a) and PF (b).

The error levels of model and observations are essential parameters in the updating process. Therefore, they must be correctly set before running EnKF and PF. As described in section 4.10.1, a

reference CGM was used to generate a synthetic LAI data series. A non-calibrated CGM ("CGM to update") was simulated by modifying the reference LUE value. The model and observation errors were calculated by comparing synthetic LAI observations and simulations by the "CGM to update" with the reference LAI data series. The effect of overestimation and underestimation were simulated for a range of ± 50% of the reference errors for the model and the observations.

The percentage of variation of LAI error between updated CGM and reference CGM for EnKF and PF with overestimated or underestimated model and observation errors is sketched in Figure 35: (a) observation error and (b) model error.

The effect of underestimation of the observation error is similar for EnKF and PF, with an error increase of 20 %. The underestimation error has a direct consequence in the misrepresentation of observation variability during the updating process. On the other hand, a sharply different trend is observed for an overestimation of the observation error; while for EnKF the overestimation reduces the error of the updated LAI, for PF the error increases. This difference is related to the principle of each filter. In EnKF the updating is carried out using two ensembles, observation and model. Hence, increasing the observation error allows a better representation of its variability. However, it is important to highlight that the increase of the observation error requires the increment of the ensemble size to achieve a good representation of observation's variability. Therefore, the demand of computational resources is also increasing.

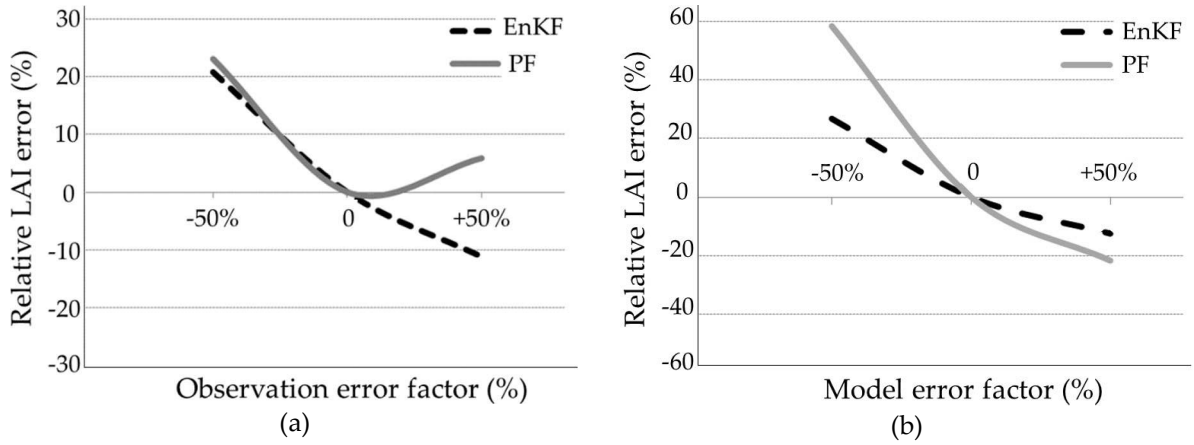

Figure 35. LAI updating error according to observation (a) and model (b) overestimation and underestimation error.

On the other hand, for PF, the LAI observation is simulated using a unique value. The "simulated observation" is calculated using the retrieved LAI from EO-data, its estimation error, and a Gaussian noise. Therefore, an excessively large error could generate a non-expected simulation of the LAI observation. Then, the raise of the observation error, does not necessarily improve the performance of PF, although the observation error has a lower impact in the updating process compared to the underestimation error.

Regarding the effects of model errors, Figure 35 (b) shows a similar behavior for both filters. An underestimation has a negative impact due to the underrepresentation of the model's error. The impact is stronger for PF with a reduction of the LAI updating accuracy of around 60%. Any model error overestimation has for both filters a positive effect reducing the error 12% for EnKF and 21% for PF. It is important to highlight the different slopes between overestimation and underestimation sections. The underestimation of the model error has a stronger effect in the updating performance, thus, it is crucial to implement an accurate model error.

A representation of updating techniques by EnKF and PF is shown in Figure 36. The LAI curve corresponding to the CGM "to update" (gray line) is clearly shifted towards the reference LAI curve as a response of the strong influence of LUE in the LAI simulation. The LAI observations show a larger variability from the second half of the growing period to anthesis. The red-dashed curve corresponds to the LAI data series simulated by the updated CGM.

The main difference between filters shown in Figure 36 is the degree of fitting between the updated curves and the LAI observations. The CGM updated by EnKF follows tightly the LAI observations. On the other hand, the LAI updated by PF are smoother with a larger mismatch between simulated and LAI observations. The global error is 20% lower than the CGM updated by EnKF.

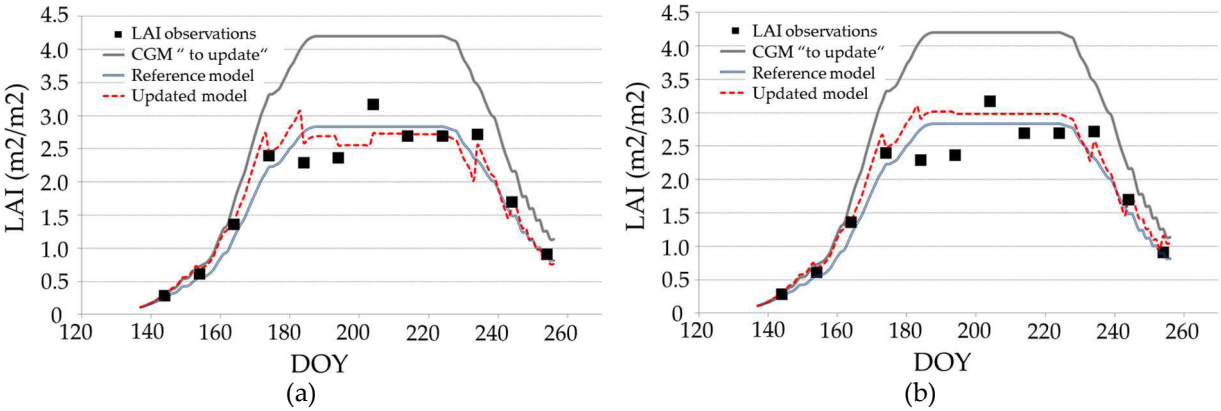

Figure 36. Comparison of updating techniques; (a) EnKF, (b) PF.

Regarding the yield estimation error, the best fit was obtained by EnKF. As the LAI reference is overestimated and underestimated in different ranges along the crop season, the impact of the error in the yield estimation is reduced. This direct relationship between LAI and yield estimation is applicable only in this case because the CGM parameters are constant in both examples.

The improvement of yield estimation by updating is significant for both models. The yield estimated by the CGM "to update" was modified from 122 (q/ha) to 94 (q/ha) for the model updated by EnKF and 98 (q/ha) for the model updated by PF. This represents a reduction of yield estimation error in relation to the reference value of 50% and 39%, respectively.

5.7.2-Yield estimation

The EnKF and PF were implemented in the GRAMI and SAFY models calibrated by the iLUT and PSO techniques. An ensemble size of 200 particles was used for EnKF and PF resampling (PF r) and 500 particles for the PF non-resampling (PF nr).

The RMSE calculated between the LAI field measurements and the LAI estimations by the CLAIR model (§ 5.2) was used as observation error in the updating process. The model error was estimated using pixel data. First, the NRMSE between LAI observations from each pixel and LAI simulated by the calibrated CGM at plot scale was calculated. Then, the maximum NRMSE value was selected as model error. The goal of calculating the error at pixel scale was to incorporate the intra-plot variability in the updating process considering that for the parameter calibration an average LAI data series was used as representative for the plot.

The results obtained for each filter in combination with CGM and calibration technique are presented in Table 22. The best result was achieved by SAFY + PSO + EnKF (highlighted in italic-bold). A similar regional and plot accuracy was obtained by SAFY + PSO in combination with PF nr and PF

r. These three techniques, using SAFY model, outperformed all the calibration and updating combinations tested for GRAMI. Additionally, low EEP and EER errors were obtained by using the iLUT calibration (SAFY + iLUT + EnKF). Together, this proves the strong influence of the CGM on the yield estimation accuracy independently of the calibration technique.

Regarding the effect of resampling in PF, we found that using a large ensemble (PF nr) or a resampling (PFr) technique had low impact on PF performance.

The effect of updating on the yield estimation accuracy is compared in Table 23. The calibration techniques implemented at plot scale for each CGM are contrasted with the combination CGM + calibration + updating at pixel scale.

Table 22. Goodness-of-fit parameters for combinations CGM + calibration + updating

CGM	**GRAMI**						**SAFY**					
Calibration	**ILUT**			**PSO**			**ILUT**			**PSO**		
Filter	**EnKF**	**PF nr**	**PF r**	**EnKF**	**PF nr**	**PF r**	**EnKF**	**PF nr**	**PF r**	**EnKF**	**PF nr**	**PF r**
Slope	1.23	1.19	1.12	0.95	1.01	1.03	1.04	1.02	1.03	**1.04**	1.03	1.03
Offset	-17.3	-14	-10.2	-10.1	-13.8	-16	-4.6	0.75	1.8	**-3.7**	-3.5	-3.6
R^2	0.73	0.69	0.65	0.79	0.8	0.80	0.77	0.73	0.69	**0.84**	0.8	0.81
NRMSEf	14.3	15.3	16.3	12.5	12.6	12.3	13.4	14	15.9	**11.2**	12.2	11.9
EER	2.9	0.9	3.4	21.1	18.3	19.5	3.6	1.4	4.3	**2.3**	2.7	3.3
EEP	13.0	13.7	14.4	21.9	19.5	20.4	11.7	12.8	14.6	**9.7**	10.7	10.5

The performance of the GRAMI + iLUT was not improved by updating. The goodness-of-fit parameters between calibrated and calibrated + updated CGM are similar. Regarding GRAMI + PSO, updating increased the correlation between estimated and simulated yield by 7 %. However, the error at plot and pixel scale (EEP and EER) was raised. Overall, updating was not able to improve the performance of the calibrated GRAMI model.

On the other hand, for SAFY + iLUT the updating at pixel scale allowed improving the correlation between simulated and observed yield. The NRMSEf was reduced by 16 % and the EEP by 17 % in relation to the SAFY calibrated at plot scale. In the same direction and with similar proportion was improved the accuracy of the SAFY model calibrated by PSO with reduction by 15% and 18% for NRMSEf and EEP respectively.

Table 23. Comparison of calibration techniques at plot scale with the combination CGM + calibration + updating at pixel scale for each CGM.

	GRAMI				**SAFY**			
Calibration	**iLUT**		**PSO**		**iLUT**		**PSO**	
Updating	**-**	**EnKF**	**-**	**PF r**	**-**	**EnKF**	**-**	**EnKF**
Slope	1.07	1.23	0.88	1.03	0.81	1.04	0.86	1.04
Offset	-5	-17.3	0.67	-16	15.9	-4.06	11.6	-3.7
R2	0.73	0.73	0.76	0.80	0.61	0.77	0.75	0.84
NRMSEf	14.3	14.3	13.5	12.3	17.2	13.4	13.8	11.2
EER	3.2	2.9	14.4	19.5	0.6	3.6	0.2	2.3
EEP	12.9	13	17.4	20.4	15.7	11.7	12.5	9.7

Based on Table 23, we can state that updating could improve the yield estimation, however, the reached accuracy depends largely on the ability of the CGM to simulate the real crop conditions, as well as the values of the fixed and calibrated parameters and the driving variables used in the estimation. In our experiment, the filters acted as a fine tuning which allowed adding extra information from pixel data.

The scatter plots of the combination SAFY + PSO + EnKF and SAFY calibrated at pixel scale by PSO with three free parameters are compared in Figure 37. This strategy was preferred instead PSO with six free parameters, because, non-correlated parameters are calibrated at pixel scale. Therefore, this technique is comparable with updating in which a Gaussian error and calibrated LUE value were used to generate the model ensemble.

The main difference between the techniques is the variability of the yield estimations. Calibration + updating showed a lower variability because, in contrast to PSO, the model parameters have not been calibrated as only the LAI was updated.

The combination SAFY + PSO + EnKF improved NRMSEf and EEP by 16% in relation to SAFY + PSO with 3 free parameters. Additionally, the computational demand for updating was markedly lower in relation to the PSO routine: 2 hours for PSO against 7 minutes for updating.

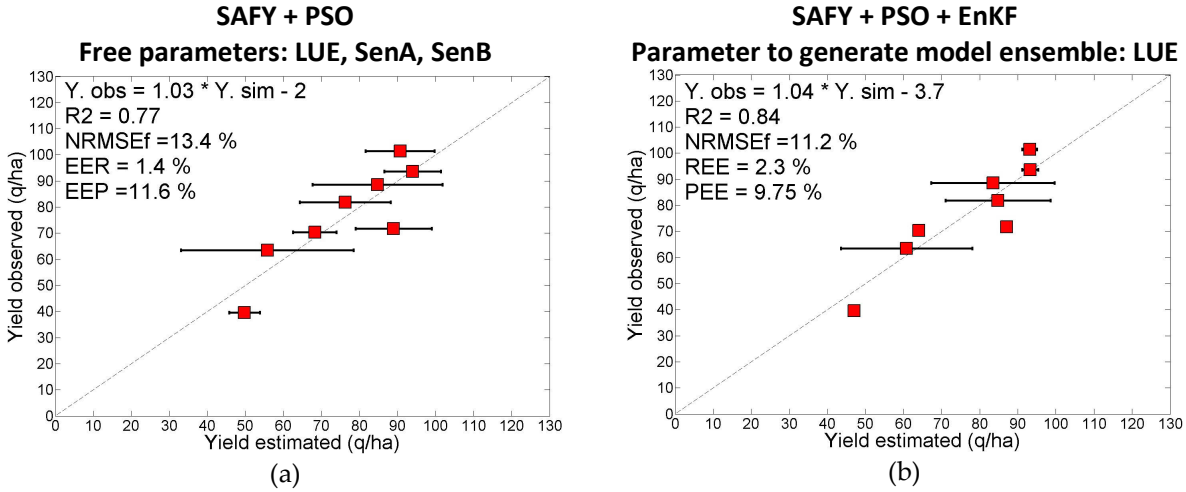

Figure 37. Comparison of calibration and updating between (a) SAFY + PSO at pixel scale using three free parameters and (b) SAFY + PSO + EnKF.

5.8 Validation of GRAMI and SAFY parameters

As introduced in section 4.11, we validated the performance of the calibrated GRAMI and SAFY models using an independent remotely sensed FAPAR dataset and the Monteith equation (Monteith, 1977). The CGM parameters used in the Monteith equation were LUE and the phenological parameters: crop emergency and maturity. Three sources of phenological data, to define the FAPAR integration period, and two type of LUE, to convert FAPAR in biomass, were compared in all their combinations. In Table 24 is presented a detail of the parameters used in the Monteith equation.

Table 24. Phenological data source and LUE used in the Monteith equation

Source of Phenological data	LUE (calibration scale)
Derived by filtering	Regional
Field observations	Plot
Calibrated in CGM	

The effect of the source of phenological data and LUE on the yield error estimation at plot scale (EEP) by Monteith equation is depicted in Figure 38. The error trend is similar for the estimation using the LUE calibrated at regional and plot scale. The variability of EEP is larger between different sources of phenological data. Therefore, in our experiment the correct estimation of the FAPAR accumulation period (emergency to maturity) had higher influence in the accuracy of the yield estimation than the type of LUE implemented.

The most accurate yield estimation was obtained using LUE and phenological cardinal points extracted from the calibrated SAFY model. The goodness-of-fit parameters between reference yield and the estimations by Monteith equation are similar to SAFY + PSO + EnKF introduced above. Therefore, we verified that LUE and the phenological parameters calibrated in SAFY model are valid to estimate maize yield using independent EO data.

The scatter plot of most accurate yield estimation by integrating FAPAR data series is represented in Figure 39. In Appendix G are presented the goodness-of-fit parameters for the complete experiment.

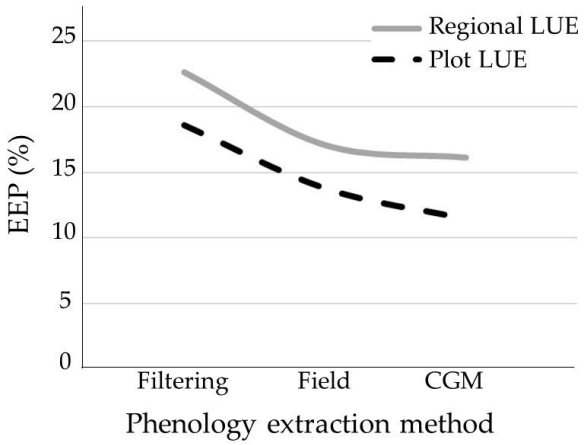

Figure 38. Effect of the phenology extraction method and LUE on the yield estimation error at plot scale (EEP) using Monteith equation.

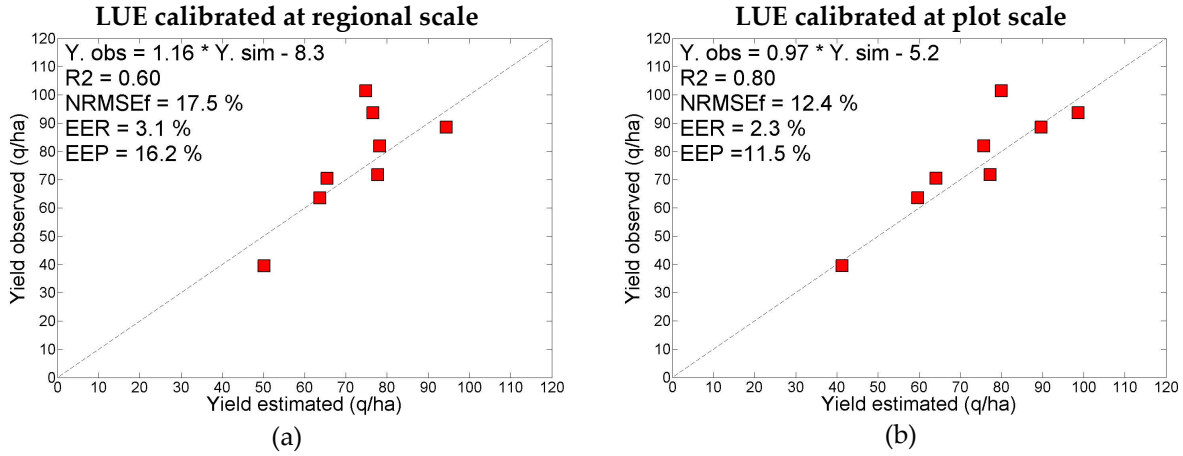

Figure 39. Comparison between observed and estimated yield by Monteith equation and FAPAR data using a) LUE calibrated at regional scale and b) LUE calibrated at plot scale.

5.9 Verification

The calibration and updating techniques were verified using a group of eight maize plots for the season 2014. The official average yield estimation for the county of Gänszendorf by Statistics Austria was 90 q/ha (0 % humidity). This represents an increase of 16.6 % in relation to the season 2013.

One of the most important differences between the seasons 2013 and 2014 was the phenology of maize crop. In 2014 the crop emergency had an average delay of 15 days with respect to the previous season (2013). Therefore, the sowing date in LUT was modified to a range from 100 to 140 DOY. Moreover, LAI observations pointed a longer growing season for 2014 with relatively high LAI values till end October. Being aware of this seasonal difference, the maximum GDD to maturity was increased in the LUT from 1580 to 1780 GDD. These two modifications allowed improving the yield estimations markedly, proving the relevance of defining a broad range of phenological parameters for CGM calibration.

The delay in maize emergency might be related to meteorological conditions. In 2013, a larger cumulative precipitation from January to May is observed (Figure 15). Therefore, the soil humidity conditions at the early season were more favorable for plant emergency in 2013 than in 2014. The mean temperatures for the emergency period (April-May) were similar in both seasons. The total precipitation from May to October was 22 % larger in season 2013 compared to 2014. However, it is worth mentioning that most of the maize fields in the study area are irrigated.

The extended maize cycle in 2014 might be the result of an higher monthly average temperature in June, July, September and October compared to 2013 (Figure 15). The cumulative GDD for maize season was 7 % larger in 2014 compared to the previous year.

The best calibration technique as well as combination calibration + updating for each CGM are depicted in Table 25. The goodness-of-fit parameters for the complete experiment are presented in Appendix H.

Some differences and similarities were observed compared to 2013. For instance, for the GRAMI model, the best iLUT performance was obtained by using the first iteration instead of the best iteration as in season 2013. However, most of the findings of 2013 matched with season 2014. The best calibration technique for GRAMI was iLUT while for SAFY, the PSO proved more efficient. Overall, SAFY showed again a better performance than GRAMI.

Table 25. Best calibration and calibration+ updating approaches for GRAMI and SAFY models for season 2014.

CGM	**GRAMI**		**SAFY**	
Calibration	**iLUT**		**PSO**	
Updating	**-**	**EnKF**	**-**	**PF**
N° FP plot	**10**	**10**	**8**	**8**
N° FP pixel	**2**	**-**	**3**	**-**
Slope	1.16	0.69	0.59	0.62
Offset	-4.5	32.3	34.8	28.9
R^2	0.5	0.5	0.68	0.73
NRMSEf	10.2	9.9	8.1	7.45
EER	15.9	18.6	7.9	1.63
EEP	12.8	15.4	10.1	11.1

FP: free parameters

The combination SAFY + PSO yielded the best accuracies at regional and plot scales. The EEP and EER values were similar in both seasons.

The accuracy of SAFY + PSO + the three filters was similar, however, a slight improvement in the regression function was obtained by using PF (Appendix H). On the other hand, for 2013, the best

performance was achieved by coupling SAFY + PSO + EnKF. Additionally, the combination SAFY + iLUT + PF yielded also good results, though, with lower R^2 and higher NRMSEf compared to the combination using PSO. Nevertheless, this alternative, in which PSO is replaced by iLUT, has a low demand of computational resources, thus, it is more suitable for regional applications.

In Figure 40 are shown the scatter plots for (a) the SAFY + PSO + PF approach for season 2014, (b) SAFY + PSO + EnKF for 2013 for grain and seeds production, and (c) for only the grain production in 2013.

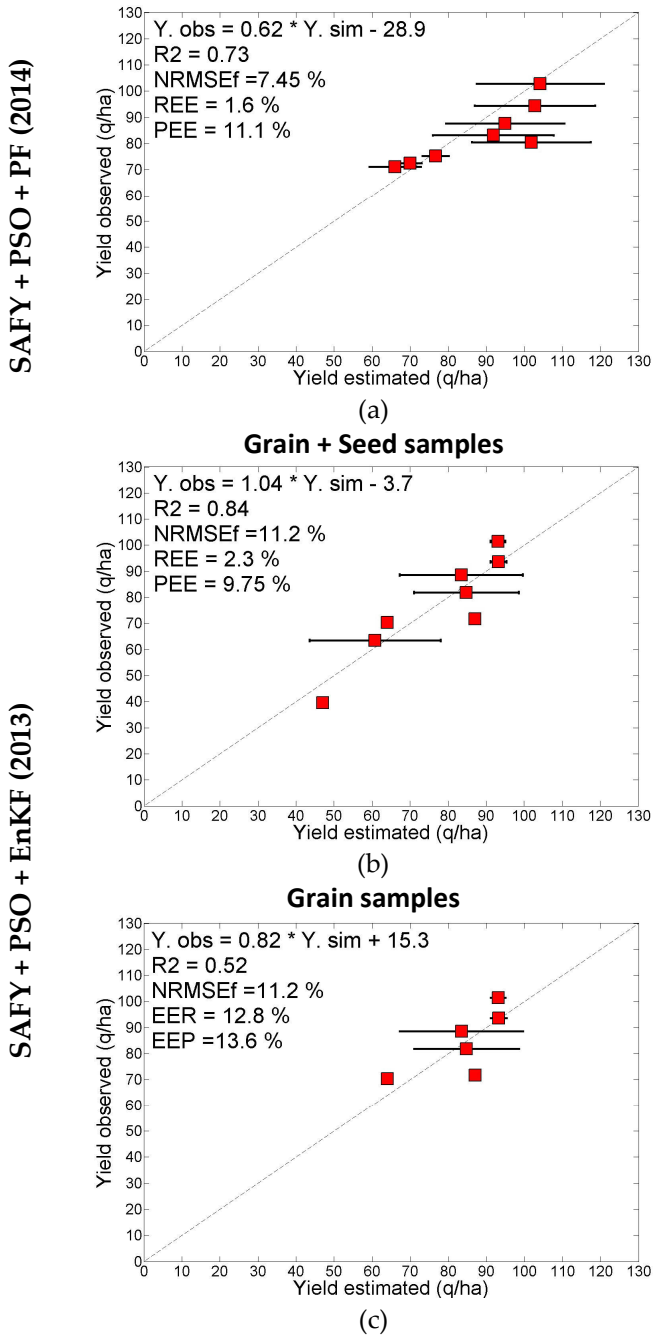

Figure 40. Scatter plot of technique SAFY + PSO + PF for season 2014 (a), SAFY + PSO + EnKF for season 2013 for grain and seed production (b) and grain production (c).

Figure 40 shows a good fitting between observed and estimated yield for season 2014 (a). A higher disagreement is observed for samples with yields larger than 80 (q/ha). For this group of

samples, the yield was overestimated. Additionally, the chart shows a larger variability of the yield estimations with respect to 2013; the average CV was increased by 22%.

Compared to 2013, the regression functions obtained in 2014 have a lower slope and larger offset. The R^2 is also lower (0.6 to 0.7) compared to 2013. However, if one only considers the maize plots for grain production, the regression functions between seasons are similar (Figure 40 c). The best fit between observed and estimated yield was found for a larger range of maize yield, from seed to grain production as observed in season 2013 (40 q/ha to 100 q/ha; 0 % humidity).

5.10 Discussion

5.10.1. Reference data of maize yield

The correct assessment of the yield estimation error is conditioned by the reliability of the reference data. We detected some error sources in the yield reported by the farmer and in the estimations by field sampling.

The main source of uncertainty of the maize yield informed by the farmers was the percentage of humidity of the harvested grain. When this datum was not reported by the farmer, we used a reference value of 14% (commercialization humidity of maize). Additionally, in some cases, the yield was reported as complete maize cob. Therefore, we used an empirical factor to express yield as maize grains. These sources of uncertainties can modify noticeably the value of maize yield.

Regarding the yield estimation by sampling in field, the main source of uncertainty was the identification of a representative cob for each sample point (Appendix A). We observed a large variability of the cob size in a short distance. Consequently, the yield was estimated with a large variability (Figure 23). The main advantages of field sampling were the possibility to calculate the yield variability and its spatial autocorrelation (Appendix A). The main disadvantage is the demand of human resources. This hampers its application in large regions.

5.10.2. LAI observations

As introduced in chapter 3, the assimilation of EO data in crop models is affected by factors such as the spatial resolution and the timing of the EO data and the error of the retrieved state variable, among others.

In our experiment the timing of the estimated LAI was well synchronized with maize crop phenology. The average frequency of LAI was 15 days; 10 observations in 2013 and 12 observations in season 2014. Therefore, an average frequency of EO data between 10 and 15 days seems suitable for maize crop monitoring.

No gaps were identified along the season. This was achieved using Landsat 5TM and DEIMOS data for season 2013 and Landsat 5TM, Landsat 8OLI and DEIMOS data for season 2014. The availability of enough LAI observations along the crop season allowed estimating accurately phenological stages such as sowing, emergency and maturity. This finding reinforces the promising results obtained by the integration of multi-source EO data in CGMs (Dente et al., 2008; Liu et al., 2014b).

Regarding the spatial resolution of the EO-data, we noticed that the pixel size of 30 m (Landsat) and 22 m (DEIMOS) was not suitable for some small plots in the study area. Therefore, to avoid the effect of mixed pixels, we discarded the plots smaller than 3.5 ha or with strip shape.

A strategy to reduce the effect of temporal and spatial resolution in EO data assimilation might be the fusion of multi-source data. The fusion algorithms allow combining fine and coarse resolution images to generate high temporal resolution data at the finer spatial scale (Gao et al., 2006; Meng et al., 2013;

Zhu et al., 2010). Moreover, a new perspective to overcome this problem is the free availability of imagery from Sentinel 2 with 10 m spatial resolution (Immitzer et al., 2016).

Finally, the error of the retrieved LAI by CLAIR model (Vuolo, et al. 2013) was calculated using field measurements for a broad range of maize samples (Figure 23). The RMSE level obtained is comparable with other research findings (Nguy-Robertson et al., 2012; Casa et al., 2010; Duan et al., 2014).

5.10.3. Reference GRAMI and SAFY parameter values

The range of GRAMI and SAFY parameters used in LUT and PSO were suitable to simulate the variability of the maize plot in the study area (Table 12). The reference ranges can be modified using ancillary data from field measurements or from parameter calibrations in previous crop seasons. The narrower fit of parameter ranges allows increasing the calibration accuracy and reducing the burden of data processing. That is valuable when the CGMs are applied in large regions.

Regarding phenological parameters, we set a range of sowing date, GDDem and GDDmt based on field observations of season 2013. However, these ranges were not suitable for season 2014 (§5.9). Therefore, we recommend defining beforehand a broad range of phenological parameters to capture better the crop variability along different seasons.

Crop yield was estimated by using total biomass and the harvest index. The value used was 0.48 and was fixed for both crop seasons. However, the harvest index value is affected by environmental factors (climate and soil) and management factors such as plant density, hybrid, fertilization and irrigation among others (Hay, 1995; Payero, et al., 2009).

The possible sources of the harvest index variability in our experiment were related, mainly, with management factors such as fertilization, irrigation and destination of the production, grain or seeds, as mentioned in section 4.4.

Although, we noted differences in management practices between plots, the possible variation of the harvest index had low impact in yield accuracy estimations. We consider that the effect of harvest index variability was compensated by the calibration of the CGM parameters, specifically SLA (specific leaf area, g/m2). Proof of that is the average difference of 20 % between the SLA calibrated for grain plots and seed plots.

5.10.4. Sensitivity of biomass and LAI to parameters variation

As presented in section 5.3.1, biomass estimation is influenced in a higher proportion by LUE. This parameter has main relevance because in simple CGMs such as SAFY and GRAMI is assumed that LUE captures the variability inter- and intra-plot related with management and environmental conditions (Duchemin et al., 2008; Claverie et al., 2012).

Regarding LAI, the parameters with most influence are SLA, A and B. The specific leaf area (SLA) changes with crop age. However, for operational purpose SLA is constant along the crop season. The coefficients A and B drive the partition of biomass to the leaves in the period from emergency to anthesis. They change depending of the type of cultivar and in less proportion on management (Penning, et al. 1989). Aware of it, Padilla et al. (2012) clustered wheat samples based on its phenological similarity and carried out an independent calibration for each group. To reduce the effect of the uncertainty of phenological parameters in the yield estimation accuracy, we decided to implement a calibration strategy at plot scale.

5.10.5. Calibration of GRAMI and SAFY parameters

Iterative Look up Table

The sensitivity analysis carried out for LUT allows defining an optimal combination of cost function and threshold to select the best combination of parameter levels (§5.4.1). The simple cost function showed an acceptable performance without requiring ancillary data. Moreover, the threshold expressed as global error allows selecting a representative number of LUT records for each plot.

Additionally, we proved the effect of filtering the retrieved LAI data series. The smoothed LAI data had a better fitting with the LAI simulations generated by the calibrated SAFY and GRAMI models. Then, the error of the yield estimation was reduced due to the new parameter levels selected. The combination filtering + cost function + threshold criterion was consistent with comparable level of error yield estimation for both seasons.

The iterative LUT (iLUT) technique showed different performance for the CGMs in each crop season. For season 2013 the best accuracy for GRAMI model was obtained by calibrating the parameters using the iLUT. However, for season 2014 the iLUT showed a low performance. The best accuracy was obtained using the initial LUT (Table 12). On the other hand, for SAFY the initial LUT yielded the best results in both seasons.

Aware of the burden of data processing and the meager results obtained by iLUT, we recommend testing a new strategy considering an iterative procedure for a group of samples instead of individual plots. We verified that the maximum LAI and the cumulated GDD from emergency to anthesis were useful to cluster the samples in two groups; plots for seed production and plots for grain production. These parameters could be calculated using the initial LUT. Then, the samples are clustered and the iterative LUT runs independently for each group of samples. This approach can be compared with a global iterative LUT in which all the samples are included in a unique group. We recommend assessing the effect of the parameters dispersion in the accuracy of CGM considering the calibration of multi (inter-) correlated parameters (ill-posed problem).

Particle Swarm Optimization (PSO)

The sensitivity analysis of PSO parameters allowed us to improve the efficiency of the algorithm by modifying some default values, for instance, the maximum velocity particle (MPV) and the maximum number of iterations (MNI). The reduction of MNI for PSO + SAFY from 2000 to 1000 allowed diminishing the time processing by 58% in relation to PSO + GRAMI (MNI=2000).

Moreover, we defined a minimum number of PSO repetitions per plot to reduce the effect of the ill-posed problem in a context of calibration of multiple parameters inter-correlated. This value should be modified if the number of free parameters is lower. For instance, we define a unique PSO repetition when the algorithm was implemented at pixel scale.

The combination PSO + SAFY showed a relatively better performance in relation to PSO + GRAMI, with a lower errors at plot and region scales. This trend was also observed when the algorithm was implemented at pixel scale with a reduced number of free parameters. However, the main drawback of PSO + SAFY was the increase of the error yield estimation at plot scale when a total of 11 parameters were calibrated (§5.5.4). The increase was due to the inclusion of phenological parameters such as Sw, GDDem, GDDmt in the optimization routine. In this scenario, it is recommended reducing the uncertainty along the optimization by using narrow searching intervals for the free phenological parameters. These ranges can be set using field observations or data collected in previous crop seasons.

Comparison between iLUT and PSO

- Sensitivity of calibration techniques to frequency and error level of LAI retrieved values

Based on the sensitivity experiment, we proved that the calibration techniques and the CGMs have different degree of sensitivity regarding the random error, the frequency and the gaps of the LAI data. In most of cases, the GRAMI model showed larger dispersion of the yield estimation in relation with SAFY. Moreover, the larger sensitivity of SAFY and GRAMI to the LAI error and temporal frequency was verified when the models were calibrated by LUT technique. A lower variability of the yield estimation was obtained by calibrating the CGM parameters using PSO. However, a larger number of outliers were registered because of the greater flexibility of the optimization algorithm in respect to LUT.

- Comparison of calibrated parameters.

We compared GRAMI and SAFY parameters calibrated by LUT and PSO. The largest difference between model parameters was for: the specific leaf area (SLA), the extinction light coefficient (K) and the light use efficiency (LUE). This difference might be directly related with the temperature stress function implemented in SAFY. Although, the temperature stress function adjusts only LUE according to the daily temperature, K and SLA were also affected during the calibration because they are strongly inter-correlated with LUE. On the other hand, the lower differences were noticed for phenological parameters such as GDD to emergency, sowing date and GDD to maturity.

Moreover, we compared the calibrated values of SLA, K and LUE with bibliographical references values: K=0.6, SLA=0.0022 m^2 / g (Penning, et al. 1989) and LUE=3.3-3.8 g/MJ (Lindquist et al., 2005; Singer, et al., 2011). We found that the SLA and K were underestimated. The ranges of values obtained by calibration were 0.45-0.55 and 0.15-0.20 respectively. A stronger underestimation of SLA was observed by PSO. However, in compensation, the coefficient K was better calibrated than by the LUT approach. A higher difference between CGMs was observed for LUE. The average value for GRAMI was 2.7 while for SAFY 3.3. The good calibration of the LUE in SAFY was already verified using Monteith equation and FAPAR data (§ 5.8). This good performance is related with the efficiency of SAFY to simulate the effect of temperature in the plant use radiation.

- Yield estimation

The combination SAFY + PSO showed the best performance with a clear reduction of EEP and EER errors in relation with GRAMI model (Table 18). This trend was also confirmed in season 2014 (Table 22). However, the main drawback of PSO approach at pixel scale is the demand of computational resources. For instance, the time required to calibrate 3 parameters at pixel scale (84 series of LAI data) was three times larger than the time required to calibrate 8 parameters at plot scale (1 series of LAI data). The sharp increase of the computational processing time depends on the number of pixels per plot. Therefore, one alternative might be to cluster automatically the pixels in homogeneous units. This option is viable if there is a suitable relationship between pixel size and plot size and the clustering technique has low computational demand.

- Yield forecasting

The calibration techniques showed a good performance to forecast maize yield one and two months before harvesting. A clear trend in yield estimation accuracy was noticed. The error was lower at regional scale than plot scale. Moreover, a better accuracy was achieved one month before crop harvesting in relation to two months before. These trends are explained by the compensation of errors at regional scale and the reduction of the meteorological data uncertainty.

The good performance of yield forecasting can be explained by two main reasons:

- the total crop biomass was simulated accurately till anthesis by the calibrated CGMs;

- there were no extreme meteorological phenomena such as pests, frosts and flooding which affected the maize production between the yield forecasting and the end of the crop season.

5.10.6. Updating of LAI in GRAMI and SAFY models

The novel experiment implemented in section 5.7.1 allowed us to estimate a suitable ensemble size. Furthermore, we assessed the effect of underestimation and overestimation of observation and model errors in EnKF and PF performance.

The ensemble size chosen by the sensitivity analyses was higher than the values used in other research (De Wit and van Diepen, 2007; Ines et al., 2013; Zhao et al., 2013). This size did not affect significantly the speed of the updating process. However, for a large burden of processing data, the number of particles could be reduced to 100 or even 50 particles.

Concerning the model and observation errors, the experiment demonstrated relevant differences between filters. The effect of the overestimation of the observation error showed a negative impact in PF accuracy while in EnKF the updating accuracy was improved. The effect of the underestimation and overestimation of the model error is comparable in both filters. However, the PF showed a larger sensitivity to error underestimation.

Aware of the sensitivity to the model error estimation, we implemented an innovative technique suitable for both filters. The pixel approach allowed assessing a more representative model error in relation with the approach based on plot data. Moreover, the code has the benefit of being directly coupled with the updating routine.

Regarding maize yield estimation, the combination calibration + updating showed good results. EnKF and PF, coupled with calibrated GRAMI and SAFY models, improved the maize yield estimation. The performance of the three filters tested was similar. The best accuracy for season 2013 was achieved using SAFY + PSO + EnKF, while in 2014 the combination SAFY + PSO + PF yielded the best accuracy. We noted that the efficiency of updating was constrained by the CGM and the calibration technique implemented. The filters acted as a fine tuning which allowed adding extra information from pixel data.

5.10.7. Model performance for simulating crop yield

The main difference between previous research using GRAMI and SAFY models with our experiment is the strategy carried out to calibrate the model parameters. For instance, Claverie et al., (2012) and Duchemin et al (2008) calibrated, at first, a group of parameters constant for each crop type such as biomass partition (A and B) and senescence (SenA and SenB). Then, the parameters related with agro-environmental conditions such as emergence date and LUE were calibrated at plot scale. Moreover, Chahbi et. al. (2014), Padilla et al. (2012) and Ko et al. (2005) calibrated a reduced combination of the model parameters at plot scale. Parameters such as K and SLA were no calibrated. They were, in most of the cases, measured in field. On the other hand, we assessed the calibration of 10 parameters for GRAMI and 11 for SAFY. The phenological parameters sowing date, emergency and maturity were also included in the group. In most of the previous researches, sowing date was fixed and GDD to emergency was calibrated. Then, maturity (total plant senescence) was defined by a minimum LAI threshold.

Table 23 presents the accuracy obtained for biomass and yield estimation for different crops. The biomass estimations were generally more accurate than yield. This is probably related to the fact that the yield assessment in GRAMI and SAFY models is too much simplified compared to reality

(Duchemin et al, 2008). Moreover, some factors mentioned in previous research as sources of uncertainty in CGMs estimations are:

- using a unique planting date and phenological parameters for all the fields in a given year (Padilla, et al., 2012);
- inefficiency to capture differences in crop management between the plots by LUE (Duchemin, et al. 2008);
- keeping a constant LUE value along the crop season (Lecoeur et al. 2011, Claverie 2012);

Aware of these drawbacks, we carried out an innovative approach. To avoid the effect of unrepresentative phenological data, we calibrate the CGMs parameters independently for each plot. Moreover, to capture better the effect of crop management, we tested the calibration at plot and pixel scales and the combination between calibration (plot scale) with the updating (pixel scale).

As presented in Table 26, the results of our experiment are promising considering the minimum input data required and the high accuracy obtained at regional and plot scale. We have achieved a good performance in both seasons. The regional estimation copied accurately the inter-season variation of the maize yield. Furthermore, our results are comparable whit the accuracy obtained by complex crop growth models such as EPIC, CERES or STICS. For instance, Fang et al (2011) obtained a regional accuracy of 3.5% for maize by assimilating EO-data in CERES model. Ren, et al (2009) estimated maize yield with an error of 6.4% by assimilating LAI into EPIC. Jégo et al (2012) achieved a NRMSE of 10.4% for maize estimation by assimilating retrieved LAI in STICS model.

Table 26. Examples of crop yield estimation by assimilating EO-data in GRAMI and SAFY.

Reference	Model	Crop	R^2	NRMSE	
				Region	Plot
Atzberger el al. (2001)	GRAMI	Wheat	0.29		25.9
Ko et al (2005)	GRAMI	Cotton	0.67		
Padilla et al. (2012)	GRAMI	Wheat		6.8	21
Duchemin et al (2008)	SAFY	Wheat	0.48	25	
Claverie et al. (2012)*	SAFY	Maize	0.86		26
Chahbi et al, (2014)	SAFY	Wheat	0.45		
SAFY + PSO + EnKF - 2013	SAFY	Maize	0.84	2.3	11.2
SAFY + PSO + PF - 2014			0.73	1.6	7.45

*biomass estimation

6. Conclusions and recommendations

This chapter is divided in five sections. General conclusions about crop monitoring are presented in item 6.1. Aspects related with retrieval of biophysical variables (chapter 2) and assimilation of EO-data in crop growth models (chapter 3) are introduced in section 6.2 and 6.3 respectively. The findings about maize yield estimation using GRAMI and SAFY models calibrated and updated by EO data are presented in section 6.4. Finally, in section 6.5 are introduced recommendations and further research regarding crop yield monitoring at regional and plot scale.

6.1. General overview about crop monitoring

The demand for reliable crop intelligence at suitable scales and within a short lag-time is constantly increasing. Crop growth models are valuable tools to deliver useful information to planners and decision makers for optimizing agricultural activities and for increasing the efficiency in the production process. The integration of EO data in CGM allows spatializing model application and minimizing model uncertainties. The added value of integration results from the combination of the synoptic and repetitive data from EO systems with the continuous – and knowledge-based – description of crop status derived by crop models.

Operational system for regional crop growth modeling has to address several issues of uncertainty related to model formulation, model inputs, data assimilation algorithm, and assimilated observations. Simple crop models have generally low(er) data requirements compared to complex models and therefore might be more easily transferable to other regions. Simple crop growth models can therefore outperform complex models in which most parameters are set to standard values. However, simple CGM usually estimate only few state variables compared to complex models, which can simulate variables related to crop water balance, nitrogen balance among others in addition to yield and biomass. Hence, the challenge of implementing complex model at regional scale is the feasibility of fine-tuning parameters and providing the necessary input and driving variables to represent the spatial variability in an appropriate manner.

6.2 Retrieval of vegetation bio-physical variables

Numerous techniques have been implemented to retrieve biophysical variables. In the last years, the challenge of retrieval techniques is focused on developing routines able to quantify the uncertainty of the retrieved vegetation bio-physical variables. This has a paramount importance regarding the quality level and consistency required to assimilate EO-data in CGM.

Based on the review of vegetation bio-physical data retrieval techniques, we recommend to focus the research on the development of flexible and robust routines able to select and apply context-dependent algorithms, to make use of a priori constraints. In this way, it could provide realistic ranges of uncertainties together with the retrieved vegetation bio-physical variables. At the same time, computational requirements have to be considered in particular with regards to an operational mapping of biophysical variables at regional and global scales at deca-metric spatial resolution.

6.3 Assimilating remotely retrieved biophysical variables in crop models

Aiming to reduce uncertainties at regional scale, EO data have been integrated with crop models using different assimilation techniques. In the last years, updating technique has been widely used thanks to its flexibility. This sequential approach allows assimilating state variables or combination of parameters and state variables while taking into account model and observation errors. In new

studies, updating has been integrated with variational techniques. The hybrids approaches have shown good performance because take advantage of strength of both techniques.

As a matter of fact, EO data availability will steadily increase in the future. Data will be delivered from sensors with diverse technical characteristics. In this scenario more research is needed with respect to:

- multisource EO data assimilation techniques (optical and microwave data) testing new filter and hybrid approaches;
- fusion of EO data to match the CGMs spatial and temporal scale with user demands;
- coupled CGM, atmosphere and radiative transfer models (RTM), aiming to further reducing uncertainties.

6.4 Maize yield estimation by using GRAMI and SAFY models

6.4.1 Sensitivity analyze of GRAMI and SAFY parameters

The present work proves that crop biomass estimation is highly influenced by Light Use Efficiency. The effect of parameters such as sowing date, GDD to emergence and GDD to maturity is conditioned by the daily temperature. The role of senescence in biomass estimation is stronger in the GRAMI model because there is a direct connection between biomass synthetized and senescence. In the SAFY formulae these two processes are decoupled.

The parameters with a stronger influence in the calibration of the LAI are SLA, A, B and LUE for both models. Moreover, the study shows that these parameters together with K and LAI at emergency (LAIin) are highly correlated. This high correlation explains the ill-posed problem when they are calibrated together. On the other hand, parameters related with senescence and GDD to maturity had a low correlation with the rest of the parameters.

6.4.2 Sensitivity of LUT and PSO to the error level, frequency and gaps of LAI data

The experiment shows that a minimum LAI frequency suitable to calibrate GRAMI and SAFY models is 15 days for LUT and 20 days for PSO.

The calibration techniques are strongly sensitive to LAI data gaps. The yield estimation error increases sharply if the LAI data series used in CGMs calibration has gaps during crop emergency. Therefore, the LAI observations should be well distributed in the crop season.

Finally, the average LAI random error should be no larger than 20%. This threshold has more relevance when the crop yield is estimated using GRAMI and the model parameters are calibrated by LUT approach.

6.4.3 Yield estimation using calibrated GRAMI and SAFY models by iLUT and PSO techniques

We could further prove that the filtering of the retrieved LAI using the Whittaker filter with smoothing parameter λ equal 300 improves the parameter calibration. The smoothed LAI observations have a better fitting with the LAI simulations obtained by SAFY and GRAMI models. Consequently, the biomass estimation is improved. The simple cost function shows an acceptable performance for the LUT and PSO techniques without requiring ancillary data.

Regarding iLUT technique, the regional yield is underestimated by SAFY and overestimated by GRAMI. This trend was verified in the seasons 2013 and 2014. The dispersion of parameter levels and yield as well as the global LAI error is reduced along the LUT iterations.

SAFY calibrated by PSO at plot scale achieves the best performance with a lower error at plot and regional scales in relation with GRAMI estimations. However, the error yield estimation increases when phenological parameters such as Sw, GDDem, GDDmt are included in the optimization routine.

The present work proves the increase of the yield estimation accuracy by using pixel data. The best results are observed using PSO for a reduced number of free parameters with low inter-correlation. The yield variability and the error at plot and regional scale is reduced, in most of the cases, in relation with the plot approach.

The calibration techniques perform well in forecasting maize yield one and two months before harvesting. A clear trend in yield estimation accuracy is noticed. The error is lower at regional scale than plot scale. Moreover, a better accuracy is achieved one month than two months before crop harvesting. These trends are explained by the compensation of errors at regional scale and the reduction in the uncertainty of the meteorological data.

6.4.4 Updating of GRAMI and SAFY models using EnKF and PF

The sensitivity analysis implemented for EnKF and PF shows us the effect of the model and observation error in the filter performance. The underestimation of the model error has a strong effect on updating performance. Therefore, this study applies an innovative technique, using pixel-based data, to calculate a representative model error.

Regarding the maize yield estimation, the combination calibration + updating shows a good performance. For 2013 SAFY + PSO + EnKF achieve the best accuracy. While in 2014 the combination SAFY + PSO + PF yields the best results. This confirms the better performance of SAFY compared with GRAMI in our study. We further note that the efficiency of updating is constrained by the accuracy of the CGM calibration. The study shows that the filter acts as a fine tuning which allows adding extra information from pixel scale.

Considering the good performance of PF in seasons 2013 and 2014, we recommend the calibration of the SAFY model at plot scale using PSO and the updating at pixel scale using PF. This combination between techniques results in a suitable accuracy both at regional and plot scale. Additionally, the low computational demand of PF makes possible the updating of SAFY at pixel scale in large regions.

As a whole, the study confirms the robustness of simple crop growth models. The main assumption of the GRAMI and SAFY models is verified. The LUE calibrated by LAI observations is able to model the agro-environmental conditions of maize. The approach achieves a good accuracy at regional and plot scale with a minimum demand of input data. The strategy of parameter calibration at plot scale and updating at pixel scale is suitable to estimate accurately maize yield in Marchfeld.

Finally, based on the results, we state that the SAFY model calibrated and updated by remote sensing is able to monitor the dynamics of vegetation, to detect anomalies in crop phenology and to predict accurately above-ground biomass at regional and plot scales.

6.5 Recommendations and further research

Being aware of the computational demand of applying CGM in large regions, we recommend testing a strategy to calibrate cluster of samples instead of individual plots. Then an iterative LUT could run independently for each group of samples. We suggest assessing the effect of the parameter dispersion on the accuracy of CGM estimations. This is relevant when calibrated multi (inter-) correlated parameters (ill-posed problem).

Considering the availability of multi-source remote sensing data and the impact of the LAI accuracy in the calibration of CGMs, further research should focus on testing a routine to assimilate

the surface reflectance collected by remote sensors directly in SAFY model. Then, SAFY would be coupled with a radiative transfer model and atmosphere model. The main advantage of this strategy would be to avoid the error of the LAI retrieval and the possibility to assimilate multi-source remote sensing data.

We recommend validating our assimilation routine (calibration + updating) in rain feed regions aware of the sensitivity of the crops to the spatial distribution of rainfall and to the soil water content. In this way, the following assumptions can be validated:

- the LUE is an efficient indicator of the global agro-environmental stress;
- the crop yield can be calculated accurately using the total above biomass and a constant harvest index;

Moreover, one can compare the efficiency of senescence simulation using GRAMI and SAFY approaches.

Finally, we encourage implementing the SAFY model calibrated at plot scale and updated at pixel scale to estimate yield of other crops with importance in the commodities world market such as winter cereals and soybean.

7. References

Alexandratos, N.; Bruinsma, J. World agriculture towards 2030/2050: The 2012 revision. *ESA Working Paper* **2012**, 12(03).

Alganci, U.; Ozdogan, M.; Sertel, E.; & Ormeci, C. Estimating maize and cotton yield in southeastern Turkey with integrated use of satellite images, meteorological data and digital photographs. *Field Crop Res* **2014**, *157*, 8–19.

Arulampalam, M. S.; Maskell, S.; Gordon, N.; Clapp, T. A tutorial on particle filters for online nonlinear/non-Gaussian Bayesian tracking. *IEEE Trans Signal Process* **2002**, *50*(2), 174–188.

Asrar, G.; Kanemasu, E.T.; Jackson, R.D.; Pinter, P.J. Jr. Estimation of total above-ground phytomass production using remotely sensed data. *Remote Sens. Environ.* **1985**, *17* (3), 211-220.

Atzberger, C. Advances in Remote Sensing of Agriculture: Context Description, Existing Operational Monitoring Systems and Major Information Needs. *Remote Sens* **2013a**, *5*(2), 949–981.

Atzberger, C.; Darvishzadeh, R.; Schlerf, M.; Le Maire. Suitability and adaptation of PROSAIL radiative transfer model for hyperspectral grassland studies. *Remote Sens Lett* **2013b**, *4* (1), 55-64.

Atzberger, C.; Guérif, M.; Baret, F.; Werner. Comparative analysis of three chemometric techniques for the spectroradiometric assessment of canopy chlorophyll content in winter wheat. *Comput Electron Agric* **2010a**, *73* (2), 165-173.

Atzberger, C. Inverting the PROSAIL canopy reflectance model using neural nets trained on streamlined databases. *J Spectr Imaging* **2010b**, *1* (1), 1–13.

Atzberger, C. Estimates of winter wheat production through remote sensing and crop growth modeling. A case study on the Camargue region..Verlag für Wissenschaft und Forschung. VWF, Universität Trier, Berlin, 1997.

Atzberger, C. Object-based retrieval of biophysical canopy variables using artificial neural nets and radiative transfer models. *Remote Sens Environ* **2004**, *93*(1-2), 53–67.

Atzberger, C.; Darvishzadeh, R.; Immitzer, M.; Schlerf, M.; Skidmore, A.; le Maire, G. Comparative analysis of different retrieval methods for mapping grassland leaf area index using airborne imaging spectroscopy. *Int. J. Appl. Earth Obs. Geoinf* **2015**, *43*, 19-31.

Atzberger, C.; Guérif, M.; Delécolle, R. The use of GRAMI crop growth model and SPOT data for biomass estimations in winter wheat. Physical measurements and signatures in remote sensing. 8th international symposium, Aussois, France, 1-12/08/2001; Leroy, Marc; Balkema, 2001; pp. 705-711.

Atzberger, C.; Klisch, A.; Mattiuzzi, M.; Vuolo, F. Phenological Metrics Derived over the European Continent from NDVI3g Data and MODIS Time Series. *Remote Sens*. **2014**, *6*(1), 257-284; doi:10.3390/rs6010257.

Atzberger, C.; Richter, K. Spatially constrained inversion of radiative transfer models for improved LAI mapping from future Sentinel-2 imagery. *Remote Sens Environ* **2012**, *120*, 208–218.

Atzberger.C.; Eilers P.H.C. Evaluating the effectiveness of smoothing algorithms in the absence of ground reference measurements, *Int J Remote Sens* **2011**, *32*(13), 3689-3709.

Aubert, D.; Loumagne, C.; Oudin, L. Sequential assimilation of soil moisture and streamflow data in a conceptual rainfall-Runoff model. *J Hydrol* **2003**, *280*(1-4), 145–161.

Awika, J.M. Advances in Cereal Science: Implications to Food Processing and Health Promotion. ACS Symposium Series; American Chemical Society: Washington, DC, 2011; doi: 10.1021/bk-2011-1089.ch001. Available on: http://pubs.acs.org

Bala, S. K.; and Islam, A. S. Correlation between potato yield and MODIS-derived vegetation indices. *Int J Remote Sens* **2009**, 30 (10), 2491–2507.

Baret, F.; & Buis, S. Estimating canopy characteristics from remote sensing observations: Review of Methods and Associated Problems. In *Advances in Land Remote Sensing. System, Modeling, Inversion and Application.*; Liang, S.; Springer: Netherlands, 2008; Volume 2, pp. 172–301.

Baret, F.; Guyot, G. Potentials and limits of vegetation indices for LAI and APAR assessment. *Remote Sens Environ* **1991**, *35*, 161–173.

Baret, F.; Guyot, G.; Major, D.J. Crop biomass evaluation using radiometric measurements. *Photogrammetria* **1989**, *43*, 241–256.

Bazargan, J.; Hashemi, H.; Mousavi, S.M.; Zamani Sabzi, H. Optimal Operation of Single-Purpose Reservoir for Irrigation Projects under Deficit Irrigation Using Particle Swarm Algorithms. *Canadian Journal on Environmental* **2011**, 2(7), 164-171.

Becker-Reshef, I.; Vermote, E.; Lindeman, M.; Justice, C. A generalized regression-based model for forecasting winter wheat yields in Kansas and Ukraine using MODIS data. *Remote Sens. Environ.* **2010**, *114*(6), 1312–1323.

Bocquet, M.; Sakov, P. An iterative ensemble Kalman smoother. *Q. J. Roy. Meteor Soc* **2014**, *140*, 1521–1535.

Boote, K.J.; Jones, J.W.; Pickering, N.B. Potential uses and limitations of crop models. *Agron. J.* **1996**, *88*, 704-716.

Bouman, B.A.M.; van Keulen, H.; van Laar, H. H.; Rabbinge, R. The 'School of de Wit' crop growth simulation models: A pedigree and historical overview. *Agric Syst* **1996**, *52* (2–3), 171–198.

Bouallègue,S.; Haggège, J.; Benrejeb, M. A New Method for Tuning PID-Type Fuzzy Controllers Using Particle Swarm Optimization. Available on: http://cdn.intechopen.com/pdfs-wm/39486.pdf (accessed on 29/03/2016).

Brisson N.; Mary B.; Ripoche D.; Jeuffroy M.H.; Ruget F.; Nicoullaud B.; Gate P.; Devienne-Barret F.; Antonioletti R.; Durr C.; Richard G.; Beaudoin N.; Recous S.; Tayot X.; Plenet D.; Cellier P.; Machet J.M.; Meynard J.-M.; Delécolle R.; STICS: a generic model for the simulation of crops and their water and nitrogen balances. I. Theory and parametrization applied to wheat and corn, *Agronomie* **1998**, *18*, 311–346.

Brisson, N.; Gary, C.; Justes, E.; Roche, R.; Mary,B.; Ripoche,D.; Zimmer, D.; Sierra, J.; Bertuzzi, P.; Burger, P.; Bussiere, F.; Cabidoche, Y.M.; Cellier, P.; Debaeke, P.; Gaudillére, J.P.; Hénault, C.; Maraux, F.; Seguin, B.; Sinoquet, H. An overview of the crop model STICS. *Eur. J. Agron*. **2003**, *18*, 309–332.

Burgers, G.; van Leeuwen, P.J.; Evensen, G. Analysis scheme in the ensemble Kalman filter. *Mon Wea* Rev **1998**, *126*, 1719–172

Caicedo, J.P.R.; Verrelst, J.; Munoz-Mari, J.; Moreno, J.; Camps-Valls. Toward a Semiautomatic Machine Learning Retrieval of Biophysical Parameters. *IEEE J Sel Top Appl* **2014**, *7* (4), 1249-1259.

Calvao, T.; Pessoa, M.F. Remote sensing in food production–a review. *Emir. J. Food Agric* **2015**, *27*(2), 138-151.

Cannell, M.G.R.; Sheppard, L.J.; Milne, R. Light Use Efficiency and Woody Biomass Production of Poplar and Willow. *Forestry* **1988**, *61* (2), 125-136.

Casa, R.H.; Varella, S.; Buis, M.; Guérif, B.; De Solan, F.; Baret. Forcing a wheat crop model with LAI data to access agronomic variables: Evaluation of the impact of model and LAI uncertainties and comparison with an empirical approach. *Eur J Agron* **2012**, *37* (1), 1-10.

Cernicharo, J.; Verger, A.; Camacho, F. Empirical and Physical Estimation of Canopy Water Content from CHRIS/PROBA Data. *Remote Sens* **2013**, *5*(10), 5265-5284.

Chahbi, A.; Zibri, M.; Lili-Chabaane, Z.; Duchemin, B.; Shabou, M.; Mougenot, B.; Boulet, G. Estimation of the dynamics and yields of cereals in a semi-arid area using remote sensing and the SAFY growth model. *Int J Remote Sens* **2014**, *35* (3), 1004-1028.

Chahbi, A.; Zibri, M.; Lili-Chabaane, Z.; Duchemin, B.; Shabou, M.; Mougenot, B.; Boulet, G. Estimation of the dynamics and yields of cereals in a semi-arid area using remote sensing and the SAFY growth model. *Int. J. Remote Sens.* **2014**, *35* (3), 1004-1028.

Chander, G.; Hewison, T.J.; Fox, N.; Wu, X.; Xiong, X.; Blackwell, W.J. Overview of Intercalibration of Satellite Instruments. *IEEE Trans. Geosci. Remote Sens*. **2013**, *51*(3), 1056-1080.

Chandran, K. P.; Pandit, A.; Pandey, N. K. Evaluation of models for estimating potato production trends in major states of India. *Potato J* **2005**, *32*(3-4), 219-220.

Chaudhari, K.N.; Tripathy, R.; Patel, N.K. Spatial wheat yield prediction using crop simulation model, GIS, remote sensing and ground observed data. *J Agrometeorol* **2010**, *12*, 174–180.

Chen, Y; Cournède, P-H. Data assimilation to reduce uncertainty of crop model prediction with Convolution Particle Filtering. *Ecol Model* **2014**, *290*, 165–177.

Claverie, M.; Demarez, V.; Duchemin, B.; Hagolle, O.; Ducrot, D.; Marais-Sicre, C.; Dedieu, G. Maize and sunflower biomass estimation in southwest France using high spatial and temporal resolution remote sensing data. *Remote Sens Environ* **2012**, *124*, 844–857.

Clevers, J. G. P.; Vonder, O.; Jongschaap, R. E.; Desprats, J.; King, C.; Prévot, L.; & Bruguier, N. A semi-empirical approach for estimating plant parameters within the RESEDA-Project. *Int Arch Photogramm Remote Sens* **2000**, 33, 272–279.

Clevers, J.G.P.W. Application of a weighted infrared-red vegetation index for estimating leaf Area Index by Correcting for Soil Moisture. *Remote Sens. Environ*. **1989**, *29*, 25–37.

Combal, B.; Baret, F.; Weiss, M. Improving canopy variables estimation from remote sensing data by exploiting ancillary information. Case study on sugar beet canopies. *Agronomie* **2002a**, *22*, 205-215.

Combal, B.; Baret, F.; Weiss, M.; Trubuil, A.; Mace, D.; Pragnère, A.; Myneni, R.; Knyazikhin, Y.; Wang, L. Retrieval of canopy biophysical variables from bidirectional reflectance using prior information to solve the ill-posed inverse problem. *Remote Sens Environ* **2002b**, *84*, 1–15.

Combal, B.; Baret, F.; Weiss, M.; Trubuil, A.; Macé, D.; Pragnère, A.; Wang, L. Retrieval of canopy biophysical variables from bidirectional reflectance using prior information to solve the ill-posed inverse problem. *Remote Sens Environ* **2003**, *84*(1), 1–15.

Confalonieri, R.; Bellocchi, G.; Bregaglio, S.; Donatelli, M.; Acutis, M. Comparison of sensitivity analysis techniques: A case study with the rice model WARM. *Ecol. Model.* **2010**, *221*(16), 1897–1906.

Cournède, P.-H.; Chen, Y.; Wu, Q.; Baey, C.; Bayol, B. Development and Evaluation of Plant Growth Models: Methodology and Implementation in the PYGMALION platform. *Math Model Nat Phenom* **2012**, *8*, 112-130.

Crow, W. T. Correcting Land Surface Model Predictions for the Impact of Temporally Sparse Rainfall Rate Measurements Using an Ensemble Kalman Filter and Surface Brightness Temperature Observations. *J Hydrometeorol* **2003**, *4*, 960–973.

Crow, W. T.; & Van Loon, E. Impact of Incorrect Model Error Assumptions on the Sequential Assimilation of Remotely Sensed Surface Soil Moisture. *J Hydrometeorol* **2006**, *7*(3), 421–432.

Curnel, Y.; de Wit, A. J. W.; Duveiller, G.; Defourny, P. Potential performances of remotely sensed LAI assimilation in WOFOST model based on an OSS Experiment. *Agric For Meteorol* **2011**, *151*(12), 1843–1855.

Dadhwal, V. K. Crop Growth and Productivity Monitoring and Simulation using Remote Sensing and GIS. Proceedings of a Training Workshop held 7-11 July 2003 in Dehra Dun, India, Edited by M.V.K. Sivakumar, P.S. Roy, K. Harmsen, and S.K . Saha, AGM-8, WMO/TD-No. 1182.

Danson, F.; Rowland, C.; & Baret, F. (2003). Training a neural network with a canopy reflectance model to estimate crop leaf area index. *Int. J. Remote Sens* **2003**, 24(23), 4891–4905.

Darvishzadeh, R.; Atzberger, C.; Skidmore, A.; Schlerf, M. Mapping grassland leaf area index with airborne hyperspectral imagery: A comparison study of statistical approaches and inversion of radiative transfer models. *ISPRS J Photogramm Remote Sens* **2011**, *66*(6), 894-906.

Das, P. K; Seshasai, M. V. R. Multispectral sensor spectral resolution simulations for generation of hyperspectral vegetation indices from Hyperion data. *Geocarto Int.* **2015**, *30* (6), 686-700.

De Leeuv, J.; Vrieling A.; Shee, A.; Atzberger, C.; Hadgu, K.M.; Biradar, C.M.; Keah, H.; Turvey, C. The Potential and Uptake of Remote Sensing in Insurance: A Review. *Remote Sens.* **2014**, *6*, 10888-10912; doi:10.3390/rs61110888.

De Wit, A.; Duveiller, G.; Defourny, P. Estimating regional winter wheat yield with WOFOST through the assimilation of green area index retrieved from MODIS observations. *Agric For Meteorol* **2012**, *164*, 39–52.

De Wit, J. W.; Diepen van, C. Crop model data assimilation with the Ensemble Kalman filter for improving regional crop yield forecasts. *Agr Forest Meteorol* **2007**, *146*(1-2), 38–56.

Delécolle, R.; Maas, S.J.; Guérif, M.; Bareta, F. Remote sensing and crop production models: present trends. *ISPRS J Photogramm Remote Sens* **1992**, *42*, 145-161.

Dente, L.; Satalino, G.; Mattia, F.; Rinaldi, M. Assimilation of leaf area index derived from ASAR and MERIS data into CERES-Wheat model to map wheat yield. *Remote Sens Environ* **2008**, *112*(4), 1395–1407.

Diepen van, C.A.; Wolf, J. Keulen van, H. WOFOST: a simulation model of crop production. *Soil Use Manage* **1989**, 5(1), 16-24.

Dong, Y.; Luo, R.; Feng, H.; Wang, J.; Zhao, J.; Zhu, Y.; Yang, G. Analysing and Correcting the Differences between Multi-Source and Multi-Scale Spatial Remote Sensing Observations. *PLoS One*. **2014**, 9(11), 1-10.

Dong, Y.; Wang, J.; Li, C.; Yang, G.; Wang, Q.; Liu, F.; Huang, W. Comparison and analysis of data assimilation algorithms for predicting the leaf area index of crop canopies. *IEEE J Sel Top Appl Earth Obs Remote Sens* **2013**, *6*(1), 188–201.

Dongwei, W.; JinDi, W.; ShunLin, L. Retrieving crop leaf area index by assimilation of MODIS data into a crop growth model. *Sci China Earth Sci* **2010**, *53*(5), 721–730.

Dongwei, W.; Jindi, W.; Yongmei, C.; Haobo, L.; Shunlin, L.; Zhiqiang, X. Crop LAI retrieval from MODIS bidirectional reflectance observations using the particle filter algorithm and a crop growth model. Geoscience and Remote Sensing Symposium (IGARSS) 2008, (5), 2008–2011.

Doraiswamy, P. C.; Moulin, S.; Cook, P. W.; & Stern, A. Crop Yield Assessment from Remote Sensing. *Photogramm Eng Remote Sens* **2003**, *69*(6), 665–674.

Dorigo, W.; Richter, R.; Baret, F.; Bamler, R.; Wagner, W. Enhanced Automated Canopy Characterization from Hyperspectral Data by a Novel Two Step Radiative Transfer Model Inversion Approach. *Remote Sens* **2009**, *1* (4), 1139-1170.

Dorigo, W.; Zurita-Milla, R.; de Wit, J. W.; Brazile, J.; Singh, R.; Schaepman, M. E. A review on reflective remote sensing and data assimilation techniques for enhanced agroecosystem modeling. *Int J Appl Earth Obs Geoinf* **2007**, *9*(2), 165–193.

Duan, Q.; Sorooshian, S.; Gupta, H. V. Effective and efficient global optimization for conceptual rainfall-runoff models. *Water Resour Res* **1992**, *28*(4), 1015–1031.

Duan, S-B.; Liang Li, Z.; Wu,H.; Li, C. Inversion of the PROSAIL model to estimate leaf area index of maize, potato, and sunflower fields from unmanned aerial vehicle hyperspectral data. *Int J Appl Earth Obs* **2014**, *26*(1), 12–20.

Duchemin, B.; Maisongrande, P.; Boulet, G.; Benhadj, I. A simple algorithm for yield estimates: Evaluation for semi-arid irrigated winter wheat monitored with green leaf area index. *Environ Model Softw* **2008**, *23*(7), 876–892.

Dumont, B.; Vancutsem, F.; Seutin, B.; Bodson, B.; Destain, J.P.; Destain, M.F. Wheat growth simulation using crop models: a review of methods, and their potential and limitations. *Biotechnol. Agron Soc Environ* **2012**, *16*(3), 382-392.

Duveiller, G.; Weiss, M.; Baret, F.; Defourny, P. Retrieving wheat green area index during the growing season from optical time series measurements based on neural network radiative transfer inversion. *Remote Sens Environ*, **2011**,*115* (3), 887-896.

Dzotsi, K. A.; Basso, B.; Jones, J. W. Parameter and uncertainty estimation for maize, peanut and cotton using the SALUS crop model. *Agr Syst* **2015**, *135*, 31-47.

Edgertong, M.D. Increasing Crop Productivity to Meet Global Needs for Feed, Food, and Fuel. *Plant Physiol*. **2009**, *149*(1), 7–13; doi: 10.1104/pp.108.130195.

Ehrendorfer, M. A review of issues in ensemble-based Kalman filtering. Meteorol Z **2007**, *16*(6), 795-818.

Eilers, P.H.C. A perfect smoother. *Anal Chem* **2003**, *75*, 3299–3304.

Emerick, A. A; Reynolds, A. Ensemble smoother with multiple data assimilation. *Comput Geosci* **2013**, *55*, 3–15.

Eskes, H.J.; Piters, A.J.M.; Levelt, P.F.; Allaart, M.A.F. and Kelder, H. Variational data assimilation: How to extract more information from GOME total ozone data. *EOQ-GOME special* **1998**, *58*, 35-38.

Evensen, G. Sequential data assimilation with a nonlinear quasi-geostrophic model using Monte Carlo methods to forecast error statistics. *J Geophys Res* **1994**, *99*, 10143–10162.

Evensen, G. The ensemble Kalman filter for combined state and parameter estimation. Control Systems, *IEEE Control Syst. Mag* **2009**, 29(3), 83–104.

Evensen, G. The Ensemble Kalman Filter: Theoretical formulation and practical implementation. *Ocean Dynamics* **2003**, *53*(4), 343–367.

Evers, G. PSO Research Toolbox Documentation (Version 20110515i). Available on: http://www.georgeevers.org/pso_research_toolbox_documentation.pdf (accessed on 15/01/2016)

Faivre, R.; Leenhardt, D.; Marc, V.; Marc, B.; Francois, P.; & Dedieu, G. Spatializing crop models. *Agronomie **2004**, 24*, 205–217.

Fang, H.; Liang, S.; Hoogenboom, G. Integration of MODIS LAI and vegetation index products with the CSM-CERES-Maize model for corn yield estimation. *Int J Remote Sens* **2011**, *32*(4), 1039-1065.

Fang, H.; Liang, S.; Hoogenboom, G.; Teasdale, J.; Cavigelli, M. Corn yield estimation through assimilation of remotely sensed data into the CSM-CERES Maize model. *Int. J. Remote Sens.* **2008**, *29*(10), 3011–3032.

Fang, H.; Liang, S.; Kuusk, A. Retrieving leaf area index (LAI) using a genetic algorithm with a canopy radiative transfer model. *Remote Sens Environ* **2003**, *85*(3), 257–70.

Fang, S., Le, Y., Liang, Q., Liu, X. Leaf Area Index Estimation Using Time-Series MODIS Data in Different Types of Vegetation. *J Indian Soc Remote* **2014**, *42* (4), 733-743.

FAO-World Soil Classification. Available on: http://www.fao.org/soils-portal/soil-survey/soil-classification (accessed on 29/03/2016)

Ferencz, C.;. Bognar, P.; Lichtenberger, D.; Hamar, G.; Tarcsai, G.; Timár, G.; Molnár, S.; Pásztor, P.; Steinbach, B.; Székely, Y.; Ferencz, O. E.; Ferencz-Árkos, I. Crop yield estimation by satellite remote sensing. *Int. J. Remote Sens.* **2004**, 25 (20), 4113-4149.

Ferreyra, R.A.; Podestá, G.P.; Messina, C.D.; Letson, D.; Dardanelli, Guevara, E.; Meira, S. A linked-modeling framework to estimate maize production risk associated with ENSO-related climate variability in Argentina. *Agric For Meteorol* **2001**, *107* (3), 177–192.

Filella,I.; Penuelas, J.The red edge position and shape as indicators of plant chlorophyll content, biomass and hydric status. *Int J Remote Sens* **1994**, *15* (7), 1459-1470.

Foley, J. A.; Ramankutty, N.; Brauman, K. A.; Cassidy, E. S.; Gerber, James. S.; Johnston, M.; Mueller, N. D.; O'Connell, C.; Ray, D. K.; West, P. C.; Balzer, C.; Bennett, E. M.; Carpenter, S. R.; Hill, J.; Monfreda, C.; Polasky, S.; Rockström. J.; Sheehan, John.; Siebert, S.; Tilman, D.; Zaks, D. P. M. Solutions for a cultivated planet. *Nature* **2011**, *478*, 337–342.

Gao, F.; Masek, J.; Schwaller, M.; Hall, F. On the blending of the Landsat and MODIS surface reflectance: Predicting daily Landsat surface reflectance. *IEEE Trans Geosci Remote Sens* **2006**, *44*(8), 2207–2218.

Gehlhar, M; Coyle W. Global Food Consumption and Impacts on Trade Patterns. In Changing Structure of Global Food Consumption and Trade; Regmi A.; Economic Research Service/USDA , Washington, 2001, pp. 4-13.

Glenn, E.P.; Huete, A.R.; Nagler, P.L.; Nelson, S.G. Relationship between remotely-sensed vegetation indices, canopy attributes and plant physiological processes: What vegetation indices can and cannot tell us about the landscape. *Sensors* **2008**, *8* (4), 2136-2160.

Goel, N.S. Models of vegetation canopy reflectance and their use in estimation of biophysical parameters from reflectance data. *Remote Sensing Reviews* **1988**, *4*(1), 1-222.

Gómez-Dans, J.L.; Lewis, P.E.; Disney, M. Efficient Emulation of Radiative Transfer Codes Using Gaussian Processes and Application to Land Surface Parameter Inferences. *Remote Sens*. **2016**, 8, 119; doi:10.3390/rs8020119.

Gommes, R. Agrometeorological Models and Remote Sensing for Crop monitoring and Forecasting. Report of the Asia-Pacific Conference on Early Warning, Preparedness, Prevention and Management of Disasters, 12-15 June 2001, Chiang-Mai. RAP Publication 2001/14, FAO, Bangkok. 75-92.

Google Earth (Version 7.1.5.1557) [Software]. Mountain View, CA: Google Inc. (2015). Available on: http:// kh.google.com.

Guérif, M.; Duke, C. Adjustment procedures of a crop model to the site specific characteristics of soil and crop using remote sensing data assimilation. *Agr Ecosyst Environ* **2000**, *81*(1), 57–69.

Guérif, M.; Duke, C. Calibration of the SUCROS emergence and early growth module for sugar beet using optical remote sensing data assimilation. *Eur J Agron* **1998**, *9*(2-3), 127–136.

Guérif, M.; Philipe, O.; Delécolle, R. Statistical modelling of winter wheat at a regional scale. In: Wheat Growth and Modelling. NATO ASI Series, Series A: Life Sciences W. Day and R.K. Atkin (Editors), 1985, 86, pp. 371-379.

Guindin-Garcia, N. Estimating Maize Grain Yield from Crop Biophysical Parameters Using Remote Sensing. Doctor of Philosophy, University of Nebraska-Lincoln, USA, December 2010.

Haboudane, D.; Miller, J.R.; Pattey, E.; Zarco-Tejada, P.J.; Strachan I.B. Hyperspectral vegetation indices and novel algorithms for predicting green LAI of crop canopies: modeling and validation in the context of precision agriculture. *Remote Sens. Environ* **2004**, *90*, 337–352.

Hadria, R.; Duchemin, B.; Lahrouni, A.; Khabba, S.; Er-Raki, S.; Dedieu, G.; Chebouni, A.; Olioso, A. Monitoring of irrigated wheat in a semi-arid climate using crop modelling and remote sensing data: Impact of satellite revisit time frequency. *Int. J. Remote Sens.* **2006**, *27*(5-6), 1093–1117.

Han, X.; Li, X. An evaluation of the nonlinear/non-Gaussian filters for the sequential data assimilation. *Remote Sens. Environ.* **2008**, *112*(4), 1434–1449.

Hanrahan, G. Swarm intelligence metaheuristics for enhanced data analysis and optimization. *Analyst* **2011**, 136, 3587.

Hay, R.K.M. Harvest index: a review of its use in plant breeding and crop physiology. *Annals of Applied Biology*, **1995**, *126* (1), 197-216.

He, B.B.; Li, X; Quan, X.W.; Qiu, S. Estimating the Aboveground Dry Biomass of Grass by Assimilation of Retrieved LAI into a Crop Growth Model . *IEEE J Sel Top Appl* **2015**, *8*(2), 550-561.

Hedley, J.; Roelfsema, C.; Phinn, S, R. Efficient radiative transfer model inversion of remote sensing applications. *Remote Sens Environ* **2009**, *113*(11), 2527-2532.

Hofmann, H. Violin plot based on kernel density estimation, using default ksdensity function. Available on: https://de.mathworks.com/matlabcentral/fileexchange/45134-violin-plot

Hoogenboom, G. Contribution of agrometeorology to the simulation of crop production and its applications. *Agric For Meteorol* **2000**, *103*, 137–157.

Huang, J.X.; Ma, H.Y.; Su, W.; Zhang, X.D.; Huang, Y.B.; Fan, J.L.; Wu, W.B. Jointly Assimilating MODIS LAI and ET Products into the SWAP Model for Winter Wheat Yield Estimation. *IEEE J Sel Top Appl*. **2015a**, *8* (8), 4060-4071.

Huang, J.X.; Tian, L.Y.; Liang, S.L.; Ma, H.Y.; Becker-Reshef, I.; Huang, Y.B.; Su, W, Zhang, X.D.; Zhu, D.H.; Wu, W.B. Improving winter wheat yield estimation by assimilation of the leaf area index from Landsat TM and MODIS data into the WOFOST model. *Agric For Meteorol* **2015b**, *204*, 106-121.

Huang, Y.; Zhu, Y.; Li, W.; Cao, W.; Tian, Y. Assimilating Remotely Sensed Information with the WheatGrow Model Based on the Ensemble Square Root Filter for Improving Regional Wheat Yield Forecasts. *Plant Prod Sci* **2013**, *16*(4), 352—364.

Huemmrich, K.F. The GeoSail model: a simple addition to the SAIL model to describe discontinuous canopy reflectance. *Remote Sens Environ* **2001**, *75* (3), 423-431.

Huete, A. R. A soil-adjusted vegetation index (SAVI). *Remote Sens Environ* **1998**, *25*, 295-309.

Huete, A.; Justice, C.; Leeuwen Van, W. Modis Vegetation Index (MOD13). Algorithm Theoretical Basis Document. Available on: http://modis.gsfc.nasa.gov/data/atbd/atbd_mod13.pdf (accessed on 02/04/2016).

Immitzer, M.; Vuolo, F.; Atzberger, C. First Experience with Sentinel-2 Data for Crop and Tree Species Classifications in Central Europe. *Remote Sens* **2016**, *8*, 166.

Ines, A. V. M.; Das, N. N.; Hansen, J. W.; Njoku, E. G. Assimilation of remotely sensed soil moisture and vegetation with a crop simulation model for maize yield prediction. *Remote Sens. Environ.* **2013**, *138*, 149–164.

Inoue, Y. Synergy of remote sensing and modeling for estimating ecophysiological processes in plant production. *Plant Prod Sci* **2003**, *6* (1), 3-16.

Jacquemoud, S.; Baret, F. PROSPECT: A model of leaf optical properties spectra. *Remote Sens Environ* **1990**, *34*, 75–91.

Jacquemoud, S.; Verhoef, W.; Baret, F.; Bacour, C.; Zarco-Tejada, P. J.; Asner, G. P.; Ustin, S. L. PROSPECT + SAIL models: A review of use for vegetation characterization. *Remote Sens Environ*, **2009**, *113*, 56–66.

Jégo, G.; Pattey, E.; Liu, J. Using Leaf Area Index, retrieved from optical imagery, in the STICS crop model for predicting yield and biomass of field crops. *Field Crops Res* **2012**, 131, 63–74.

Jiang, Z.; Chen, Z.; Chen, J.; Ren, J.; Li, Z.; & Sun, L. The Estimation of Regional Crop Yield Using Ensemble-Based Four-Dimensional Variational Data Assimilation. *Remote Sens* **2014a**, *6*(4), 2664–2681.

Jiang, J.; Xiao, Z.; Wang, J.; Song, J. Sequential Method with Incremental Analysis Update to Retrieve Leaf Area Index from Time Series MODIS Reflectance Data. *Remote Sens* **2014b**, *6*(10), 9194–9212.

Jiang, Z.; Chen, Z.; Chen, J.; Liu, J.; Ren, J.; Li, Z.; Li, H. Application of Crop Model Data Assimilation With a Particle Filter for Estimating Regional Winter Wheat Yields. *IEEE J Sel Top Appl Earth Obs Remote Sens* **2014c**, *7*(11), 4422–4431.

Jones C.A.; Kiniry J. CERES-MAIZE, a simulation model of maize growth and development, Texas A&M University Press, 1986, pp.194.

Jones, H.G.; Vaughan, R.A. Radiative properties of vegetation, soils, and water. In *Book Remote Sensing of Vegetation: Principles, Techniques, and Applications*, 1st ed.; Publisher: Oxford University Press, Great Britain, 2010; pp. 36–67.

Jones, J. W.; Hoogenboom, G.; Porter, C.H.; Boote, K.J.; Batchelor, W.D.; Hunt, L.A.; Wilkens, P.W.; Singh, U.; Gijsman, A.J. Ritchie, J.T. The DSSAT cropping system model. *Eur J Agron* **2003**, *18*, 3-4.

Kalman, R. E. A New Approach to Linear Filtering and Prediction Problems. *J Basic Eng-T ASME* **1960**, *82*(Series D), 35–45.

Kang, B.; Leeb, K.; Choea, J. Improvement of ensemble smoother with SVD-assisted sampling scheme. *J Petrol Sci Eng* **2016**, *141*, 114–124.

Kennedy, J.; Eberhart, R.C. Particle swarm optimization. *Proceedings of IEEE International Conference on Neural Networks* **1995**, 1942-1948.

Kim, H.; Chang, S.; Kang, T-G. Enhancement of Particle Swarm Optimization by Stabilizing Particle Movement. *ETRI Journal* **2013**, 35 (6), 1168-1171.

Ko, J.; Maas, S. J.; Lascano, R. J.; Wanjura, D. Modification of the GRAMI Model for Cotton. *Agron J* **2005**, *97*(5), 1374.

Ko, J.; Maas, S. J.; Mauget, S.; Piccinni, G.; Wanjura, D. Modeling Water-Stressed Cotton Growth Using Within-Season Remote Sensing Data. *Agron J* **2006**, *98*(6), 1600.

Koetz, B.;Baret, F, Poilvé, H, Hill, J. Use of coupled canopy structure dynamic and radiative transfer models to estimate biophysical canopy characteristics. *Remote Sens Environ* **2005**, *95* (1), 115-124.

Künsch, H. R. Particle filters. *Bernoulli* **2013**, *19*(4), 1391–1403.

Lahoz, W.; Schneider, P. Data assimilation: making sense of Earth Observation. *Front Environ Sci* **2014**, 2, 1–28.

LAI-2200C Plant Canopy Analyzer, Instruction Manual. Available on: https://app.boxenterprise.net/s/fqjn5mlu8c1a7zir5qel (accessed on 05/04/2016)

Lantz, N. Estimating plant area index for monitoring crop growth dynamics using Landsat-8 and RapidEye images. *J Appl Remote Sens* **2014**, *8*, 085196-1-12.

Lauer, Joe. Methods for Calculating Corn Yield. Agronomy Advice, Univ. of Wisconsin-Madison. Available on: http://corn.agronomy.wisc.edu/AA/pdfs/A033.pdf (accessed on 15/04/2013).

Launay, M.; & Guérif, M. Assimilating remote sensing data into a crop model to improve predictive performance for spatial applications. *Agric. Ecosyst Environ* **2005**, *111*(1-4), 321–339.

Lauvernet, C.; Baret, F.; Hascoët, L.; Buis, S.; & Le Dimet, F. X. Multitemporal-patch ensemble inversion of coupled surface-atmosphere radiative transfer models for land surface characterization. *Remote Sens Environ* **2008**, *112*(3), 851–861.

Le Dimet, F. X. Talagrand, O. Variational algorithms for analysis and assimilation of meteorological observations: theoretical aspects. *Tellus* **1986**, *38*, 97–110.

Le Maire, G.; François, C.; Soudani, K.; Berveillera, D.; Pontaillera, J.Y.; Brédac, N.; Genetc, H.; Hendrik, H.; Dufrênea, E. Calibration and validation of hyperspectral indices for the estimation of broadleaved forest leaf chlorophyll content, leaf mass per area, leaf area index and leaf canopy biomass. *Remote Sens Environ* **2008**, *112* (10), 3846-3864.

Lecoeur, J.; Poire-Lassus, R.; Christophe, A.; Pallas, B.; Casadebaig, P.; Debaeke, P. Quantifying physiological determinants of genetic variation for yield potential in sunflower. SUNFLO: A model-based analysis. *Functional Plant Biology* **2011**, 38, 246–259.

Leeuwen Van, P.J. Particle Filtering in Geophysical Systems. *Mon Weather Rev* **2009**, *137*, 4089–4114.

Lewis, P.; Gómez-Dans, J.; Kaminski, T.; Settle J.; Quaife, T.; Gobron, N.; Styles, J.; Berger, M. An Earth Observation Land Data Assimilation System (EO-LDAS), *Rem. Sens. Environ*. **2012**, *120*, 219-235.

Li, R.; Li, C.; Dong, Y.; Liu, F.; Wang, J.; Yang, X.; & Pan, Y. Assimilation of Remote Sensing and Crop Model for LAI Estimation Based on Ensemble Kalman Filter. *Agric Sci China* **2011**, *10*(10), 1595–1602.

Li, X.; Zhang, Y.; Bao, Y.; Luo, J.; Jin, X.; Xu, X.; Song, X.; Yang, G. Exploring the Best Hyperspectral Features for LAI Estimation Using Partial Least Squares Regression. *Remote Sens.* **2014a**, *6*, 6221-6241.

Li, Y.; Zhou, Q.; Zhou, J.; Zhang, G.; Chen, C.; Wang, J. Assimilating remote sensing information into a coupled hydrology-crop growth model to estimate regional maize yield in arid regions. *Ecol Model* **2014b**, *291*, 15–27.

Li, Z.H.; Jin, X.L.; Zhao, C.J.; Wang, J.H.; Xu, X.G.; Yang, G.J.; Li, C.J.; Shen, J.X. Estimating wheat yield and quality by coupling the DSSAT-CERES model and proximal remote sensing. *Eur. J. Agron*. **2015**, *71*, 53-62.

Liang, L, Di, L.P.; Zhang, L.P.; Deng, M.X.; Qin, Z.H.; Zhao, S.H.; Lin, H. Estimation of crop LAI using hyperspectral vegetation indices and a hybrid inversion method. *Remote Sens Environ* **2015**, *165*, 123-134.

Liang, S. Recent developments in estimating land surface biogeophysical variables from optical remote sensing. *Prog Phys Geogr* **2007**, *31*(5), 501–516.

Lin, W.L.W.; Zhao, M.Z.M.; Liu, Y.L.Y.; Gao, J.G.J.; Wang, C.W.C. Winter wheat yield estimation model with MODIS normalized near-infrared spectral index. International Workshop on Earth Observation and Remote Sensing Applications, 30/06-2/07/2008, Beijing, China.

Lindquist, J.L.; Arkebauer, T.J.; Walters, D.T.; Cassman, K.G.; Dobermann, A. Maize Radiation Use Efficiency under Optimal Growth Conditions. Available on: http://digitalcommons.unl.edu/agronomyfacpub/92.

Liu, B.; Ait-El-Fquih, B.; Hoteit, I. Efficient Kernel-Based Ensemble Gaussian Mixture Filtering. *Mon Weather Rev* **2016**, *144*, 781-800.

Liu, J.; Huang, J.; Tian, L.; Ma, H.; Su, W.; Wu, W.; Zhu, D. Regional winter wheat yield prediction by integrating MODIS LAI into the WOFOST model with sequential assimilation technique. *J Food Agric Environ*, **2014a**, *12* (1), 180-187.

Liu, Q.; Liang, S.; Xiao, Z.; & Fang, H. Retrieval of leaf area index using temporal, spectral, and angular information from multiple satellite data. *Remote Sens. Environ.* **2014b**, 145, 25–37.

Liu, J.; Pattey, E.; Jégo, G. Assessment of vegetation indices for regional crop green LAI estimation from Landsat images over multiple growing seasons. *Remote Sens Environ* **2012**, *123*, 347–358.

Liu, J.; Pattey, E.; Miller, J. R.; McNairn, H.; Smith, A.; Hu, B. Estimating crop stresses, aboveground dry biomass and yield of corn using multi-temporal optical data combined with a radiation use efficiency model. *Remote Sens. Environ.* **2010**, *114*(6), 1167–1177.

Lobell, D. The use of satellite data for crop yield gap analysis. *Field Crops Res* **2013**, *143*, 56–64.

Locherer, M.; Hank, T.; Danner, M.; Mauser, W. Retrieval of Seasonal Leaf Area Index from Simulated EnMAP Data through Optimized LUT-Based Inversion of the PROSAIL Model. *Remote Sens* **2015**, *7* (8), 10321-10346.

Lyle, G.; Lewis, M.; Ostendorf, B. Testing the Temporal Ability of Landsat Imagery and Precision Agriculture Technology to Provide High Resolution Historical Estimates of Wheat Yield at the Farm Scale. *Remote Sens* **2013**, *5*(4), 1549–1567.

Ma, G.; Huang, J.; Wu, W.; Fan, J.; Zou, J.; & Wu, S. Assimilation of MODIS-LAI into the WOFOST model for forecasting regional winter wheat yield. *Math Comput Model* **2013b**, *58*(3-4), 634–643.

Ma, H.; Huang, J.; Zhu, D.; Liu, J.; Su, W.; Zhang, C.; & Fan, J. Estimating regional winter wheat yield by assimilation of time series of HJ-1 CCD NDVI into WOFOST-ACRM model with Ensemble Kalman Filter. *Math Comput Model* **2013a**, *58*(3-4), 759–770.

Maas, S.J. GRAMI: A crop growth model that can use remotely sensed information; US Department of Agriculture, Agricultural Research Service, Washington, USA, 1992, pp 78.

Maas, S.J. Using satellite data to improve model estimates of crop yield. *Agron J* **1988**, *80*(4), 655–662.

Maas, S.J. Within-season calibration of modeled wheat growth using remote sensing and field sampling. *Agron J* **1993,** *85*, 669–672.

Machwitz, M.; Giustarini, L.; Bossung, C.; Frantz, D.; Schlerf, M.; Lilienthal, H.; Thomas Udelhoven. Enhanced biomass prediction by assimilating satellite data into a crop growth model. *Environ Model Softw* **2014**, *62*, 437–453.

Makowski, D.; Jeuffroy, M.; Guérif, M. Bayesian methods for updating crop- model predictions, applications for predicting biomass and grain protein content. *Frontis* **2004**, *3*, 57–68.

Manjunath, K. R.; Potdar, M. B.; Purohit, N. L. Large area operational wheat yield model development and validation based on spectral and meteorological data. *Int. J. Remote Sens.* **2002**, *23* (15), 3023-3038.

Mansouri, M.; Destain, M.-F. An improved particle filtering for time-varying nonlinear prediction of biomass and grain protein content. *Comput Electron in Agric* **2015**, *114*, 145–153.

Mansouri, M.; Dumont, B.; Leemans, V.; & Destain, M.-F. Bayesian methods for predicting LAI and soil water content. *Precis Agric* **2014**, *15*, 184–201.

Meng, J.; Du, X.; Wu, B. Generation of high spatial and temporal resolution NDVI and its application in crop biomass estimation. *Int J Digit Earth* **2013**, *6*, 203-218.

Meroni, M.; Marinho, E.; Sghaier, N.; Verstrate, M.; Leo, O. Remote Sensing Based Yield Estimation in a Stochastic Framework—Case Study of Durum Wheat in Tunisia. *Remote Sens*, **2013**, *5*(2), 539–557.

Monteith, J. L. Climate and efficiency of crop production in Britain. *Phil. Trans. R. Soc. B* **1977**, *281*, 277–294.

Montzka, C.; Pauwels, V. R. N.; Franssen, H.J. H.; Han, X.; Vereecken, H. Multivariate and multiscale data assimilation in terrestrial systems: a review. *Sensors,* **2012**, *12*(12), 16291-16333.

Moradkhani, H.; Sorooshian, S.; Gupta, H. V.; Houser, P. R. Dual state-parameter estimation of hydrological models using ensemble Kalman filter. *Adv Water Resour* **2005**, *28*(2), 135–147.

Morel, J.; Begue, A.; Todoroff, P.; Martine, J.; Lebourgeois, V.; Petit, M. Coupling a sugarcane crop model with the remotely sensed time series of fIPAR to optimise the yield estimation. *Eur. J. Agron*, **2014**, *61*, 60–68.

Moriondo, M.; Maselli, F.; Bindi, M. A simple model of regional wheat yield based on NDVI data. *Eur J Agron* **2007**, *26*(3), 266–274.

Mosleh, M.; Hassan, Q. H.; Chowdhury, E.H. Application of Remote Sensors in Mapping Rice Area and Forecasting Its Production: A Review. *Sensors* **2015**, *15*(1), 769-791.

Moulin, S.; Fischer, A.; Dedieu, G.; Delècolle, R. Temporal variations in satellite reflectances at field and regional scales compared with values simulated by linking crop growth and SAIL models. Remote *Sens. Environ* **1995**, 54, 261–272.

Mousivand, A.; Menenti, M.; Gorte, B.; & Verhoef, W. Multi-temporal, multi-sensor retrieval of terrestrial vegetation properties from spectral–directional radiometric data. *Remote Sens Environ* **2015**, *158*, 311–330.

Mridha, N; Sahoo, N.R.; Kumar, D.N.; Sehgal, V.K.; Krishna, G.; Pradhan, S.; Gupta, V.K. Genetic Algorithm based Inversion Modelling of PROSAIL for Retrieval of Wheat Biophysical Parameters from Bi-directional Reflectance Data. *Int. Agrophys*, **2014**, 14, 87-95.

Mridha, N; Sahoo, N.R.; Sehgal, V.K.; Krishna, G.; Pargal, S.; Pradhan, S.; Gupta, V.K.; Kumar, D.N. Comparative evaluation of inversion approaches of the radiative transfer model for estimation of crop biophysical parameters. *Int. Agrophys*., **2015**, 29, 201-212

Müller,W. Agroklimatische Kennzeichnung des zentralen Marchfeldes. *Beihefte zu den Jahrbüchern der ZAMG, Klimatologie* **1993**, *3*(348).

Murmu, S.; Biswas, S. Application of Fuzzy Logic and Neural Network in Crop Classification: A Review. *Aquat. Procedia*, **2015**, *4*, 1203–1210.

Murthy, V.R.K. Crop Growth Modeling and its Applications in Agricultural Meteorology. Proceedings of a Training Workshop, Dehra Dun, India, 7-11 July 2003.

Myneni, R.B.; Ross, J. Photon-Vegetation Interactions. Applications in Optical Remote Sensing and Plant Ecology; Springer Science & Business Media, Berlin Heidelberg, Germany, 1991; pp 565.

Nearing, G. S.; Crow, W. T.; Thorp, K. R.; Moran, M. S.; Reichle, R. H.; & Gupta, H. V. Assimilating remote sensing observations of leaf area index and soil moisture for wheat yield estimates: An observing system simulation experiment. *Water Resour Res* **2012**, *48*(5), 1–13.

Nguy-Robertson, A.; Gitelson, A.; Peng, Y.; Viña, A.; Arkebauer, T.; Rundquist, D. Green Leaf Area Index Estimation in Maize and Soybean: Combining Vegetation Indices to Achieve Maximal Sensitivity. *Agron. J.* **2012**, *104*, 1336–1347.

Nightingale, J.M.; Morisette, J.T.; Wolfe, R.E.; Tan, B.; Gao, F.; Ederer, G.; Collatz, G.J.; Turner, D.P. Temporally smoothed and gap-filled MODIS land products for carbon modelling: application of the fPAR product. *Int. J. Remote Sens.* **2009**, 30(4), 1083-1090.

Oteng-Darko, P.; Yeboah, S.; Addy S. N. T.; Amponsah, S.; Owusu Danquah, E. Crop modeling: A tool for agricultural research–A review. *E3 Journal of Agricultural Research and Development* **2013**, *2*(1), 1-6.

Ozdogan, M. The spatial distribution of crop types from MODIS data: Temporal unmixing using Independent Component Analysis. *Remote Sens Environ* **2010**, *114*(6), 1190–1204.

Padilla, F.L.M.; Maas, S.J.; González-Dugo, M.P.; Mansilla, F.; Rajan, N.; Gavilán, P.; Dominguez, J. Monitoring regional wheat yield in Southern Spain using the GRAMI model and satellite imagery. *Field Crop Res* **2012**, *130*, pp. 145–154.

Patel, N. R.; Bhattacharjee, B.; Mohammed, A. J.; Tanupriya, B.; Saha, S. K. Remote sensing of regional yield assessment of wheat in Haryana, India. *Int. J. Remote Sens.* **2006**, *27* (19), 4071 – 4090.

Payero, J. O.; Tarkalson, D.; Irmak, S.; Davison, D.; Petersen J. L. Effect of timing of a deficit-irrigation allocation on corn evapotranspiration, yield, water use efficiency, and dry mass. *Agric. Water. Mgmt.* **2009**, *96*(10), 1387-1397.

Pellenq, J.; Boulet, G. A methodology to test the pertinence of remote-sensing data assimilation into vegetation models for water and energy exchange at the land surface. *Agronomie* **2004**, *24*(4), 197-204.

Peng, Y.; Gitelson, A.; Keydan, G.; Rundquist, D. C.; Moses, W. Remote estimation of gross primary production in maize and support for a new paradigm based on total crop chlorophyll content. *Remote Sens. Environ.* **2011**, *115*(4), 978–989.

Penning de Vries, F.W.T.; Jansen, D.M.; Berge, H.F.M.; Bakema, A. Assimilation and dissimilation of carbon. In Simulation of ecophysiological processes of growth in several annual crops. Simulations Monographs, PUDOC, Wageningen, The Netherlands, 1989, pp. 28-40.

Pino, F. A. Estadísticas agrícolas para el siglo XXI. *Revista Agricultura de San Pablo* **1999**, *46*(2), 71-105.

Plummer, S. E. Perspectives on combining ecological process models and remotely sensed data. *Ecol Model* **2000**, *129*(2-3), 169–186.

Pragnère, A.; Baret, F.; Weiss, M.; Myneni, R.; Knyazikhin, Y.; Wang, L.B. Comparison of three radiative transfer model inversion techniques to estimate canopy biophysical variables from remote sensing data. Geoscience and Remote Sensing Symposium; (IGARSS) 1999, 2, 1093-1095.

Prévot, L.; Chauki, H.; Troufleau, D.; Weiss, M.; Baret, F.; Brisson, N. Assimilating optical and radar data into the STICS crop model for wheat. *Agronomie* **2003**, *23* (4), 297-303.

Qi, J.; Chehbouni, A.; Huete, A. R.; Kerr, H. Y.; Sorooshian, S. A modified soil adjusted vegetation index. *Remote Sens Environ* **1994**, *48*,119−126.

Qu,Y.; Wang. J.; Wan, H.; Li, X.; Zhou, G. A Bayesian network algorithm for retrieving the characterization of land surface vegetation. *Remote Sens Environ*, **2008**, *112*, 613–622

Rahman, A.;Roytman, L.; Krakauer, N.Y.; Nizamuddin,M.; Goldberg, M. Use of Vegetation Health Data for Estimation of Aus Rice Yield in Bangladesh. *Sensors* **2009**, *9*(4), 2968–2975.

Rauff, K.; Bello, R. A Review of Crop Growth Simulation Models as Tools for Agricultural Meteorology. *Agricultural Sciences* **2015**, *6*, 1098-1105. DOI: 10.4236/as.2015.69105.

Reichle, R. H.; Walker, J. P.; Koster, R. D.; Houser, P. R. Extended versus Ensemble Kalman Filtering for Land Data Assimilation. *J Hydrometeorol* **2002a**, *3*(6), 728–740.

Reichle, R.; McLaughlin, D. B.; Entekhabi, D. Hydrologic data assimilation with the ensemble Kalman filter. *Monthly Weather Review* **2002b**, *130*(1), 103–114.

Rembold, F.; Atzberger, C.; Savin, I.; & Rojas, O. Using Low Resolution Satellite Imagery for Yield Prediction and Yield Anomaly Detection. *Remote Sens* **2013**, *5*(4), 1704–1733.

Ren, J.; Yu, F.; Du, Y.; Qin, J.; & Chen, Z. Assimilation of field measured LAI into crop growth model based on SCE-UA optimization algorithm. *International Geoscience and Remote Sensing Symposium* (IGARSS) 2009, *3*, 573–576.

Richardson, A.J.; Wiegand, C.L.; Wanjura, D.F.; Dusek, D.; Steiner, J.L. Multisite analyses of spectral biophysical data for sorghum. *Remote Sens Environ* **1992**, *41*, 71-82.

Richter, G. M.; Acutis, M.; Trevisiol, P.; Latiri, K.; Confalonieri, R. Sensitivity analysis for a complex crop model applied to Durum wheat in the Mediterranean. *Eur J Agron* **2010**, *32*(2), 127–136.

Richter, R. Correction of satellite imagery over mountainous terrain. *Appl. Opt*. **1998**, *37*, 4004–4015.

Rivera, J. P.; Verrelst, J.; Gómez-Dans, J.; Muñoz-Marí, J.; Moreno, J.; Camps-Valls, G. An Emulator Toolbox to Approximate Radiative Transfer Models with Statistical Learning. *Remote Sens* **2015**, *7*(7), 9347-9370.

Rizzi, R.; Rudorff, B.D.T.; Shimabukuro, Y. E. Analysis of MODIS leaf area index product over soybean areas in Rio Grande do Sul State, Anais XII Simpósio Brasileiro de Sensoriamento Remoto, Goiânia, Brasil, April 2005; pp. 253-260.

Rouse, J.W.; Haas, R.H.; Schell, J.A.; Deering, D.W. Monitoring vegetation systems in the great plains with ERTS. In Proceedings of the Third ERTS Symposium; NASA SP-351; NASA: Washington, DC, USA, 1973; pp. 309–317.

Royce, F.S.; Jones, J.W.; Hansen, J.W. Model-based optimization of crop management for climate forecast applications. *Trans ASAE* **2001**, *44*(5), 1319-1327.

Rudorff, B.F.T.; Batista, G.T. Spectral response of wheat and its relationship to agronomic variables in the tropical region**.** *Remote Sens. Environ.* **1990**, *31*(1), 53-63.

Ruiz, J.J.; Pulido, M.; Miyoshi, T. Estimating Model Parameters with Ensemble-Based Data Assimilation: A Review. *J. Meteor. Soc. Japan* **2013**, *91* (2), 79-99.

Sakamoto, T.; Gitelson, A.; Arkebauer, T. J. MODIS-based corn grain yield estimation model incorporating crop phenology information. *Remote Sens. Environ.* **2013**, *131*, 215–231.

Salazar, L.; Kogan, F.; Roytman, L. Use of remote sensing data for estimation of winter wheat yield in the United States. *Int. J. Remote Sens.* **2007**, *28*(17), 3795–3811.

Sellers, P.J. Canopy reflectance, photosynthesis and transpiration, II. The role of biophysics in the linearity of their interdependence. *Int. J. Remote Sens.* **1987**, *21*, 143-183.

Serrano, L.; Filella, I.; Penuelas, J. Remote sensing of biomass and yield of winter wheat under different nitrogen supplies. *Crop Science* **2000**, *40* (3), 723-731.

Shanahan, J. F.; Schepers, J. S.; Francis, D. D.; Varvel, G. E.; Wilhem, W. Use of Remote-Sensing Imagery to Estimate Corn Grain Yield. *Agron J* **2001**, *93*, 583–589.

Shang, J.; Liu, J.; Huffman, T.; Qian, B.; Pattey, E.; Wang, J.; Zhao, T.; Geng, X.; Kroetsch, D.; Dong, T.;

Shen, Z.Q.; Tang, Y.M. A modified ensemble Kalman particle filter for non-Gaussian systems with nonlinear measurement functions. *J Adv Model Earth Sy* **2015**, *7*(1), 50-66.

Shi, Y.; Ji, S.P.; Shao, X.W.; Tang, H.J.; Wu, W.B.; Yang, P.; Zhang, Y.J.; Ryosuke, S. Framework of SAGI agriculture remote sensing and its perspectives in supporting national food security. *J Integr Agric* **2014**, *13* (7), Pages 1443-1450.

Shin D. W.; Baigorria G. A, Lim Y.-K.; S. Cocke, T. E. LaRow, O'Brien, J.J.; Jones, J-W. Assessing Crop Yield Simulations with Various Seasonal Climate Data. Science and Technology Infusion Climate Bulletin NOAA's National Weather Service 7th NOAA Annual Climate Prediction Application Science Workshop, Oklahoma, USA, 24-27 October 2009.

Šimůnek, J. Models of water flow and solute transport in the unsaturated zone. In *Encyclopedia of hydrological sciences;* Anderson, M.G and McDonnell, J.J; John Wiley & Sons, Chichester, UK, 2005; pp. 1171–1180.

Singer, J.W.; Meek, D.W.; Sauer, T.J.; Prueger, J. H.; Jerry L.; Hatfield, J.L. Variability of light interception and radiation use efficiency in maize and soybean. *Field Crop Res*, **2011**, *121* (1), 147–152.

Soundharajan, B.; Sudheer, K. P. Sensitivity analysis and auto-calibration of ORYZA2000 using simulation-optimization framework. *Paddy Water Environ* **2013**, *11* (1-4), 59-71.

Spitters C.J.T.; van Keulen H.; Van Kraalingen D.W.G. A simple and universal crop growth simulator: SUCROS87. In *Simulation and system management in crop protection*; Rabbinge R., Ward S.A.; Van Laar H.H; Pudoc, Wageningen, The Netherlands, 1989, pp. 147–181.

Spitters, C.J.T. Crop growth models: their usefulness and limitations. *Acta Hortic*. **1990**, *267*, 349-368.

Steinmetz, S.; Guerif, M.; Delecolle, R.; Baret, F. Spectral estimates of the absorbed photosynthetically active radiation and light-use efficiency of a winter wheat crop subjected to nitrogen and water deficiencies. *Int. J. Remote Sens*. **1990**, *11*, 1797–1808.

Stol W.; Rouse, D.I.; van Kraalingen, D.; Klepper O. FSEOPT a FORTRAN program for calibration and uncertainty analysis of simulation models; Simulation Report CABO-TT, CABO-DLO and Agricultural University, Netherlands, 1992, 24, pp 1-24.

Thenkabail, P.S.; Smith, R.B.; De Pauw, E. Hyperspectral vegetation indices and their relationship with agricultural crop characteristics. *Remote Sens Environ* **2000a**, *71* (2), 158-182.

Thenkabail, P.S. Biophysical and yield information for precision farming from near-real-time and historical Landsat TM images. *Int. J. Remote Sens.* **2000b**, 24 (14), 2879-2904.

Thenkabail, P.S.; Knox, J.W.; Ozdogan, M.; Gumma, M. K.; Congalton, R.G.; Wu, Z.; Milesi, C.; Finkral, A.; Marshall, M.; Mariotto, I.; You, S.; Giri, C.; Nagler, P. Assessing future risks to agricultural productivity, water resources and food security: How can remote sensing help? *Photogramm Eng Remote Sensing* **2012**, 78 (8), 773-782.

Tian, L.Y.; Li, Z.X.; Huang, J.X.; Wang, L.M.; Su, W.; Zhang, C.; Liu, J.M. Comparison of Two Optimization Algorithms for Estimating Regional Winter Wheat Yield by Integrating MODIS Leaf Area Index and World Food Studies Model. *Sensor Letters* **2013**, *11*(6-7), 1261-1268.

Tian, X.; Xie, Z.; & Dai, A. An ensemble-based explicit four-dimensional variational assimilation method. *J Geophys Res* **2008**, *113*(D21), 1–13.

Tippett, M.K.; Anderson, J.L.; Bishop, C.H.; Hamill, T.M.; Whitaker, J.S. Ensemble square-root filters. *Mon Weather Rev* **2003**, *131*, 1485–1490.

Trelea I.C. The particle swarm optimization algorithm: convergence analysis and parameter selection. *Information Processing Letters* **2003**, *85*, 317-325.

Tremblay, Marie; Wallach, Daniel. Comparison of parameter estimation methods for crop models. *Agronomie* **2004**, *24*, 351–365.

Tripathy, R.; Chaudhari, K.N.; Mukherjee, J.; Ray, S.S.; Patel, N.K.; Panigrahy, S.; Parihar, J.S. Forecasting wheat yield in Punjab state of India by combining crop simulation model WOFOST and remotely sensed inputs. *Remote Sens Lett* **2013**, *4*(1), 19–28.

Trombetta, A.; Iacobellis, V.; Tarantino, E. ; Gentile, F . Calibration of the Aqua Crop model for winter wheat using MODIS LAI images. *Agric Water Manag* **2016**, *164*(2), 304-316.

Trudinger, C. M.; Raupach, M. R.; Rayner, P. J.; Enting, I. G. Using the Kalman filter for parameter estimation in biogeochemical models. *Environmetrics* **2008**, *19* (8), 849–870.

Tsiligirides, T. A. Remote sensing as a tool for agricultural statistics: a case study of area frame sampling methodology in Hellas. *Comput Electron Agric* **1998**, *20* (1), 45-77.

UN Sustainable Development Goals. Available online: http://www.un.org/sustainabledevelopment (accessed on 29/03/2016).

Van der Tol, C.; Verhoef, W.; Timmermans, J.; Verhoef, A.; Su, Z. An integrated model of soil-canopy spectral radiances, photosynthesis, fluorescence, temperature and energy balance. *Biogeosciences* **2009**, *6*, 3109–3129.

Vazifedoust, M.; van Dam, J. C.; Bastiaanssen, W. G. M.; Feddes, R. Assimilation of satellite data into agrohydrological models to improve crop yield forecasts. *Int. J. Remote Sens.* **2009**, *30*(10), 2523–2545.

Verger, A.; Baret, F.; Camacho, F. Optimal modalities for radiative transfer-neural network estimation of canopy biophysical characteristics: Evaluation over an agricultural area with CHRIS/PROBA observations. *Remote Sens Environ* **2011**, *115* (2), 415–426.

Verhoef, W.; Bach, H. Coupled soil-leaf-canopy and atmosphere radiative transfer modeling to simulate hyperspectral multi-angular surface reflectance and TOA radiance data. Remote Sens Environ **2007**, 109,166−182.

Verhoef, W.; Xiao, Q.; Jia, L.; & Su, Z. Unified optical-thermal four-stream radiative transfer theory for homogeneous vegetation canopies. *IEEE Trans Geosci Remote Sens* **2007**, *45*, 1808-1822.

Verhoef,W. Light scattering by leaf layers with application to canopy reflectance modeling: the SAIL model. *Remote Sens Environ* **1984**, *16*,125−141.

Verrelst, J.; Camps-Valls, G.; Muñoz-Marí, J.; Rivera, J. P.; Veroustraete, F.; Clevers, J. G.; Moreno, J. Optical remote sensing and the retrieval of terrestrial vegetation bio-geophysical properties–A review. *ISPRS J Photogramm Remote Sens* **2015b**, *108*, 273-290.

Verrelst, J.; Rivera, J.P.; Gómez-Dans, J.; Camps-Valls, G.; Moreno, J. Replacing radiative transfer models by surrogate approximations through machine learning. International Geoscience and Remote Sensing Symposium (IGARSS) 2015c, 633–636.

Verrelst, J.; Rivera, J.P.; Veroustraete, F.; Munoz-Mari, J.; Clevers, J.G.P.W.; Camps-Valls, G.;Moreno, J. Experimental Sentinel-2 LAI estimation using parametric, non-parametric and physical retrieval methods -A comparison.*ISPRS J Photogramm Remote Sens* **2015a**, *108*, 260-272.

Vohland, M.; Mader, S.; Dorigo, W. Applying different inversion techniques to retrieve stand variables of summer barley with PROSPECT+ AIL. *Int J Appl Earth Obs Geoinf* **2010**, *12*(2), 71–80.

Vuolo, F.; Atzberger, C.; Richter, K.; Dash, J. Retrieval of Biophysical Vegetation Products from Rapideye Imagery. ISPRS TC VII Symposium, Vienna, Austria, 5–7/7/2010; IAPRS, Vol. XXXVIII, Part 7A; pp. 281–286.

Vuolo, F.; Neugebauer, N.; Bolognesi, S.; Atzberger, C.; & D'Urso, G. Estimation of Leaf Area Index Using DEIMOS-1 Data: Application and Transferability of a Semi-Empirical Relationship between two Agricultural Areas. *Remote Sens* **2013**, *5*(3), 1274–1291.

Vuolo, F.; Żółtak, M.; Pipitone, C.; Zappa, L.; Wenng, H.; Immitzer, M. Data service platform for Sentinel-2 surface reflectance and value-added products: system use and examples. JAG **2016** (under review).

Vuolo, F.; Wai, T.; Atzberger. Innovative approach for smoothing and gap-filling of high resolution multi-spectral time series: Example of Landsat data. Transactions on Geoscience and Remote Sensing **2016** (under review).

Wallach, D.; Goffinet, B.; Bergez, J.-E.; Debaeke, P.; Leenhardt, D.; Aubertot, J.-N. Parameter Estimation for Crop Models. *Agron J* **2001**, *93*(4), 757.

Wang, F.; Huang, J.; Tang, Y.; Wang, X. New Vegetation Index and Its Application in Estimating Leaf Area Index of Rice. *Rice Sci* **2007**, *14* (3), 195–203.

Wang, H.; Zhu, Y.; Li, W.; Cao, W.; Tian, Y. Integrating remotely sensed leaf area index and leaf nitrogen accumulation with RiceGrow model based on particle swarm optimization algorithm for rice grain yield assessment. *J Appl Remote Sens* **2014**, *8*(1), 083674.

Weiss, M.; Baret, F.; Myneni, R.B.; Pragnere, A.; Knyazikhin, Y. Investigation of a model inversion technique to estimate canopy biophysical variables from spectral and directional reflectance data. *Agronomie* **2000**, *20*, 3–22.

Whitaker, J. S.; Hamill, T. M. Ensemble Data Assimilation without Perturbed Observations. *Mon Weather Rev* **2002**, *130*(7), 1913–1924.

Widlowski, J.L..; Mio, C.; Disney, M.; Adams, J.; Andredakis, I.; Atzberger, C.; Brennan, J.; Busetto, L..; Chelleg, M.; Ceccherini, G.; Colombo, R.; Côté, J.F.; Eenmäe, A.; Essery, R.; Gastellu-Etchegorry, J. P.; Gobron, N.; Graun, E.; Haverd, V.; Homolová, L.; Huang, H.; Hunt, L.; Kobayashi, H.; Koetz, B.; Kuusk, A.; Kuusk, J.; Lang, M.; Lewis, P. E.; Lovell, J. L.; Malenovský, Z.; Meroni, M.; Morsdorf, F. The fourth phase of the radiative transfer model intercomparison (RAMI) exercise: Actual canopy scenarios and conformity testing. *Remote Sens Environ* **2015**, *169*, 418-437.

Widlowski, J.L.; Pinty, B.; Lopatka, M.; Atzberger, C.; Buzica, D.; Chelle, M.; Disney, M.; Gastellu-Etchegorry, J.P.; Gerboles, M.; Gobron, N.; Grau, E.; Huang, H.; Kallel, A.; Kobayashi, H.; Lewis, P.E.; Qin, W.; Schlerf, M.; Stuckens, J.; Xie, D. The fourth radiation transfer model intercomparison (RAMI-IV): Proficiency testing of canopy reflectance models with ISO-13528. *J Geophys Res-Atmos* **2013**, 118(13), 6869-6890.

Wiegand, C.L.; Richardson, A.J.; Jackson, R.D.; Pinter, P.J.; Aase, J.K.; Smika, D.E.; Lautenschlager, L.F.; Mcmurtrey, J.E. Development of Agrometeorological Crop Model Inputs from Remotely Sensed Information. *IEEE Trans Geosci Remote Sens* **1986**, *24* (1), 90-98.

Williams J.R.; Jones C.A.; Kiniry J.R.; Spanel D.A. The EPIC crop growth model. *Trans. ASAE* **1989**, *32*, 497–511.

Wöhling, Th.; Singh, R.; Schmitz, G. H. Physically based modeling of interactive surface-subsurface flow during furrow irrigation advance. *J. Irrig. Drain. Div* **2004**, *130*(5), 349–356.

Wold, S.; Sjostrom, M. Chemometrics: Theory and Application; American Chemical Society Simposium Series 52, Washington, 1977; pp 243.

World development report 2008. Available online: http://siteresources.worldbank.org/INTWDR2008/Resources/WDR_00_book.pdf (accessed on 29/03/2016).

World Food Programme. Available online: http://cdn.wfp.org/zerohunger (accessed on 29/03/2016).

Wu, S.; Huang, J.; Liu, X.; Fan, J.; Ma, G.; & Zou, J. Assimilating MODIS-LAI into crop growth model with EnKF to predict regional crop yield. *IFIP AICT* **2012**, *370*, 410–418.

Xiao, Z.; Liang, S.; Wang, J.; Wang, J.; Song, J.; Wu, X. A temporally integrated inversion method for estimating leaf area index from MODIS data. *IEEE Trans Geosci Remote Sens*, **2009**, *47*, 2536–2545

Xie, Q.Y.; Huang, W. J.; Cai, S.H.; Liang, D.; Peng, D. L.; Zhang, Q.; Huang, L. S.; Yang, G. J.; Zhang, D. Y. Comparative study on remote sensing inversion methods for estimating winter wheat leaf area index. *Guang pu xue yu guang pu fen xi* **2014**, *34* (5), 1352-6.

Xu, X.; Li, J.; Tolson, B. A. Progress in integrating remote sensing data and hydrologic modeling. *Prog Phys Geogr* **2014**, *38* (4), 464-498.

Yang, P.; Wu, W.; Tang, H.; Zhou, Q.; Zou, J.; Zhang, L. Mapping Spatial and Temporal Variations of Leaf Area Index for Winter Wheat in North China. *Agric Sci China* **2007**, *6*, 1437–1443.

Yao, Y.; Liu, Q.; Liu, Q.; Li, X. LAI retrieval and uncertainty evaluations for typical row-planted crops at different growth stages. *Remote Sens Environ*, **2008**, *112*(1), 94–106.

Yeom, J-M.; Ko, J.; Ok Kim, H. Application of GOCI-derived vegetation index profiles to estimation of paddy rice yield using the GRAMI rice model. *Comput Electron Agric* **2015**, *118*, 1-8.

Yuping, M.; Shili, W.; Li, Z.; Yingyu, H.; Liwei, Z.; Yanbo, H.; Futang, W. Monitoring winter wheat growth in North China by combining a crop model and remote sensing data. *Int J Appl Earth Obs Geoinf* **2008**, *10*(4), 426–437.

Zhang, H.K.; Huang,B.; Zhang, M.; Cao, K.; Yu, L. A generalization of spatial and temporal fusion methods for remotely sensed surface parameters. *Int J Remote Sens* **2015**, *36* (17), 4411-4445.

Zhang, Y.; Qu, Y.; Wang, J.; Liang, S.; Liu, Y. Estimating leaf area index from MODIS and surface meteorological data using a dynamic Bayesian network. *Remote Sens Environ* **2012**, *127*, 30–43.

Zhao, Y.; Chen, S.; & Shen, S. Assimilating remote sensing information with crop model using Ensemble Kalman Filter for improving LAI monitoring and yield estimation. *Ecol Model* **2013**, *270*, 30–42.

Zheng, G.; Moskal, M. Retrieving Leaf Area Index (LAI) Using Remote Sensing: Theories, Methods and Sensors. *Sensors* **2009**, *9*(4), 2719-2745.

Zhou, J.; Cheng, G.; Lia, X.; Hu, B. X.; Wang, G. Numerical Modeling of Wheat Irrigation using Coupled HYDRUS and WOFOST Models. *Soil Sci Soc Am J* **2012**, *76* (2), 648-662.

Zhu, X.; Zhao, Y.; Feng, X. A methodology for estimating Leaf Area Index by assimilating remote sensing data into crop model based on temporal and spatial knowledge. *Chin Geogr Sci* **2013**, *23*(5): 550−561.

Zhu, X.L.; Chen, J.; Gao, F.; Chen, X.H.; Masek, J.G. An enhanced spatial and temporal adaptive reflectance fusion model for complex heterogeneous regions. *Remote Sens. Environ.* **2010**, *114*, 2610–2623.

Zurita-Milla, R.; Laurent, V.C.E.; van Gijsel, J.A.E. Visualizing the ill-posedness of the inversion of a canopy radiative transfer model: A case study for Sentinel-2. *Int J Appl Earth Obs Geoinf* **2015**, 43, 7-18.

8. Index of tables

9. Index of figures

10. Index of abbreviations

4DVAR	Four Dimensional Variational Data Assimilation
A	Leaf partition fraction
ANN	Artificial neural network
B	Leaf partition fraction
CCC	Canopy chlorophyll content
CGM	Crop growth models
CPF	Convolution Particle Filtering
EEP	Estimation error at plot scale
EER	Estimation error at regional scale
EKF	Extended Kalman filter
EnKF	Ensemble Kalman filter
EnSRF	Ensemble square root filter
fCOVER	Fractional cover
fPAR	Fraction of photosynthetically active radiation absorbed by the canopy
GDD	Growing degree days
GDDem	GDD emergency
GDDmt	GDD maturity
GDP	Gross domestic product
HI	Harvest index
iLUT	iterative Look Up Table
IPF	Improved Particle Filter
K	Extinction coefficient
LAI	Leaf area index
LAIin	Initial LAI
LCC	Leaf chlorophyll content
LKf	Linear Kalman filter
LLS	Leaf span
LUE	Efficiency light use
LUT	Look up table
MCMC	Hamiltonian Markov Chain Monte Carlo
MLR	Multiple linear regression
NDII	Normalized-Difference-Infrared-Index
NDVI	Normalized difference vegetation index
NN	Neural nets
NRMSE	Normalized RMSE
NRMSEf	Mean square error for the regression function
PAR	Photosynthetically active radiation
PCR	Principal component regression
PF	Particle filter
PLSR	Partial least square regression
PSO	Particle Swarm Optimization

PSRI	Plant Senescence Reflectance Index
R2	Determination coefficient
REIP	Red edge inflection point
RENDVI	Red Edge Normalized Difference Vegetation Index
RFF	Random forest regression
RS	Remote sensing
RTM	Radiative transfer models
SAFY	Simple Algorithm For Yield estimate
SDI	Simple difference index
SenA	Senescence factor A
SenB	Senescence factor B
SLA	Specific leaf area
SR	Simple ratio
SRTM	Shuttle Radar Topography Mission
SVM	Support vector machines
SW	Sowing date
UN	United Nations
VI	Vegetation indices
WDVI	Weighted Difference Vegetation Index

11. Appendices

Appendix A-Estimating maize yield prior to harvest using the "Yield Component Method"

The method used to estimate maize yield was originally described in the University of Illinois. It is based on the premise that one can estimate grain yield from estimates of the yield components that constitute grain yield (http://www.agry.purdue.edu/ext/corn/news/timeless/YldEstMethod.html).

The yield components measured were:

1) number of ears per ha
2) number of kernel's rows per ear
3) number of kernels per row
4) kernel weight

The first three components were measured in field. The last component was estimated using 1000 seeds extracted from some average ears. The samples were dried at 100°c during two days and then they were weighted.

Yield (kg/ha) = ears/ha * average rows per ear * average kernels per row * weight of 1000 kernel

In the "yield component method" is suggested to sample several sites in the field and at each site, measure off a length of row equal to 1/1000th acre. In the sample site must be counted the number of harvestable ears and every fifth ear must be counted the number of rows per ear and the number of kernel per row. Then, it is calculated for this sample the average number of kernel per ear. This procedure must be repeated for at least four additional sites across the field.

Regarding the feasibility to take ear's samples and considering the size of the plots some changes were considered in the methodology suggested above. If we consider that the plot's row spacing is, in most of the cases 0.7m, the 1/1000th of length row is 14 m. To better represent the spatial variability of the plot, we defined a shorter row of 10 m and increased the number of samples in comparison with the original method. In each sample were selected two ears and the average number of kernel per ear were calculated. The samples were taken when the maize kernel began the milk stage (R3).

E. g.
Plot n° 2
Width: 54 m
Length: 840 m
N° of rows: 77 (54/0.7)
Total length row: 64680 m (77 * 840)
N° of samples: 6-7 ((64680 * 0.001)/10*)
*each sample is 10 m long.

The sampling method was systematic. For each elemental sampling unit (ESU) were taken 3 observations such as is delineated in the Figure A1. The aim of this sampling diagram was diminished the effect of the positional error in order to obtain a more precise spatial interpolation of the field data. The three yield components were measured in each ESU. The individual observations were used to estimate the average yield and the compounded samples to obtain a yield map.

In Table A1 is presented the basic data used during the maize sampling in field for the season 2013.

The autocorrelation spatial of the yield components was analized using ordinary Kriging technique. The best kriging model, nugget, sill and range were adjusted for each plot. To verified the kriging parameters, the values obtained were compared with the kriging of the same data but randomly distributed. We verified a low spatial autocorrelation of the data. The nugget values were high and the range values were similar to the distance between the samples. Therefore, the kriging functions had an important component of random error (high nugget) and the influence of the neighbor observations was low.

The low spatial autocorrelation might be related with the sampling method used, the homogeneity of the plot and the agricultural management. We believe that probably a more intensive sampling could capture the spatial autocorrelation of the maize. However, the influence of the factor with more relevance in the spatial pattern of the yield, the soil, was minimized by the influence of the irrigation. Spatial patterns of crop yield associated with soil conditions might be better detected in rain-feed regions.

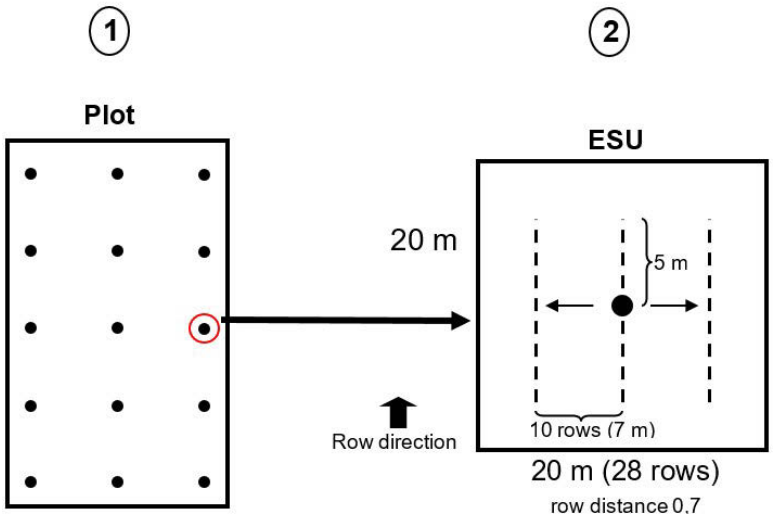

Figure A1- Sampling procedure to measure yield components and extract maize samples in field.

Table A1. Basic data for maize sampling in the season 2013

Sampling rate = 0,1% of the total meters of maize in one hectare.									
Plot	**Width (m)**	**Lenght (m)**	**n° rows**	**Total lenght**	**Number of samples**	**Samples x line**	**Number of lines**	**Row interval**	**Dist x sampl (m)**
2	54	840	77	64680	6	3	2	25	210
3	153	344	219	75336	8	4	2	70	70
4	45	755	64	48320	6	3	2	20	200
5	213	350	304	106400	12	4	3	80	70
7	74	533	106	56498	6	3	2	35	130
8	172	409	247	101023	10	5	2	80	80
9	70	500	100	50000	6	3	2	23	125
11	220	264	314	82896	9	3	3	80	70
12	49,7	640	71	45440	6	3	2	24	160
14	270	287	386	110782	12	4	3	100	60
16	150	280	214	59920	6	3	2	70	70
17	154	418	220	91960	9	4+1	2	70	80

Appendix B-Mathemathical description of GRAMI and SAFY models

B1. GRAMI

1.1. Calculation of the cumulative degree days

$\Delta GDD_t = GDD_{t-1} + (T_t - T_b)$

1.2. Fraction of the incident radiation energy absorbed by the canopy

$FAPAR_t = 1 - e^{-K * LAI(t-1)}$

1.3. Production of new dry mass

$\Delta DM_t = LUE * PAR_t * FAPAR_t$

1.4. Partitioning of new dry mass

- ***From Emergence to Anthesis***

  -New biomass to Leaf

  $LPF_t = 1 - SPF_t$

  $\Delta LAI_t = \Delta DM_t * LPF_t * SLA$

  $Sen_t = (\sum LAI > LLs) - Sen_{t-1}$

  When the age of the leaves exceeds LLs is assumed that they have senesced

  $LAI_t = LAI_{t-1} + (\Delta LAI_t - Sen_t)$

  -New biomass to Stem

  $SPF_t = A * e^{B * GDD}t$

  $\Delta Stem_t = \Delta DM_t * SPF_t$

  $Steam_t = Stem_{t-1} + \Delta Stem_t$

- ***From Anthesis to maturity*** *(The biomass is not partitioned to the Leaf)*

  -Leaf biomass

  $Sen_t = \sum LAI > LLs - Sen_{t-1}$

  $LAI_t = LAI_{t-1} - Sen_t$

  -New biomass to Stem

  $SPF_t = A * e^{B * GDD}t$

  $\Delta Stem_t = \Delta DM_t * SPF_t$

  $Steam_t = Stem_{t-1} + \Delta Stem_t$

  -New biomass to Grain

  $YPF_t = 1 - SPF_t$

  $\Delta Grain_t = \Delta DM_t * YPF_t$

  $Grain_t = Grain_{t-1} + \Delta Grain_t$

t: loop step
T: Average daily air temperature (ºC)
Tb: Base temperature specific to a crop species (ºC)
GDD: Growing degree days (ºC)
PAR: Photosynthetically Active Radiation (MJ/m²)
LAI: Leaf Area Index
ΔDM: Dry matter produced at day t
Grain: yield production (g/m2)
LUE: Light Use Efficiency (g/MJ). It represents the efficiency to convert absorbed PAR into biomass.

SLA: Specific leaf area (m^2/g). It determines the square meters of leaf that can be created per kg of leaf biomass.
K: Light extinction coefficient. It is directly related with leaf structure and canopy architecture assuming a specific value for a given crop.
SPF: fraction of **ΔD**M partitioned to Stem
LPF: fraction of **ΔD**M partitioned to Leaf
YPF: fraction of **ΔD**M partitioned to Grain
A: Coefficient
B: Coefficient
SPF increases from zero in an exponential manner as a function of the GDDs. The curvature of the SPF function is controlled by the parameters A (define the maximum value of SPF curve) and B (define the slope of SPF curve).
Sen: senescence biomass
LLs: Leaf Lifespan

B2. SAFY
The SAFY model is defined by similar formulas to GRAMI; however, there are some differences detailed as follows:

2.1. Effect of temperature stress in dry mass production:
In SAFY the calculation of dry matter increment (ΔDM) is modified by a factor which depends of the air temperature (Tps). The coefficient is defined by a range of optimum temperature and a function which can take the power 1 to 3. The following logic rule is applied:

if $T < T_{min}$ or $T > T_{max}$	$Tps = 0$
if $T_{max} > T > T_{opt}$	$Tps = 1 - ((T_{opt}-T)/(T_{opt}-T_{max}))^{ß}$
if $T_{min} < T < T_{opt}$	$Tps = 1 - ((T_{opt}-T)/(T_{opt}-T_{min}))^{ß}$

Tmax: maximum temperature;
Tmin: minimum temperature;
Top: optimum temperature.

For maize the range of temperatures suggested by Claverie, et al. (2012) was:
Tmax: 45°C;
Tmin: 8°C;
Top: 30°C.

For instance, if T= 18°C and ß=2
Tps = 0.45
then $\Delta DM_t = LUE * APAR *. 0.45$

2.2. Calculation of senescence:
Unlike GRAMI in SAFY senescence is driven by two parameters; Sum of Temperature for Senescence (Sen A) express in °C, which indicate the beginning of senescence and the Rate of Senescence (Sen B) express in °C day^{-1}, which mimic the velocity of the senescence process.
$Sen_t = LAI_{(t-1)} * ((\sum GDD - Sen\ A)/Sen\ B)$

2.3. Partition to grain

The grain biomass is calculated based in the partition yield coefficient (Py) which represents a percentage of the total biomass partitioned to the grain every day along the period from flowering to maturity, instead of GRAMI, which is considered a percentage (YPF) of the daily biomass produced.

$GM_t=GM_{(t-1)}+Py*\Delta DM_t$

GM: grain dray matter;
DM: dry matter;
Py: Partition yield.

Appendix C-Cost functions and logical rules of iterative LUT

C1. Cost functions

Before introducing the cost functions tested in LUT experiment, it is important to define the meaning of individual error used hereinafter. Individual error is defined as the error between LAI observed and LAI estimated in a time t ($LAIobs_t$ - $LAIest_t$). The term "total error" refers to the sum of individual errors along the crop season. The error was, in all the cases, expressed as percentage with respect to the total sum of LAI observations.

C1.1. Simple cost function

The function considers the same weight for each individual errors.

$$\text{Error} = (\sum_{t=1}^{n} \sqrt{(\text{LAIobs}_t - \text{LAIest}_t)^2} \ / \ \sum_{t=1}^{n} (\text{LAIobs}_t)\ ) * 100 \quad (1)$$

C1.2. Weighted cost function by phenology

A correct identification of anthesis period has a direct impact on the yield estimation because in both models the partition of biomass to the grain starts at anthesis. Therefore, if the anthesis identification is not precise enough, the period of grain filling could be shorter or longer compared to real conditions. Being aware of this situation, a cost function has been tested in which the weight of each individual error is defined depending on the related crop phenology. Assuming that maize anthesis matches with the maximum LAI value, 50% of the weight of the cost function was assigned to the three individual errors centered in the date of maximum LAI. The rest of weight was distributed proportionally to the rest of individual errors.

$$\text{Error}_{wphen} = (\ \sum_{t=1}^{n} w_t \sqrt{(\text{LAIobs}_t - \text{LAIest}_t)^2} \ / \ \sum_{t=1}^{n} (\text{LAIobs}_t)\ ) * 100 \quad (2)$$

C1.3. Weighted cost function by LAI uncertainty

As mentioned in section 4.9.1, the estimation of LAI is affected by uncertainties such as non-random distribution of the canopy elements. This effect is maximized at the beginning of the crop cycle, mainly, in row crops such as maize. The evolution of LAI error measured in the field with LICOR 2200 was analyzed verifying that the initial estimations had a perceptual error between 30 and 40%. Then, along the crop season the measurement error sank to around 5 %. A logical rule was defined to state a threshold tolerance error depending on the LAI observation values which is described below:

$LAI\_diffe_t = (|LAIobs_t - LAIest_t| / LAIobs_t) * 100$
If $LAIobs_t < 1$ and $LAI\_diffe_t < 30$ %; $Bval_t = 1$ *else* $Bval_t = 0$
If $LAIobs_t > 1$ and $LAI\_diffe_t < 10$ %; $Bval_t = 1$ *else* $Bval_t = 0$

The error is expressed as percentage considering the number of individual errors, which fulfill the logical rule above with respect to the total number of LAI observations.

$$\text{Error}_{w\_uncer} = (\sum_{t=1}^{n} \text{Bval}_t / \text{n° total of observations}) * 100 \quad (3)$$

C1.4. Balanced cost function

The weight of each individual error in a simple cost function (1) would be 0.1. However, an uneven temporal distribution of LAI observations can produce an unbalanced objective function calculation because observations in one part of the crop season receive much more weight than in other parts. To minimize this effect, a balanced cost function was tested that introduces weights to two

crop periods: emergence to anthesis and anthesis to maturity. The weights are defined inversely proportional to the number of observations registered in the corresponding growth period. For instance, if there are three LAI observations from emergence to flowering period and seven observations from flowering to maturity, the weights are calculated as follows:
weightP1=0.5*(1/3) = 0.16 weight of observation in the first phenological period
weightP2=0.5*(1/7) = 0.071 weight of observation in the second phenological period

C2. Logical rule for the iterative LUT

A group of logical rules, detailed as follow, were implemented to select parameter levels along the iterative LUT.

1. The sum of frequencies of the parameter levels selected must represent, together, at least 50% of the total number of treatments;
2. If the second and third parameter level, sorted by frequency, had the same frequency, the parameter level with the largest difference respect to the most frequent parameter level is selected;
3. If a parameter level had a frequency larger than 75% it is assumed to be constant in the next iteration.

Appendix D-4DVAR cost function

The 4DVAR cost function is composed of two error terms; a first one which measures the distance between the reinitialized parameter and a background parameter and a second term which represents the summation of disagreement between LAI observations and simulations in the time-frame considered.

In our experiment parameter values extracted from iLUT were considered as background parameters while the reinitialized parameters were calculated along the optimization process by PSO. The standard deviation calculated in iLUT approach represented the background error for each parameter. The equation of 4DVAR function is detailed as follows:

$$J(x) = (x_o - x_b)^T B^{-1} (x_o - x_b) + \sum_{K=1}^{S} (y_{(k)} - H(x_{(k)}))^T R_{(k)}^{-1} (y_{(k)} - H(x_{(k)})) \quad (1)$$

$\mathbf{x_o}$ initial condition at the beginning of the assimilation window
$\mathbf{x_b}$ background value
B background error covariance matrix
R observation error covariance matrix
H is the nonlinear observational model
K observational time

Appendix E-Representation of the correlation of GRAMI and SAFY parameters

A complementary visual representation of the correlation analysis for both CGMs (§5.3.2) based on stepwise technique are presented in Figures E1 (GRAMI) and E2 (SAFY).

In this stepwise analysis the parameters are considered as variables. Then, in each dispersion diagram is represented the trend between the residual of the dependent variable and a new independent variable. The rest of variables are included in the model as independent. The stepwise technique allows analyzing the marginal effect of the inclusion of a new independent variable in the model. For instance, the row LUE and column K indicates the relation between the residuals of K and the incorporation of LUE as new explanatory variable; the rest of parameters are already included in the model. The variable K is strongly related with LUE demonstrated by the sharp correlation between LUE and K residuals. The parameters A and B are another example of strong correlation. This additional analysis permits scaling the complexity of correlation between parameters.

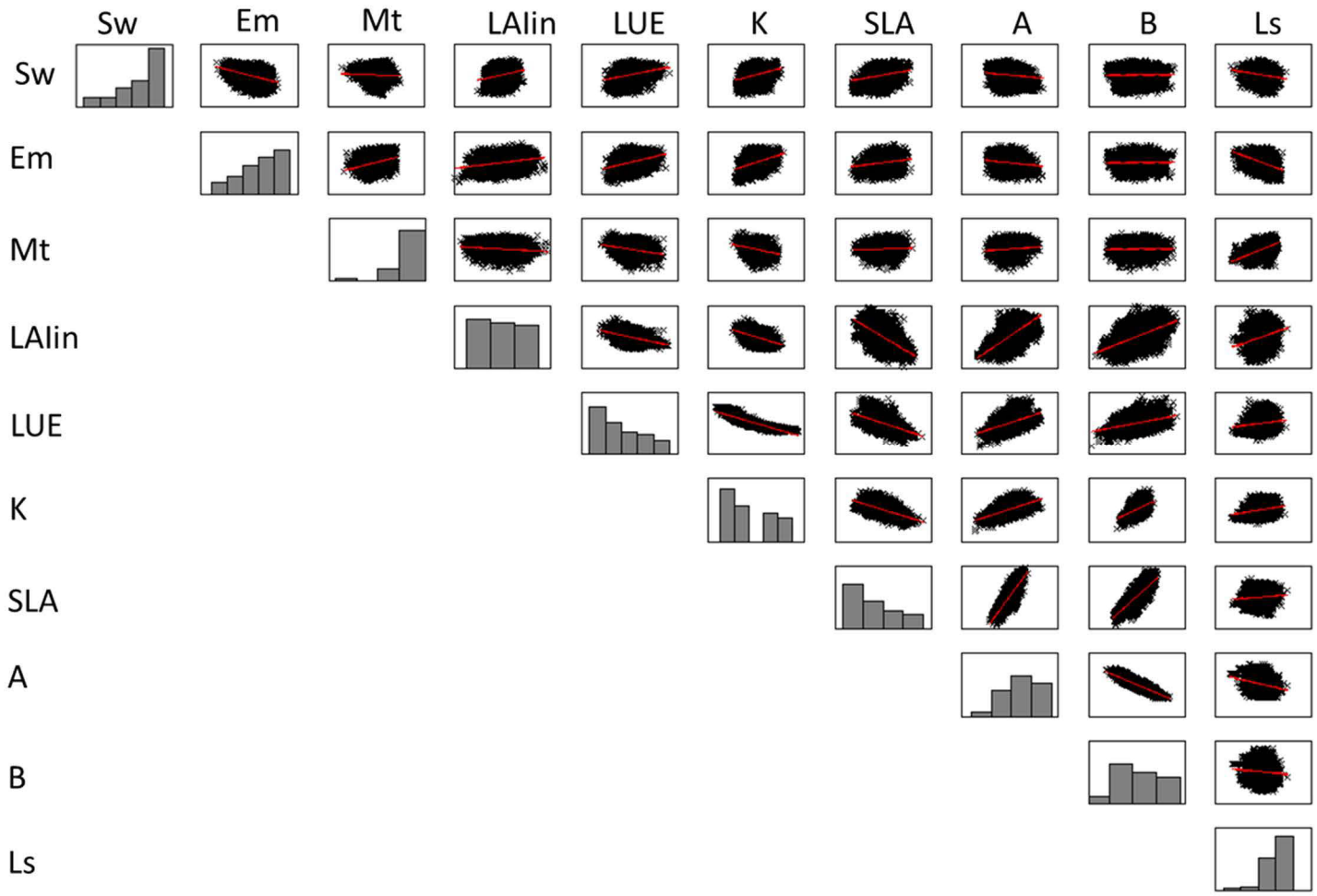

Figure E1- GRAMI parameters dispersion matrix

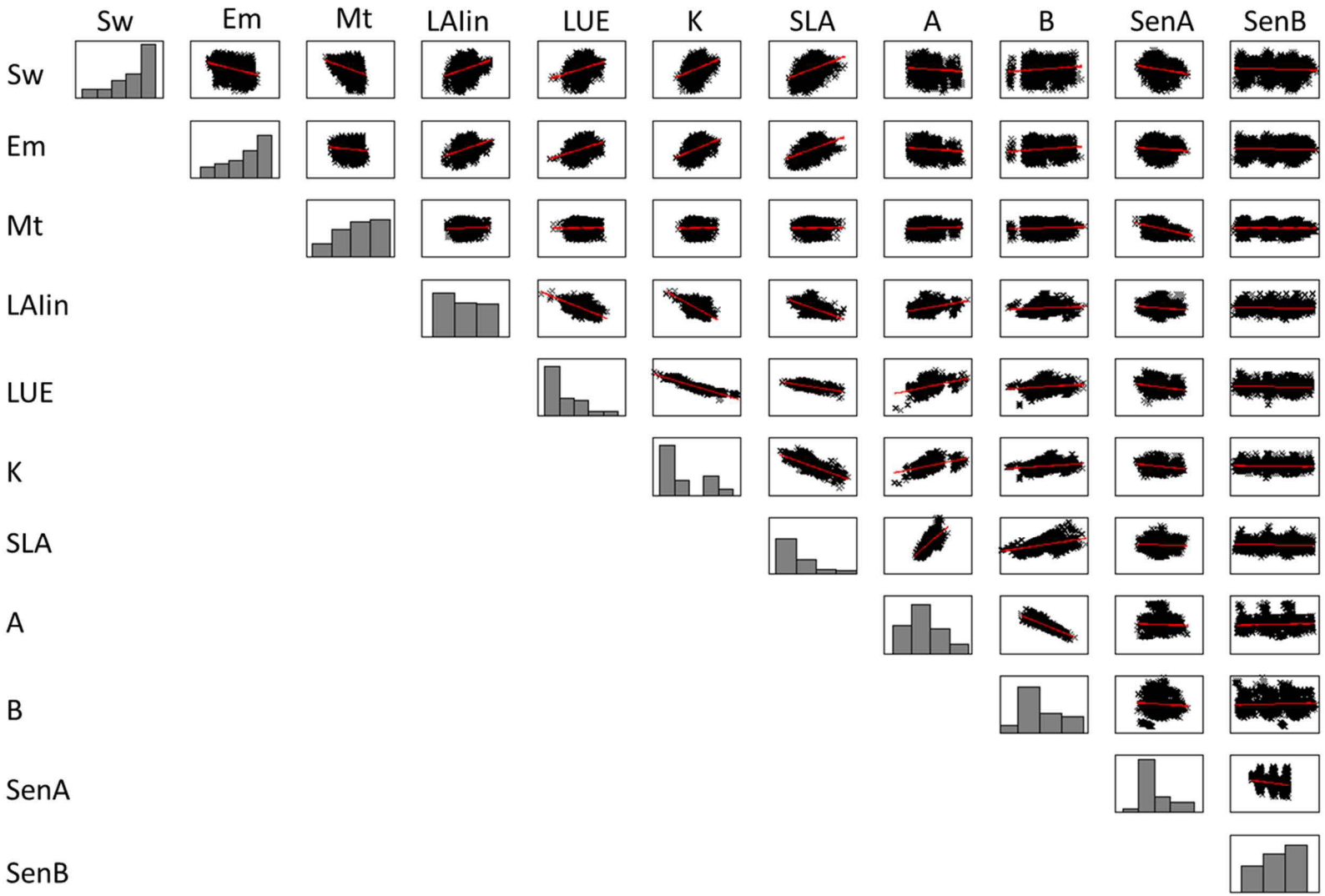

Figure E2- SAFY parameters dispersion matrix

Appendix F-Goodness-of-fit parameters for iLUT and PSO approaches for season 2013

Table F1. Goodness-of-fit parameters for iLUT approach for season 2013

CGM	GRAMI			SAFY		
	1° it	Best it	x Pixel	1° it	Best it	x Pixel
Slope	1.05	1.07	1.09	0.81	1.03	1.3
Offset	1.76	-5	-13.7	15.9	8.1	-8.7
R2	0,66	0.73	0.86	0.61	0.65	0.85
NRMSEf	16	14.3	10.2	17.2	15.4	10.8
REE	5.2	3.2	10.3	0.6	10.4	12.2
PEE	15,5	12.9	12.3	15.7	18.5	17.3

Best it: best iteration

Table F2. Goodness-of-fit parameters for PSO approach for season 2013

CGM	GRAMI			SAFY		
	Plot	pixel-2 free parameters	pixel-5 free parameters	Plot	pixel-3 free parameters	pixel 6 free parameters
Slope	0.88	1.23	1.14	0.86	1.03	1.03
Offset	0.67	-20	-23	11.6	-2	-5.6
R2	0.76	0.72	0.89	0.75	0.77	0.90
NRMSEf	13.5	14.5	8.8	13.8	13.4	8.5
REE	14.4	4.5	16.5	0.2	1.4	5.6
PEE	17.4	13.4	12.6	12.5	11.6	8.3

Appendix G-Goodness-of-fit parameters for yield estimation by FAPAR

Table G1. Goodness-of-fit parameters for yield estimation by FAPAR accumulation-Regional LUE.

CGM	GRAMI			SAFY		
Phenology	Filtering	Field	CGM	Filtering	Field	CGM
Slope	1.28	1.38	1.28	1.17	1.25	1.16
Offset	-23.1	-12.3	-8.2	-23.15	-12.3	-8.2
R2	0.35	0.62	0.60	0.35	0.62	0.6
NRMSEf	22.3	17	17.5	22.3	17	17.5
REE	3	14.7	12.1	13.5	6.1	3.1
PEE	19.2	22.5	20.8	22.6	17.1	16.1

Table G2. Goodness-of-fit parameters for yield estimation by FAPAR accumulation-Plot LUE**.**

CGM	GRAMI			SAFY		
Phenology	Filtering	Field	CGM	Filtering	Field	CGM
Slope	0.86	0.97	0.92	0.95	0.94	0.97
Offset	9.12	13.3	14.7	-4.65	9.7	5.22
R2	0.42	0.59	0.59	0.65	0.75	0.80
NRMSEf	21.1	17.5	17.6	16.3	13.8	12.4
REE	3.6	13.9	11.3	14.1	5.1	2.3
PEE	18.5	21.6	20	18.6	13.8	11.5

Appendix H Goodness-of-fit parameters for season 2014

Table H1. Goodness-of-fit parameters for iLUT approach for season 2014

CGM	GRAMI			SAFY		
	1° it	Best it	x Pixel	1° it	Best it	x Pixel
Slope	0.67	0.57	1.16	0.62	0.40	0.79
Offset	21.83	43.47	-4.50	32.87	52.98	28.13
R2	0.42	0.63	0.50	0.38	0.46	0.57
NRMSEf	10.99	8.80	10.18	11.37	10.57	9.49
REE	2.50	21.86	15.87	9.14	16.13	22.70
PEE	14.77	19.00	12.84	11.10	18.19	18.70

Best it: best iteration

Table H2. Goodness-of-fit parameters for PSO approach for season 2014

CGM	GRAMI			SAFY		
	Plot	pixel-2 free parameters	pixel-5 free parameters	1° it	pixel-3 free parameters	pixel 6 free parameters
Slope	0.35	0.46	0.35	0.43	0.59	0.61
Offset	50.81	41.70	50.78	45.73	34.78	31.94
R2	0.42	0.41	0.35	0.76	0.68	0.69
NRMSEf	10.99	11.07	11.59	7.10	8.09	7.98
REE	2.13	0.58	2.69	3.66	7.92	5.45
PEE	20.19	15.83	19.98	15.87	10.10	9.87

Table H3. Goodness-of-fit parameters for Updating approach for season 2014.

CGM	GRAMI						SAFY					
Calibration	ILUT			PSO			ILUT			PSO		
Filter	EnKF	PF nr	PF r	EnKF	PF nr	PF r	EnKF	PF nr	PF r	EnKF	PF nr	PF r
Slope	0.69	0.71	0.68	0.35	0.38	0.39	0.86	0.89	0.86	0.60	0.61	0.62
Offset	32.82	33.06	35.16	47.27	46.94	46.13	5.82	6.98	9.51	30.22	29.30	28.92
R2	0.53	0.48	0.47	0.33	0.31	0.32	0.48	0.49	0.48	0.72	0.72	0.73
NRMSEf	9.89	10.39	10.50	11.77	11.92	11.87	10.35	10.31	10.35	7.59	7.61	7.45
REE	18.58	21.62	20.81	14.11	6.98	7.12	0.62	4.33	4.61	1.75	2.14	1.63
PEE	15.43	18.21	17.66	28.48	21.78	21.72	12.46	9.54	9.53	11.32	10.88	11.10